ESD-TR-81-339

Semiannual Technical Summary

Seismic Discrimination

30 September 1981

Prepared for the Defense Advanced Research Projects Agency
under Electronic Systems Division Contract F19628-80-C-0002 by

Lincoln Laboratory

MASSACHUSETTS INSTITUTE OF TECHNOLOGY

Lexington, Massachusetts

AIR FORCE MAY 4, 1982--225

The work reported in this document was performed at Lincoln Laboratory, a center for research operated by Massachusetts Institute of Technology. This research is a part of Project Vela Uniform, which is sponsored by the Defense Advanced Research Projects Agency under Air Force Contract F19628-80-C-0002 (ARPA Order 512).

This report may be reproduced to satisfy needs of U.S. Government agencies.

MASSACHUSETTS INSTITUTE OF TECHNOLOGY

LINCOLN LABORATORY

SEISMIC DISCRIMINATION

SEMIANNUAL TECHNICAL SUMMARY REPORT TO THE DEFENSE ADVANCED RESEARCH PROJECTS AGENCY

1 APRIL — 30 SEPTEMBER 1981

12 APRIL 1982

LEXINGTON MASSACHUSETTS

ABSTRACT

This Semiannual Technical Summary describes the Lincoln Laboratory Vela Uniform program for the period 1 April through 30 September 1981. During this period, the first working prototype of a Seismic Data Center has been completed. In this report, Sec. I describes this prototype system, Sec. II describes a series of activities in seismic processing related to the Center, and Sec. III describes a series of investigations in General Seismological Research.

CONTENTS

SUMMARY

This is the thirty-fifth Semiannual Technical Summary (SATS) report describing the activities of Lincoln Laboratory funded under Project Vela Uniform. This report covers the period 1 April through 31 September 1981. Project Vela Uniform is a program of research into the discrimination between earthquakes and nuclear explosions by seismic means. An important recent emphasis of the project is in the development of data-handling and analysis techniques that may be appropriate for the monitoring of a potential Comprehensive Test Ban Treaty. The FY 1981 program consists of the development of a Prototype Seismic Data Center (SDC), which will fulfill U. S. obligations that may be incurred under such a Treaty, and which will also provide a data resource to the seismological research community. The program also contains an element of seismic research, with emphasis on those areas directly related to the operations of the SDC.

During this period, the first working Prototype SDC has been completed. This system is described in Sec. I of this report. It is capable of accepting input of both parameter and continuous waveform data, carrying out automatic signal detection and parameter extraction on the waveform data, merging all parameters, and carrying out automatic association to produce an event list. Review by a human analyst is provided for, both after automatic signal processing and after automatic association. Analyst interaction utilizes a single-user interactive computer graphics system called the Seismic Analysis Station (SAS). This Prototype will form the basis for future SDC development.

In Sec. II, several studies in the area of Seismic Processing are described. One study demonstrates that augmented transition network (ATN) grammars can be of significant use in the recognition of glitch noise. Another compares ATN grammars with dynamic time warping as means for the recognition and characterization of seismic signals. A third study describes the affinity technique for the analysis of the morphological structure and information content of seismic signals. We are beginning to apply the concepts of expert systems to the problem of automatic association (AA), and expect that this will lead to much more intelligent AA programs. Another investigation examines the use of hash functions, and the application of entropy concepts to measure their performance. These functions may have an important application to the retrieval of information from database storage. We have begun to study potential improvements in signal detection. It is shown that the number of significant detections obtained in a given time period can be increased by carrying out signal detection on the horizontal components of 3-component instruments. And we have completed an extensive comparison of the performance of automatic techniques and the human analyst in picking the first arrivals of seismic signals. While the automatic methods produce more false alarms, they are comparable to the analyst in detecting real signals. Analysts were shown to be less reliable than commonly assumed.

Section III contains reports on a number of areas of general seismological research. A detailed review of frequency-dependent anelasticity has been carried out. Additional evidence for absorption-band models is given. Another study approaches the problem of including transverse isotropy in ray theoretic calculations. Several new extensions of a method, developed earlier, for the simultaneous estimation of seismic moment tensor and event hypocenter

are described. Application of these methods to several recent earthquakes is also included. In one case, evidence is given that a complex series of motions occurred at the seismic source. Finally, an application of a new method for the analysis of mantle waves shows how these can be used to extract direct information on Earth structure.

M. A. Chinnery

SEISMIC DISCRIMINATION

I. PROTOTYPE SEISMIC DATA CENTER

A. SYSTEM FUNCTIONS

The Prototype Seismic Data Center (SDC) described in this and later sections of this report has been assembled at Lincoln Laboratory. The Prototype SDC has been based on a Lincoln Laboratory overall system design,[1] and various stages in the development of the system have been documented in previous SATS.[2-4] The intent of this Prototype SDC is that it should be a working system, capable of carrying out all the basic functions that will be required in a full-scale SDC, and able to be used to test out a variety of design concepts and operational procedures. The system described in this report has been successfully demonstrated to DARPA, and, with minor improvements, will form the basis for further SDC development.

The functions that the Prototype SDC will perform are:

(1) Accept input data in the form of both lists of parameters describing seismic arrivals and also continuous waveform data. Neither of these data types is currently available on-line, so the Prototype SDC is based on input from magnetic tape.

(2) Entry of both parameter and waveform data into a suitable database management system. The INGRES system designed by Lawrence Berkeley Laboratory has been chosen for this task.

(3) Automatic processing of the continuous waveform data, to both detect seismic signals and also extract parameters describing those signals. The outputs of this stage are a list of arrival parameters and a set of waveform segments each containing at least one detected signal.

(4) Analyst review of the output of the automatic processing algorithms, including the elimination of false alarms, the identification of seismic phases, and the refinement of the various seismic parameters measured, such as origin time, amplitude, etc.

(5) Merging of the refined arrival data extracted from the waveforms with all other arrival data in the INGRES database management system.

(6) Automatic association of the arrival data into a Preliminary-Event List (PEL).

(7) Analyst review of the PEL, including changing arrival associations, adding depth-phase information and refinement of calculated hypocenters. Also, review of those arrivals not associated with events in the PEL, with a view to adding new events.

(8) Preparation and publication of a completed Final-Event List (FEL).

In the sections that follow, we describe how each of these functions is accomplished.

M. A. Chinnery

B. HARDWARE CONFIGURATION

The hardware configuration of the Prototype differs in scale from the projected SDC and in a few details in the subsystems represented. This section details the configuration in use for the Prototype at this time.

The logical configuration, as shown in Fig. I-1, includes the Seismic Analysis Station (SAS), Database Subsystem (DBS), and Automatic Processing Subsystem. The Communications Interface Subsystem is represented only by routines used to enter parameter and waveform data into the DBS. A change from the SDC design is the use of a direct link between the VAX 11/780 which supports all the subsystems except the SAS and the PDP-11/44 which implements the SAS. This direct link uses the DEC DMC-11 high-speed communication link to send data between the machines. The DMC is used with a command which transmits files between the two machines. This command, as well as the details of the capabilities of the other subsystems, is covered in subsequent sections.

The hardware configuration is covered in detail by Fig. I-2, a schematic presentation of the hardware configuration used by the Prototype system. The hardware configuration is listed by computer in Table I-1 which gives the part number and supplier for all major components of both computers.

A. G. Gann

C. DATABASE MANAGEMENT

This report describes the database for the SDC Prototype system. The database contains both waveform and parametric data and is based on INGRES. INGRES is a relational database management system. A relation can be thought of as a table of information. In INGRES terminology, a "tuple" is a row of a table (relation) and a "domain" is a column. Commands to INGRES are given in a language called "Quel." Quel commands can be used to extract from, modify, and do computations on a relation or combinations of relations. INGRES can be accessed directly through the INGRES monitor or indirectly from a C program using Equel, a C preprocessor. Most of the primitive database commands are implemented as Quel macros. Only the waveform primitives and the primitives that perform seismic calculations need to be implemented in Equel.

1. Database Structure

Parametric data are measurements made from seismograms, such as arrival times, amplitude, and periods. Such data are determined by the SDC itself and also from data sent to it from other sources. These data will be organized into events using automatic and interactive methods.

Parameter data related to an event are organized into a 4-level structure as shown in Fig. I-3. An event consists of a number of origins – each origin being an estimate of the event's location based upon evidence from the arrivals with which the origins are associated. One origin, referred to as the preferred origin, will be used to represent the best estimate of the origin of the event. Allowing an event to have multiple origins is useful for several reasons:

(a) Historically, data centers have reprinted epicenter estimates provided by other agencies.

(b) Multiple origins allow an analyst to have several competing hypotheses for one event during the association process. Normally, after association is complete, one origin is chosen to represent the event while others are discarded.

TABLE I-1

DEMONSTRATION HARDWARE COMPONENTS

VAX 11/780 (Model SV-AXHHB-CA), (4 bays), with		
1	LA-120 console	(DEC)
	4.0-Mbyte Memory	(2.5 MB DEC, 1.5 MB Motorola)
1	H7112-A Battery backup for memory	(DEC)
1	FP780-AA Floating-point accelerator	(DEC)
2	DW780-AA Unibus adapter	(DEC)
1	BA11-KE Unibus extension	(DEC)
2	RK07 28-Mbyte disk drives with Unibus controller	(DEC)
	32-port terminal controller, DZ11	(DEC)
1	DMC-11 1-Mbaud intercomputer link to SAS	(DEC)
1	600-lpm line printer	(Southern Systems)
2	STC tape drives (1600/6250 bpi, 75 ips) with AVIV controller	(AVIV/STC)
4	CDC 675-Mbyte (nonremovable) disk drives with SI controller	(SI/CDC)
2	CDC 300-Mbyte disk pack drives with SI controller	(SI/CDC)
	Dial-in modem (300/1200 bd)	(Racal Vadic)
	Datagraphix (132-column) video display terminal for SAS	(GD)
	32-V BSD 4.0 UNIX operating system	(WECo/UCB)
PDP-11/44 (Seismic Analysis Station) with		
1	LA-120 console	(DEC)
	512-kbyte memory	(DEC)
	Battery backup for memory	(DEC)
1	FP11-F Floating-point processor	(DEC)
1	DD11-DK Unibus expansion	(DEC)
2	RL02 10-Mbyte disk cartridge drives with controller	(DEC)
	16-port terminal controller, DZ11	(DEC)
1	DMC-11 1-Mbaud intercomputer link	(DEC)
1	LA180 line printer with parallel interface	(DEC)
2	Cipher tape drives (800/1600 bpi, 45 ips) with AVIV controller	(AVIV/Cipher)
1	CDC 300-Mbyte disk pack drives with SI controller	(SI/CDC)
	UNIX V7 operating system	(WECo)
	Megatek 7000 refresh graphics display system with M702 controller, IPCU, data tablet, joystick, HCRST 2-dimensional hardware, 10-mil monitor, extra memory, rasterizer and interface for Versatec hardcopy unit	
	Versatec printer/plotter (200-dot/in. resolution)	
	Datagraphix (132-column) video display terminal	(GD)

(c) As new processing methods are developed, new results can be added to the database without erasing older published results.

Each origin contains information describing the hypocenter as well as a list of arrivals which are associated with that origin.

A Related Arrival Group (RAG) is a group of arrivals recorded by one station which are related to one event, such as a p- and an s-arrival.

Only an index to the waveform data is maintained in the database. The actual waveforms exist as UNIX files in gram-file format. This allows some flexibility in managing disk space. The connection between arrivals and waveform data is not maintained explicitly in the database. Only when portions of the database are extracted for analysis is the correspondence set up.

2. Database Primitives

The database primitives are only an initial set, and are designed to maximize ease of implementation at the expense of ease of use. Once these primitives are working satisfactorily, a more convenient user interface can be developed.

To use the primitives, the user establishes a working context within the database structure:

EVENTS
  ORIGINS
    RAGS
      ARRIVALS

One can define the context at any of the four levels, with or without respect to the other levels. For example, to work on origin 51 of event 5131, specify:

```
work event 5131
work origin 51
```

All subsequent commands will now be with respect to this context.

The analyst can define a new RAG without first defining the event or origin context, which may be unknown:

```
work event 0
new rag (range = "1")
    new arrival (day = 80105, time = 1013.1, \
    phase = "pg", qual = "i")
  new arrival (day = 80105, time = 1045.0, \
  phase = "lg", qual = "e")
  ...
new rag ()
  ...
work rag 0
work event 0
```

A primitive continued on another line requires a backslash, (\).

a. Arrival Primitives

new arrival (attribute = value, ...)

Creates a new arrival and makes it the working arrival

update arrival arrival-id (attribute = value, ...)

Modifies an existing arrival

remove arrival arrival-id

Removes an arrival from the database

add arrival arrival-id

Adds an arrival to the working RAG

sub arrival arrival-id

Removes an arrival from the working RAG

pr arrival [arrival-id]

Prints an arrival

b. RAGs Primitives

new rag (attribute = value, ...)

Creates a new RAG and makes it the working RAG

work rag rag-id

Sets up a new working RAG

update rag rag-id (attribute = value, ...)

Modifies an existing RAG

remove rag rag-id

Removes a RAG from the database

pr rag [rag-id]

Prints information about a RAG

c. Origin Primitives

new origin (attribute = value, ...)

Creates a new origin and makes it the working origin

work origin origin-id

Sets up a new working origin

update origin (attribute = value, ...)

Modifies an existing origin

copy origin

Makes a copy of the working origin

remove origin [origin-id]

Removes an origin and its associated arrivals

prefer origin [origin-id]

Identifies an origin as the preferred origin

pr origin

Prints a summary of the working origin

d. Association Primitives

assoc arrival [arrival-id]

Associate an arrival to the working origin

assoc rag [rag-id]

Associate the arrivals from a RAG to the working origin

unassoc arrival arrival-id

Unassociate an arrival from the working origin

unassoc rag rag-id

Unassociate the arrivals of a RAG from the working origin

def arrival-id

Makes the arrival identified by arrival-id defining for the working origin of the working event

nondef arrival-id

Makes an arrival nondefining in the working origin

nondef resid tolerance

Any arrival associated to the working origin that has an absolute residual less than tolerance is made nondefining

e. Event Primitives

new event (attribute = value. . .)

Create a new event and make it the working event

work event event-id

Make an event the working origin

remove event event-id

Remove an event and all of its origin information

pr event

Prints a summary of the working event including the preferred origin and arrival information

print olist

Prints a summary of the list of origins for the working event

evbul day1 time1 day2 time2

Print an event bulletin for the corresponding time interval

loc [-o]

Adjust the working event location using the working origin as the starting location

match [-t toler] [-i interval] [-p] [-r]

Finds all arrivals which match the working origin of the working event to within a given tolerance

f. Waveform Primitives

loadgi

Adds waveforms from a gram database into the waveform database

gdbs [-IXvsc] ingresdb gdbdir gdbname start interval station [channel]. . ."

Create a gram file by station for a given time interval

gdbp [-IXGPvaoepd] ingresdb dir gdbname [-s, +s] [date] [id. . .]

Create a new gram-file database for arrivals extracted by event, or origin

K. R. Anderson
P. Kreps
K. J. Schroder

D. AUTOMATIC SIGNAL PROCESSING

In the Prototype SDC, input continuous waveform data are subjected to a series of automatic processing steps which are summarized as follows:

(1) Signal detection, and the extraction of a waveform segment containing the detected signal

(2) Estimation of signal onset time

(3) Discrimination between local and teleseismic signals, based on the frequency content of the signal

(4) Measurement of signal-to-noise ratio (SNR)

(5) Measurement of the direction of first motion for impulsive signals

(6) Measurement of signal amplitude and dominant period.

In the first version of the Prototype SDC, input waveform data are stored on disk on the VAX (see Secs. A and B above) and then retrieved for analysis. The output waveforms segments and signal parameters are then entered into the DBS. Later versions of the Prototype SDC will utilize the DBS for both input and output data. The various automatic processing steps are described individually below.

Signal detection is accomplished using a "Z-statistic" algorithm based on that formulated by Swindell and Snell.[5] This detector has been described earlier.[4] The various parameters describing this detector are listed in Table I-2, together with typical values of these parameters which are loaded at run time.

Following a detection, a waveform segment extending from 1 min. before the detector "on" time to 1 min. after the detector "off" time is passed to a signal analysis program. This program is based on the algorithm of Allen[6] and has been described earlier.[4] This program first estimates the signal onset time by refiltering the input waveform, and then applying a compressed LTA (10 s)/STA (0.1 s) method. It also measures signal power in two frequency bands, and makes a qualitative estimate of event distance[2] (local or teleseismic). Current frequency bands have been based on SRO data, and may need to be revised for RSTN waveforms. For teleseismic events, amplitude is measured as the maximum observed in the 5 s following signal onset and converted to millimicrons of ground motion, and a dominant period is measured for this maximum peak. The quality of the arrival (impulsive or emergent) is determined by the SNR in the vicinity of the onset time (if the STA/LTA ratio is greater than 10, the signal is designated impulsive). When the signal is impulsive, a direction of first motion is measured.

The signal analysis program then outputs a "new-arrival" primitive for entry into the INGRES database. This primitive contains station, channel, date, onset time, quality, phase

TABLE I-2
SIGNAL DETECTOR PARAMETERS

Parameter	Typical Value
Bandpass filter, low corner frequency	0.9 Hz
Bandpass filter, high corner frequency	3.5 Hz
Length of LTA window	45 s
Length of STA window	3 s
LTS to STA lag	15 s
Interval between successive STA values	1.5 s
Freeze LTA between detections (yes/no)	No
Maximum LTA freeze time	5 min.
Initializing mean of filtered trace	12
Initializing standard deviation of filtered trace	0.35
Detection threshold (standard deviations)	4
Successive triggers needed to define detection	2
Time after last trigger before detection declared over	20 s

identification (normally P) first-motion direction, distance range, amplitude, and period. An author entry is also included to distinguish parameters determined automatically from those measured by an analyst.

Future enhancements of automatic signal processing include the addition of synthetic analysis using augmented transition network grammars. With these tools it will be possible to identify and remove glitches, calibration pulses, and various kinds of nonseismic noise. They should also be applicable to the problem of identifying S signals, particularly for local events.

M. A. Tiberio
M. W. Shields

E. INTERCOMPUTER COMMUNICATION

Two major efforts have been completed for data communication between the VAX 11/780 database system and PDP-11/44 of the SAS. The major projects were installation of the Bell Laboratory UUCP package and development of wideband data bus (1-Mbaud Digital Equipment Corporation DMR-11) with file transfer protocol (Fig. I-4). This hardware eventually will be replaced by the local network hardware.

1. Installation of UUCP Package

The purpose of UUCP installation between VAX 11/780 and PDP-11/44 is to provide low-speed file copy and command execution. Gradually, these features will be replaced by locally developed software. This provides an interim communication mechanism during DMR development, and provides some features not yet implemented in the DMR system.

2. 1-Mbaud DMR-11

Early development used the DEC DMC-11 hardware because the DMR-11 was not yet available. A number of hardware changes were made to fix DMC hardware problems: long DMA requests would hang the Unibus and the DMC spuriously issued RDYO interrupts when running full-duplex under heavy loads. Also, the sequencing and timing of commands to initialize the DMC were found to be critical. DEC claims that these problems have been corrected on the DMR-11 (Fig. I-5).

The DMR microcomputer provides a reliable link, performing most of the low-level protocol work such as error checking and retransmission. The host device drivers must provide general consistency checking and flow control.

Drivers have been written for the PDP-11 and VAX 11 Unibus interfaces using DMA data transfer in 512-byte packets. The latest tests show 300-kbaud bandwidth process to process between two machines separated by a DMC-11 network link. As soon as DMR installation is finished, we will try increasing the packet size to achieve better performance.

3. Easy File Transfer Protocol

Reliability, compatibility, and ease of use are the main concerns of this protocol. All transfer requests are initiated by a control program running on the VAX. File transfers (Fig. I-6) are then conducted by the control program and a server program running at the SAS via the DMR. The command syntax is made to be compatible with UUCP and CP, except that the file name is prefixed with host name. The best Unix file-to-file transfer rates are about 50 kbps.

The server program running at the Analyst Station performs like a function dispatcher. It simplifies adding future functions, e.g., virtual file, command execution, to the structure.

H. Hsiung

F. WAVEFORM DISPLAY

Work has progressed on the design and implementation of a new program for the display and manipulation of waveforms. The previous program[4] was originally designed for the Tektronix 4014, a storage display device. This program was then converted to be used on the Megatek 7000, a refresh display device. We are now working on a new program which takes advantage of the capabilities of the Megatek terminal, which include the ability to segment the elements on the display screen and manipulate them individually.

The program accepts commands from disk files, the user's keyboard, and from menu items on the Megatek screen selected by using the data tablet, a peripheral device connected to the Megatek, which tracks the location of a pen on a 1-ft^2 tablet. Figure I-7 shows a typical display, with the menu boxes on the right, the waveforms in the center, and boxes describing the waveform on the left. Commands from all sources are converted to a common set of tokens, which are then executed. Therefore, additional command sources such as a knob box or a voice analyzer can be interfaced to the system in an orderly manner. Commands are entered in postfix notation, with the arguments preceding the command name. This reduces the number of keystrokes required of the user, and eliminates the need for a delimiter at the end of a variable set of arguments and the need for a separator symbol between commands.

In addition to the capabilities available with the previous display program, the new program allows the waveforms to be altered dynamically, without requiring the entire screen to be replotted. Using a joystick as an interface, the new program allows smooth vertical and horizontal gain change, as well as left and right scrolling of waveforms. The program allows phase names to be selected upon entry to the program, and allows them to be changed during the execution of the program. We plan to add new functions to the program, such as waveform filtering and decimation.

We have developed a new set of interface routines for use with the Megatek 7000, to take the place of those originally provided by Purdue University. The new routines follow the general outlines of the ACM Siggraph Core Standard for graphics interfaces, but are optimized for both the SAS application and the Megatek 7000.

The interface routines recognize waveforms as a special type of graphics segment and exploit a short vector format supplied by the Megatek to effectively double the number of data samples which can be displayed without screen flicker. With the routines supplied by Purdue, noticeable flicker developed with three or more waveforms on the screen. With the new routines, six waveforms can be displayed without flicker.

The new routines also supply graphics capabilities not found in the Purdue routines, most importantly in the area of dynamic picture modification, as in the case of smooth scrolling of waveforms. In addition, the routines make more effective use of the Megatek display memory, allowing larger amounts of the waveform database to be loaded. This results in less-frequent requests for data from the host processor disk.

P. T. Crames
H. Lison

G. ANALYST INTERACTION WITH DATABASE

Following Arrivals Based Analyst Review (ABAR), the database markerfile contains adjustments to PPK's automatic picks, additional picks of later phases, and deletions of phases considered spurious by the analyst. It also contains markers corresponding to any amplitudes the analyst may want to measure. These markers, together with information from the .gi file, are input to the program CPAR. CPAR functions both as a reformatting program and a signal-analysis program. It is a reformatting program because it puts information it finds in the markerfile into INGRES "arrivals primitives" format and into human readable format for output to the terminal. It is a signal-analysis program because it makes measurements on the seismic signal.

As a reformatting program, CPAR uses the marker name and sample number from the database markerfile. The marker name contains the phase name, INGRES identification number, and information which identifies it as an arrival-time or amplitude marker. The sample number is used to calculate the phase arrival-time or to locate the point on the seismic trace to be analyzed.

The program utilizes marker-name information in the following way. An "A" in the first column designates the marker as an amplitude. Any other letter designates it as an arrival marker name. For markers designated as corresponding to arrivals, there are several letters which have special meanings when placed in the first column. A "D" in the first column signifies an analyst decision during the review session that the arrival is either misidentified or false. CPAR creates a "remove arrival" primitive for any arrival whose marker name begins with

a "D." Other special letters are "i," "e," and "w." CPAR understands these as estimates of arrival-time reading accuracy. The analyst calls the arrival "i" (impulsive), if he estimates the accuracy of his pick to be better than 0.2 s. For an estimated accuracy of 0.2 to 1.0 s, the arrival is called "e" (emergent). A "w" (weak) in the first column designates an arrival-time accuracy of worse than 1 s.

CPAR searches columns two through seven of both arrival and amplitude marker names, looking for the phase name of the arrival. A "t" occurring in columns three or four of an arrival-time marker means that the associated event has been identified as a teleseism. An "l" found in these columns categorizes the event as a local. CPAR inspects the phase name of an amplitude marker in order to associate the ground motion and period it calculates with the proper arrival. The first blank encountered in a column prior to the seventh terminates the phase name.

Starting with the first column following the blank column in the arrival marker name, CPAR looks for the INGRES identification number, a unique number of up to 5 digits assigned to each arrival in the INGRES database. If it finds the INGRES ID number, CPAR creates an "update arrival" primitive for those arrivals not previously eliminated because of a "D" in the first column of the marker name. If no ID number is found, the arrival is assumed to have been added during the ABAR session. In this case, CPAR places the results of its analysis in a "new arrival" primitive.

Arrival times are found by combining the seismogram start time and sample rate, supplied from the *.gi* file, with the sample number of the arrival found in the markerfile. Times are written to the terminal in the standard format: month/day/year hour:minute:second.tenths. The format for the INGRES "arrival primitive" is hard for a human to decipher. Year and day of year are represented by a 5-digit integer, where the first 2 digits on the left represent the year and the last 3 represent the day of the year. The time of day is in seconds. CPAR also finds the difference between the first arrival and all succeeding phases on the seismogram. This information is written to the terminal for the convenience of the analyst.

CPAR performs several analysis functions. It finds the direction of first motion of any first arrival which the analyst has called an "i." For any signal categorized as teleseismic, it automatically finds the greatest ground motion and associated period in the first 5 s of the signal. Furthermore, it will find the ground motion of any peak marked by the analyst, the only condition being that the amplitude marker name be associated with an identical arrival-time phase name. Ground motion is one-half peak-to-peak in millimicrons corrected for the frequency response of the instrument. The period is two times the absolute value of the time difference between the measured peak (or trough) and the greatest adjacent trough (or peak).

M. W. Shields

H. AUTOMATIC ASSOCIATION

The automatic association process attempts to determine event hypocenters from the time-ordered arrival list. The latter is obtained by merging the Level-I parameters (produced by the analyst at the station) with those parameters produced as a result of the automatic processing as described above, on the continuous and segmented waveform data tapes. We have implemented the association procedure for 2 October 1980 data. On that day there were 1051 short-period arrivals in the Level-I data collected by Sweden, of which 565 were primary

(i.e., P or PKP). The automatic processing of the 23 stations of waveform data comprising the U.S. contribution to the data-collection experiment produced 648 arrivals. Of these, 140 were identical (arrival time same to $\leq$ 1 s) to arrivals in the Level-I data, and 369 were flagged as being local, i.e., arrivals identified by the analysts as being local, or with initial phases Pn or Pg, or (S-P) times less than 60 s.

The automatic association scheme currently implemented is not yet fully incorporated into the INGRES-based data structure. At present, association is carried out by a FORTRAN program which operates upon the arrival list for a specified time interval, normally one day, and produces an event bulletin which is then supplied to INGRES for refinement using the SAS. On the latter subsystem, arrival and event information were updated using the INGRES database.

The FORTRAN association scheme consists basically of a series of procedures of event hypothesizing, testing, and merging. It does not currently include the standard association procedure, such as that used by the USGS National Earthquake Information Service, which involves testing all possible combinations of arrivals as event hypotheses. Nevertheless, it is both rapid (<10 min. VAX CPU time to process 24 h of arrivals) and, we feel, surprisingly successful in view of its simplicity. The various steps of the procedure follow.

1. Initial-Event Hypothesis

The arrivals list for 2 October 1980 contains 49 event locations contributed by seismic array sites NAO, SUF, HFS, GRFA, EKA, GBA, and YKA, and these form the backbone of the initial-event list. Next, all arrivals flagged as local are treated as event hypotheses, the event location being that of the station and the origin time being set as that of the arrival itself. Finally, groups of arrivals from four or more close stations were used to generate trial events by fitting a plane wave, as if the stations were a conventional seismic array. All hypotheses were assigned zero depth (surface focus).

2. Initial-Event Testing

Each of the hypotheses generated above is now simply tested by counting the number of arrivals consistent with it. If a given station has an onset time within 80 s of that predicted by the event hypotheses, it is considered to be possibly associated with the event. There is no guarantee that the number, distribution, and quality of the observations are sufficient to locate the event. Hypotheses with less than four consistent arrivals were rejected. In order to somewhat reduce the number of redundant hypotheses, arrivals which were deemed consistent with either array- or local-generated events were temporarily deleted from the list from which the hypotheses generated by the plane wave fit to groups of close stations are formed.

3. Initial Merging

At this stage we certainly have many duplicate hypotheses of the same events, and it is wise to attempt to reduce this redundancy before continuing the location procedure. Event hypotheses were deemed to be duplicate if their origin times differ by less than 100 s, and their locations by less than 10°. The event with the largest number of consistent arrivals as determined by step 2 is retained.

4. Second-Event Testing

Each of the remaining hypotheses is now tested for validity using a standard hypocentral location procedure (Geiger's method) with the event constrained to a surface focus. If the solution fails to converge after a certain number of iterations (here set to 15) or if there are less than 4 "defining" arrivals, the hypotheses are rejected. "Defining" arrivals were arbitrarily set to be those with residuals of 3.5 s or less.

5. Second-Event Merging

The remaining event hypotheses are now merged as in step 3, except that events are now considered duplicate if their origin times differ by less than 60 s and their location by less than 5°.

6. Final Location Process

So far, events have been constrained to surface focus. The remaining hypotheses are now retested with the depth unconstrained. If, during this location procedure, the final depth becomes greater than 100 km, the location obtained is checked against a stored list of seismic regions in which only shallow events have occurred historically. If the event lies in one of these regions, its depth is reconstrained to be surface focus.

Analyst Refinement:– The analyst now studies the event solutions for inconsistencies (e.g., in amplitude) observed in the parameter data and displays all the waveforms associated with a particular event. In the latter process, the analyst concentrates on identifying depth phases and, for close arrivals, consistent (S-P) time differences.

7. Results for 2 October 1980 Data

Of the 17 events given in the NEIS monthly summary for this date, only 11 had 4 or more arrivals in the input arrival list supplied to the automatic association procedure used above, and the remaining 6 could therefore not possibly be located on the basis of the information given.

Sixteen events were obtained by the automatic association procedure, and these include all but 1 of the locatable 11 events given in the NEIS monthly summary. The results are shown in Table I-3, where events common with the monthly summary are identified by an asterisk. Of the six new events, numbers 5, 6, and 7 are almost certainly real, but we are less confident in numbers 9, 13, and 14, which are all in the Western U.S. Subsequent analyst study of the latter three, particularly of the waveforms corresponding to the associated arrivals, cast serious doubt on the validity of these events generated by the automatic association process.

The final column in Table I-3 gives the sources of the initial event hypotheses leading to the 16 solutions given. Ten events were formulated on the basis of two or more array observations, 5 on the basis of two or more arrivals flagged as local, and one by the plane-wave fit method to groups of close stations. Of the original 1073 input primary arrivals, 684 remained unassociated; 510 of these were flagged as being local in character.

R. G. North

TABLE I-3

AUTOMATIC ASSOCIATION OUTPUT FOR 2 OCTOBER 1980

Event	Origin Time (h:m:s)	Latitude (°N)	Longitude (°E)	d (km)	No. of Arrivals	No. of Waveforms†	Source
1*	01:12:39.7	51.69	108.43	0	48	12	7 arrays
2*	03:42:45.9	50.21	−130.33	0	50	13	3 arrays
3*	03:51:11.0	−35.43	178.95	45	16	4	3 arrays
4*	05:26:04.6	−19.27	168.56	111	32	8	2 arrays
5	06:44:42.9	−22.24	170.16	130	6	2	3 locals
6	08:13:09.2	52.28	152.60	33	5	3	2 arrays
7	11:21:12.4	40.68	36.68	0	18	0	GROUP
8*	15:49:34.5	−20.92	−178.54	562	58	16	2 arrays
9	16:13:50.7	40.09	−107.74	0	5	5	2 locals
10*	17:23:12.6	52.95	18.06	0	8	1	4 locals
11*	17:47:36.1	37.56	141.06	0	16	6	5 arrays
12*	19:06:50.6	20.02	122.34	0	59	15	5 arrays
13	20:48:57.2	44.83	−115.90	0	4	4	2 locals
14	21:21:40.0	39.53	−112.72	0	4	4	2 locals
15*	22:00:10.7	43.33	135.32	355	26	6	6 arrays
16*	23:08:10.2	38.03	30.89	0	34	5	3 arrays

† Number of arrivals for which waveform data are available.

REFERENCES

1. "Design of a Seismic Data Center," Special Report to DARPA/NMRO (30 September 1979).
2. Seismic Discrimination SATS, Lincoln Laboratory, M.I.T. (31 March 1980), DTIC AD-A091107/3.
3. Ibid. (30 September 1980), DTIC AD-A097999/7.
4. Ibid. (31 March 1981), DTIC AD-A109184.
5. W. H. Swindell and S. S. Snell "Station Processor Automatic Signal Detection System: Phase I Final Report," Texas Instruments Report ALEX (01)-FR-77-01 (1979).
6. R. V. Allen, "Automatic Earthquake Recognition and Timing from Single Traces," Bull. Seismol. Soc. Am. 68, 1512-1532 (1978).

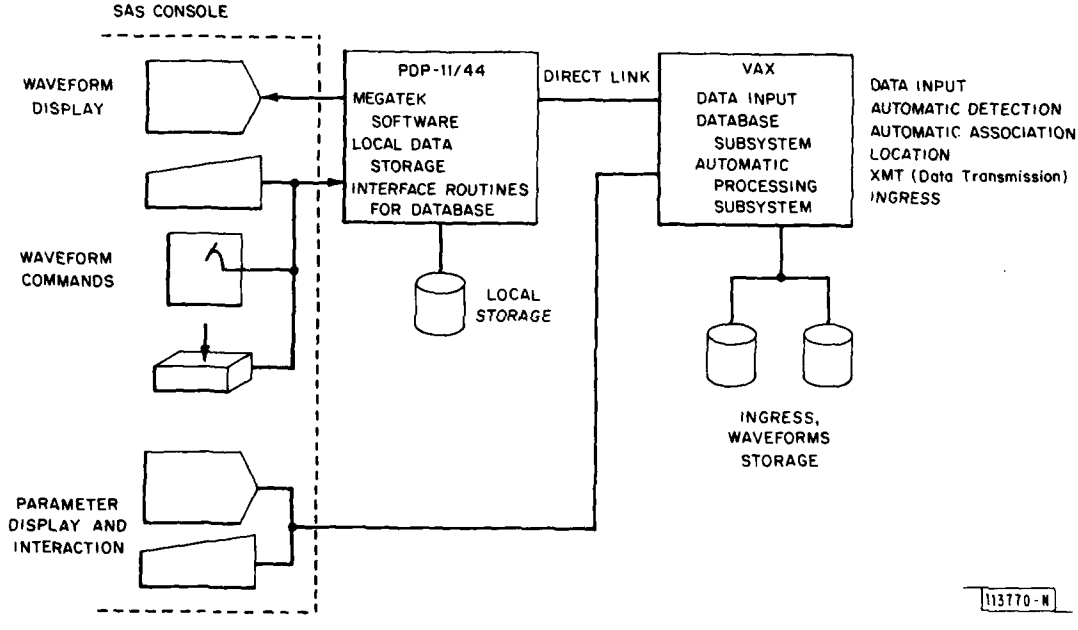

Fig. I-1. Functional configuration of Prototype SDC.

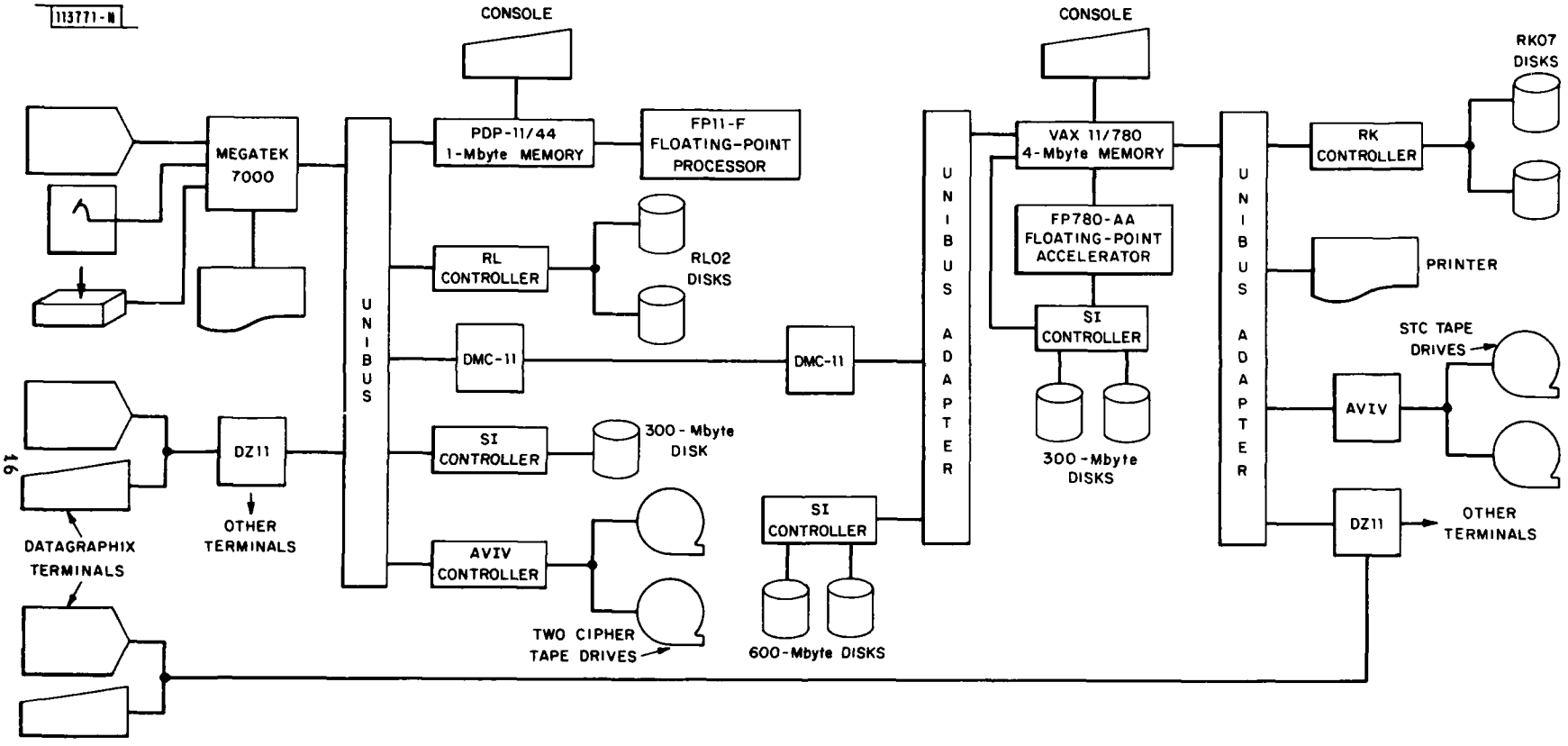

Fig. I-2. Schematic hardware configuration of Prototype SDC.

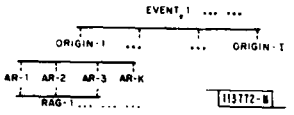

Fig. I-3. Structure of parametric data.

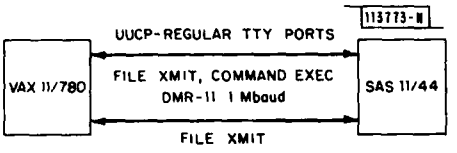

Fig. I-4. Connections between two hosts.

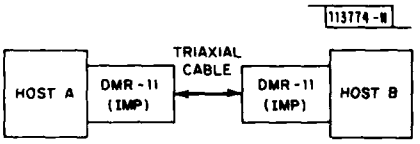

Fig. I-5. 1-Mbaud DMR link.

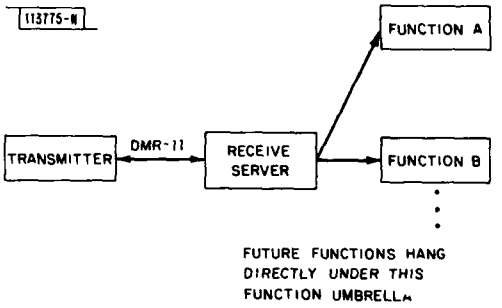

Fig. I-6. EFTP (Easy File Transfer Protocol) receiver and transmitter.

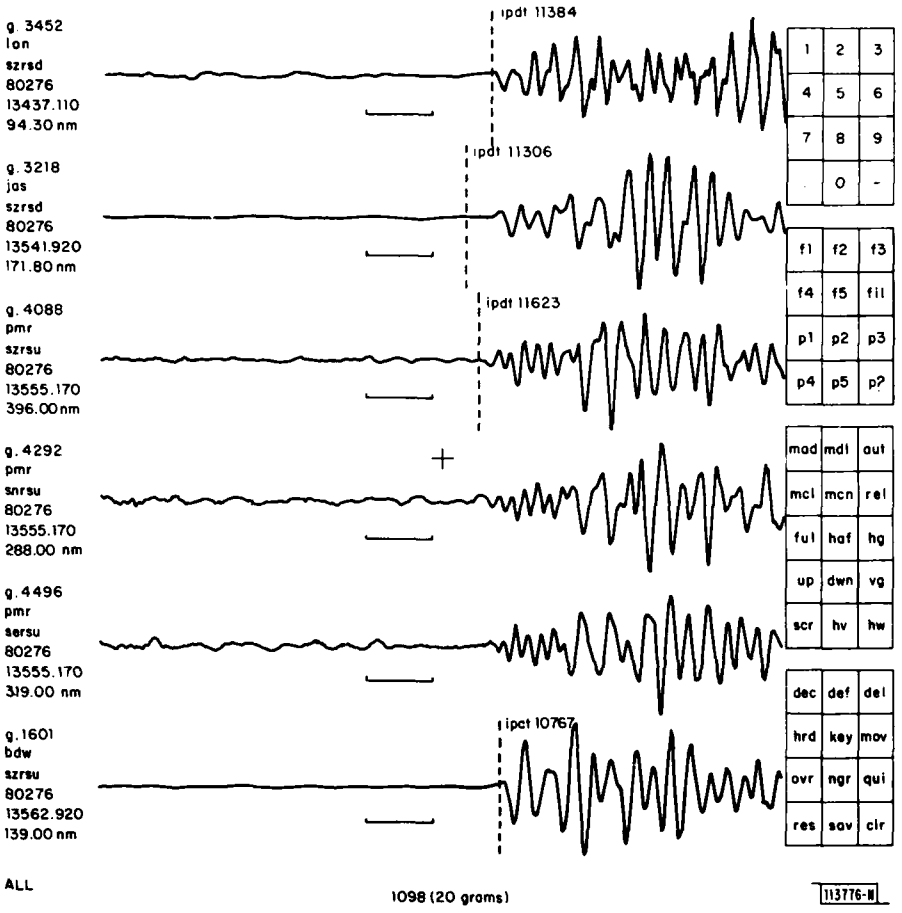

Fig. I-7. Typical display.

II. SEISMIC PROCESSING

A. GLITCH NOISE RECOGNITION USING AUGMENTED TRANSITION NETWORK GRAMMARS

Nonseismic signals such as calibration sequences, isolated glitches, glitch sequences (called buzzes), and boxes commonly cause automatic signal detectors to produce false alarms. Figures II-1 to II-3 show some examples. Thus, part of the design of a good seismic detector must be devoted to designing a glitch noise recognizer. Running median filters[1] can identify narrow isolated glitches, but may miss more complicated noise patterns. Ad hoc post-detection logic is often added to recognize glitches by features such as their duration or one-sidedness. Such tests can be difficult to implement and may not be completely effective.

On the other hand, a simple Augmented Transition Network (ATN) grammar has been designed that effectively recognizes various forms of glitch noise. The grammar can not only significantly reduce the false-alarm rate of a signal detector, but can also produce English descriptions of noise waveforms.

Since ATN grammars have been introduced in a previous SATS,[2] they will be described only briefly here. A waveform grammar is a set of rules that can be used to describe a waveform. For example, consider the calibration sequence shown in Fig. II-1. A grammar rule that describes a calibration sequence might be:

> A positive pulse followed by 60 s of noise followed by a negative pulse.

Additional rules would further describe the three components of the calibration pulse (positive pulse, noise, and negative pulse). The ATN formalism provides a powerful programming language in which grammar rules can be expressed easily.[3]

A glitch recognition system for the station ADK has been designed that operates in five steps:

S1: Detect possible seismic signal

S2: Hysteresis filter of detected waveform

S3: Segment filtered data into words

S4: Apply ATN grammar to words to produce a description of the waveform

S5: Decide if detection is due to glitch noise.

S1:– The seismic detector used has been described in a previous SATS.[2] This detector does well when compared with a human analyst; in fact, it detects weak signals more reliably than an analyst does. Unfortunately, when used on noisy data from ADK, many false alarms are produced. The detector identifies a time interval beginning 60 s before the detection and ending at a time that depends on the characteristics of the signal.

S2:– After the detection stage, the raw data are hysteresis filtered. The output of a hysteresis filter h(i) at time i is:

$$h(0) = x(0) \quad ;$$

$$h(i) = x(i) \quad , \quad |x(i) - x(i-1)| > c \quad ;$$

$$= h(i-1) \quad , \quad \text{otherwise} \quad ;$$

where x(i) is the input time series, and c is a threshold value. Thus, a hysteresis filter returns the value of the input point if it differs significantly from the last point; otherwise, it outputs the previous output. The dotted line in Fig. II-4 shows the effect of hysteresis filtering a calibration pulse. The effect of hysteresis filtering is to pass large variations unchanged while reducing low-amplitude background noise to flat segments separated by short jumps. This compresses the data and simplifies the grammar.

S3:– After hysteresis filtering, the data are divided into segments having either positive, negative, or zero slope by a simple ATN grammar. These segments, represented by their endpoints, are the words used as input to the glitch grammar.

S4:– The glitch grammar was designed on 18 data samples from ADK recorded on 4 October 1980. Only one of these signals was a true seismic signal. Since hysteresis filtering tends to destroy weak seismic signals, no attempt was made to identify true seismic signals. The only requirement was that the glitch grammar passed true signals without declaring any part of them to be glitch noise.

The glitch grammar produces a structural description of the time series.[3] This description can be translated by computer into an English description that is similar to a seismologist's. Such descriptions are used to caption Figs. II-1, II-2, and II-3.

S5:– Based on the description produced by the grammar, each detection was assigned to one of two classes, S or G. The signal was assigned to class G (glitch noise) if a box, glitch, buzz, or calibration pulse occurred within 2 s of the detector onset time; otherwise, the detection was assigned to class S (possible seismic signal).

This detector was applied to 24 h of data recorded at ADK on 2 October 1980; 39 detections occurred. Table II-1 shows a confusion matrix of the results. Over 75 percent of the signals are correctly classified. Since no class S signal was misclassified, the detector is a reliable but conservative glitch recognizer.

TABLE II-1

CLASSIFICATION PRODUCED BY ATN CLASSIFIER

	Assigned Class	
Actual Class	Seismic	Glitch
Seismic	11	0
Glitch	6	22

The six class G signals that were missed were small glitches isolated in background noise that did not occur in the training set. Thus, the grammar is completely effective at recognizing the class of signals it was trained on and can be extended easily to handle this new type of glitch.[3]

Although the class of glitches that the grammar can recognize is quite large, no attempt was made to make it general enough to work at all stations. The reason for this is that it is better to write grammars for individual stations than to try to find a general theory of glitches. A grammar should be thought of as a local expert that uses detailed knowledge to recognize glitches at one station.

K. R. Anderson

B. DYNAMIC WAVEFORM MATCHING

Although the glitch recognition grammar presented above is simple, consisting of only 41 states, other seismic applications can require more complicated grammars. For example, Liu and Fu[4] developed a grammar for distinguishing between earthquake and nuclear-explosion signals that required nearly 800 states. Thus, techniques that help automate the grammar design process are valuable. To this end, the technique of Dynamic Time Warping (DTW) is being investigated.

DTW is a technique used in speech processing to match two signals whose features need not be perfectly time aligned. This technique is used, for example, to match a word utterance to a set of word templates. DTW does a nonlinear time alignment between two patterns based on a least-error criterion. In this way, it compensates for temporal variations between the two patterns due to differences in the way a speaker says the same utterance on different occasions.

We plan to exploit the similarity between DTW and error-correcting parsing.[5,6] Both DTW and parsers match a description of a signal against an input signal. In parsing, the description is in the form of grammar rules. In DTW, the description is in the form of a matching function and a template (another signal).

Although grammatical techniques are more general than DTW, they are harder to develop. Thus, we will use DTW as a tool to understand seismic waveform recognition problems. It is not clear how far DTW will take us before we must use more grammatical methods, but there is a range of methods between these two extremes. For example, a template matcher that uses local constraints on waveform shape behaves like a simple parser.

DTW is promising in several recognition tasks involving the envelopes of local seismic signals:

(1) Template matching of signals with known characteristics against new incoming signals. For example, template matching could be used to identify portions of the signal such as the P-arrival, the S-arrival, and the coda. The interval between the P- and S-arrivals can be used to estimate the distance of the event, and information from the coda can be used to estimate spectral parameters of the earthquake as well as regional variations in attenuation. Some seismic stations receive most of their local earthquake activity from a small number of local source regions, such as quarrys. Template matching could be used to identify signals from these source regions.

(2) Cluster analysis of seismic envelopes to aid in development of template matching techniques and as an initial step in grammatical inference.[4,7]

After a brief introduction to DTW, progress in each of these areas is summarized.

1. Dynamic Time Warping (DTW)

DTW can be described as follows: Given a reference pattern R(n), $1 \leqslant n \leqslant N$, and a test pattern T(m), $1 \leqslant m \leqslant M$, find an optimal mapping from each time axis n and m onto a common time axis k:

$$n = i(k) \quad , \quad k = 1, 2, \ldots, K$$

$$m = j(k) \quad , \quad k = 1, 2, \ldots, K \quad .$$

In general, R(n) and T(n) can be multidimensional feature vectors, but in this study they are scalar quantities representing the signal envelope. The optimal mapping is one that minimizes a total distance function D of the form

$$D = \min_{[i(k), j(k)]} \frac{1}{W} \sum_{k=1}^{K} d\{R[i(k)], T[j(k)]\}\ w(k) \qquad \text{(II-1)}$$

where $d[R(i), T(j)]$ is the local distance between the point i of the reference and point j of the template, w(k) is a local weighting function, and W is a corresponding normalization. Several forms of Eq. (II-1) have been proposed and their performance in word-recognition problems has been studied by Myers.[8]

It is convenient to think of minimizing Eq. (II-1) in terms of finding an optimum path $[i(k), j(k)]$ in (n, m) space as shown in Fig. II-5. To solve Eq. (II-1) as a path finding problem, one must specify several things:

(a) Endpoint constraints – the way that the path begins and ends

(b) Local continuity constraints – constraints on motion from one point to another

(c) Global path constraints – limitations on where the path can wander in (n, m) space

(d) Range constraints – the maximum separation between i(k) and j(k) in a valid match

(e) Axis orientation – the effects of interchanging the roles between the test and reference

(f) Distance measures – both the local measure of similarity and the overall distance function used to determine the optimal path.

Myers discusses each of these factors and evaluates the performance of several combinations of them. We have investigated several of these alternatives for seismic envelope matching and have found that his type II-d matching function[8] works reasonably well.

The solution to Eq. (II-1) can be written as

$$D = \frac{D_a(N, M)}{W} \qquad \text{(II-2)}$$

where D_a is called an accumulated distance function, which for the case considered here is recursively defined as

$$D_a(n, m) = \min \begin{bmatrix} D_a(n-1, m-1) + 2d(n, m) \\ D_a(n-1, m-2) + 3d(n, m) \\ D_a(n-2, m-1) + 3d(n, m) \end{bmatrix}$$

with the initial condition

$$D_a(1, 1) = d(1, 1) \quad .$$

This type of recursive solution to Eq. (II-1) is known as Dynamic Programming.[9]

2. Waveform Matching

Figure II-6 shows an example of the DTW of the envelopes of two local seismograms. The envelope is constructed by computing nonoverlapping 3-s block averages of the rectified waveforms. This averaging smooths out high-frequency fluctuations in the envelope but provides enough detail for this application. Before matching, the envelopes are normalized by their maximum amplitude. The local matching function used is:

$$d[R(i), T(j)] = |R(i) - T(j)| \quad .$$

In other words, the waveforms are aligned based on the area under their normalized envelopes.

Dotted lines in the figure are drawn between a point in each waveform that corresponds in the match. Note that the onsets of the P- and S-arrivals have been matched.

Figure II-7 shows the match between two waveforms that are not so similar. The lower envelope has a much broader P-arrival than the top and no correspondence is found. Also, the correspondence between the S-arrivals is not very good due to the difference in their shape. Thus, time warping might be used to identify P- and S-arrivals by matching an unknown envelope against a set of templates and measuring the P-S interval from the best match, but care must be taken in choosing the set of templates.

3. Waveform Clustering

Figure II-8 shows how DTW can be used to cluster waveforms. The right part of the diagram shows the envelopes of eight local seismograms from station BDW. In the left part of the figure, a dendrogram is used to show the hierarchical clustering of the waveforms.[10] A dendrogram is a tree that shows the hierarchical clustering of a set of samples (in this case, waveforms). The leaf nodes of the tree are the waveforms themselves. Two nodes are merged into one at a level indicating their dissimilarity. For example, the dendrogram shows that:

(a) Waveforms 1 and 2 are most similar, followed by 5 and 6.

(b) Waveforms 1 through 4 are relatively similar to each other, as are waveforms 5 through 7.

(c) Waveform 8 is most unlike the other waveforms.

This clustering is similar to how a seismologist would cluster these waveforms.

The next step in the research is to cluster a large number of waveforms from several stations. These clusters will be used as templates in the design of a template matcher and as sentences in the design of waveform grammars.

K. R. Anderson
J. E. Gaby

C. WAVEFORM SEGMENTATION USING AFFINITY

The first step in syntactic waveform analysis is to divide the waveform into segments of morphological significance called words. This sequence of words should be a simplified representation of the waveform, but must have enough information to extract features of interest. The "affinity" technique[11] that has been used for region growing in scene analysis is being used to produce word sequences from the envelopes of local and regional seismograms.

Affinity is a general technique that organizes data into a binary tree structure. It groups together regions based on their relative similarity. Two similar regions are merged together to form one region at a higher node in the tree. The new node is an abstracted representation of the two regions below it.

There are several reasons why affinity is an attractive approach. First, the similarity criterion is relative, no thresholds need be set; the waveform essentially segments itself. Second, it preserves the information content of the signal. To acquire more detailed information about the signal, one need only go deeper down the tree. Although the leaves of the tree could be the individual data points themselves, it is more efficient to cut the tree off at a level that provides adequate resolution. Third, the tree is a flexible data structure that allows the waveform to be divided into word sequences in several ways. Fourth, a grammar may parse a particular sequence of words derived from a certain level in the tree. Information at lower levels in the tree can then be used to refine or verify the parse or extract useful features.

1. Introduction to Affinity

The affinity algorithm compares a segment of a waveform with its adjacent neighbors. Segments, whose descriptions closely match, are then merged together to form a new segment that is representative of the two similar segments. The i^{th} segment is described by the feature vector x(i), chosen for the particular application.

Affinity compares one segment x(i) to its adjoining neighbors x(i − 1) and x(i + 1). A distance function F determines if x(i) is more similar to x(i − 1) or x(i + 1). If $||F[x(i), x(i-1)]|| < ||F[x(i), x(i+1)]||$, segment i is linked to segment i − 1; otherwise, it is linked to i + 1. This is done for all i. Two segments (a and b) are merged if and only if segment a is linked to b and segment b is linked to a. A merge function M[a, b] takes two segments and merges them into one segment.

The tree structure is developed from a signal by successive applications of linking segments of a waveform and merging linked segments. Segments are first linked to their appropriate neighbor. Then these linked segments are merged. This forms a new, shorter sequence of segments that represents the same waveform. This process is repeated until the entire waveform has been merged into one segment whose set of features represents the waveform as a whole.

The one final segment represents the top node of the tree. It branches down to two segments that were merged to form the top node. Likewise, the two branches are nodes that branch again, in a binary fashion. Each node is a generalized representation of the node below. As you go down the tree structure, there is more detailed information about the sequence of segments that represents the signal.

2. Application of Affinity to Seismic Waveforms

To apply affinity one must determine the initial length of a segment, the feature vector that describes each segment, and the functions F and M. This decision is based on the nature of the waveform, the nature of the features to be ultimately extracted, and the resolution required.

The goal of this research is to automatically extract information from regional seismograms, such as the S-P interval. Since we are initially interested in S-P intervals larger than 5 s, a 1-s initial segment size (20 samples) provides adequate time resolution.

In this study three features were analyzed: the average magnitude (absolute amplitude), the average zero-crossing rate, and the slope between two segments. These features could be combined in different ways, but they were analyzed separately. Each of these features uses different linking and merging functions.

Affinity based on average magnitude is used because the envelope contains visual cues for the P and S onset times. Each segment is represented by three parameters – its length, its average magnitude, and the time of the middle of the segment, L(i), A(i), and T(i), respectively. The distance function F is the difference in the magnitude values between a segment and its two neighbors weighted by the segment lengths:

$$F[x(a), x(b)] = \frac{A(a)L(a) - A(b)L(b)}{L(a) + L(b)} \quad .$$

Merging two segments is accomplished by producing a new length, magnitude, and time to describe the new segment. The new length is the sum of the two lengths of the segments being merged. The new magnitude is the weighted sum of the average magnitudes of the two segments being merged. The new time is simply the center of the new segment:

$$A(new) = \frac{A(a)L(a) + A(b)L(b)}{L(a) + L(b)}$$

$$L(new) = L(a) + L(b)$$

$$T(new) = \frac{T(a) - L(a)/2 + T(b) + L(b)/2}{2} \quad .$$

Affinity based on the average number of zero crossings is similar to the average magnitude version. The only difference is that A(i) is replaced by Z(i), the average zero-crossing rate in that interval. The zero-crossing rate is a rough measure of the frequency content of the signal. It can be useful in identifying weak arrivals buried in noise, because a sudden change in the zero-crossing rate may be the only evidence for a weak arrival.

Affinity based on slope requires a different set of parameters to describe a segment. Here, the slope between the average magnitude of two segments, of the initial 1-s segmentation, is used as the feature. Each slope segment is represented by four numbers [x1(i), y1(i), x2(i), and y2(i)] where the x's are the time index and the y's are the average amplitude. The information in each segment is duplicated in the following segment. That is to say, x2(i) = x1(i + 1) and y2(i) = y1(i + 1). Because of this overlap, the information content of this initial sequence is similar to that of the average magnitude affinity.

Slope affinity compares the slopes of adjacent segments and links to the segment with the minimum change of slope. The segment is replaced by a new segment with the new start point the same as the x-y coordinates of the start point of the first segment, and the endpoint the same x-y coordinates of the endpoint of the second segment. The distance function F[a, b] is

$$F[x(a), x(b)] = y1(a)\,\frac{x2(a) - x2(b)}{x2(b) - x1(a)} + y2(a) + y2(b)\,\frac{x1(a) - x2(a)}{x2(b) - x1(a)}$$

and the parameters of a new merged segment are

$$x1(new) = x1(a)$$
$$y1(new) = y1(a)$$
$$x2(new) = x2(b)$$
$$y2(new) = y2(b)$$

3. Results

Of the three implementations studied (average magnitude, slope, and zero-crossing rate), the first two yielded good results. The zero-crossing density affinity creates word sequences that can be either misleading or show no significant information. It provides some information when the P-arrival is buried in the noise level, but it is not always reliable. A nonlinear F function that uses magnitude when the signal was strong and frequency when the signal was weak (much as a seismologist does), might provide better segmentations.

Affinity based on average magnitude produces more meaningful segmentations. Figure II-9 shows the tree structure that resulted from the application of affinity on one waveform. In this figure, and in all others, the initial segmentation is based on 3 s of the waveform and not 1 s, as used in the study. This makes the results easier to see, as the 1-s data are highly detailed and confusing. Regions with a high degree of similarity are correctly merged to form larger segments. Figure II-10(a-c) shows three different sequences of words derived from different levels in the tree. The dotted lines are the original sequences given to the affinity routine. The bold lines are the sequences of segments at different levels in the tree, the zeroth level being the top node of the tree. The two major peaks are the P- and S-waves. Word sequences produced from levels 5 and 7 show the arrival onsets clearly without showing too much detail in the coda. Thus, they provide reasonable segmentations.

Figure II-11 shows the tree produced by the slope affinity algorithm. The trees shown in this figure and in Fig. II-9 are generally similar. Figure II-12(a-c) shows different potential word sequences derived from different depths of the tree. In this segmentation, peaks stand out immediately. Both magnitude affinity and slope affinity reduce the waveform's complexity and maintain information necessary for the recognition process.

Figure II-13(a-d) shows a second method of producing word sequences from a tree. Here the word sequences are produced using a maximum length word rather than a fixed depth in the tree. In (a) and (b), all word segments are either less than 18 s in duration or are a leaf node of the tree. In (c) and (d), the length is 12 s or less. This shows how flexible the tree structure is in providing different word segmentations.

The affinity algorithm has some drawbacks. The merging does not consider the relative nature of merging things very similar and those somewhat similar at the same time. In other words, the branches of the tree all have the same relative length. This problem can be corrected by not only specifying nodes and branches, but also the relative lengths of the branches. Figure II-14(a-c) illustrates a second problem. The P-wave onset is just visible as a step before the predominate peak S-wave. The representation of the noise before the P-arrival is more detailed at a given level in the tree than the noise after the signal. This is because the length of the noise before the signal is less than the noise after, and thus requires a shallower subtree to represent it.

4. Conclusion

Studying the morphological structure of seismic signals is greatly aided by the affinity algorithm. Affinity based on average magnitude or slope yields promising results. In both cases, the waveform is broken into sections that reveal the information required to determine the P-S time interval while removing unnecessary detail.

Affinity is also useful for analyzing the waveform's structure. Structuring the data in a tree format allows the waveform to be looked at from different points of view. The tree itself could be the structure given to the grammar to analyze. The grammar could be smart enough to use the tree, with all the diversity, to break the waveform up as it needs to recognize what it wants.

J. E. Gaby
K. R. Anderson

D. AUTOMATIC ASSOCIATION USING EXPERT SYSTEMS TECHNIQUES

An automatic association (AA) program aids seismologists in associating arrivals with earthquakes. Although several AA programs have been developed,[12,13] there are still many issues that need to be worked on, among which are:

(1) AA programs can correctly associate about 70 to 80 percent of the information available to them. Can this success rate be improved?

(2) False events can be created by splitting one event into several smaller ones, or merging arrivals from two events into one. How can this be avoided?

(3) Many events created by these algorithms are based on only a few arrivals. Is there any way to estimate the probability that these events really occurred?

(4) What is the best way for an analyst to interact with the AA program?

AX, an Expert System to aid seismologists in the association problem, is under development. It is designed as a research environment that can be used to resolve these issues. AX differs from other association programs because it is based on a rule driven system capable of using knowledge about the association problem in much the same way a seismologist would. Since Expert Systems ideas are new to seismology, this report serves as an introduction to Expert Systems and as a progress report on AX.

Expert Systems is a branch of Computer Science research that studies ways to represent human expertise in computer systems. In the past few years, several Expert Systems have been developed as can be seen in Table II-2.[14-17] Although Expert Systems usually do better than an average person, they may not work as well as a true expert. PROSPECTOR works well enough that it can be used as a training tool for new human mineral prospecting experts, and even teaches established experts something new.

Two basic problems in building an Expert System are how to organize and represent knowledge and how to discover the rules required to manipulate that knowledge in the particular cognitive task. The appropriate knowledge is usually uncovered by protocol analysis. This involves observing a human expert, such as a seismic analyst, doing a task and having him explain as completely as possible his decisions and the reasoning behind them.

TABLE II-2
EXPERT SYSTEMS STUDIES

Program	Domain	Reference
MYCIN	Medical diagnosis	14
PROSPECTOR	Mineral prospecting	15
DIPMETER ADVISOR	Oil-well logging	16
DENDRAL	Chemical analysis	17

There has been one protocol session with a seismic analyst using an interactive association system at SDAC. A detailed log of his interaction with the system was kept as he associated arrivals for several events. To give some idea of the work involved in associating an event, the analyst went through over 50 different steps during the association of a medium-size event. Additional protocol sessions will be necessary during the development of AX. One advantage of the Expert Systems approach is that AX can be developed incrementally based on these protocol sessions.

Once the knowledge used by an analyst is available, it must be represented in the computer. Of course, any program that solves a problem can be said to embody knowledge of a domain. The distinguishing characteristic of an Expert System is that much of its knowledge about the task domain is stored explicitly in a database.[18] AX uses three Expert Systems programming techniques to represent knowledge:

(1) FRL, a knowledge representation language
(2) Sentinels
(3) Rules.

Each of these techniques will be described in turn.

1. Frame Representation Language (FRL)

The FRL is a package of LISP functions for manipulating data structures known as frames.[19,20] Originally motivated by Minsky,[21] frames have several features that make them convenient for knowledge representation. The objects used by AX are represented as frames in the frame database. This includes seismological objects such as events and arrivals, and also the sentinels and rules that manipulate them.

A frame is a 5-level tree structure with the following names assigned to each level:

```
FRAME
    SLOT
        FACET
            DATUM
                COMMENT
```

Each frame can contain several slots, each slot can contain several facets, and so on for each level.

Frames are used to represent objects, slots are used to represent the attributes of objects, and the datum on the value facet of a slot represents the value of the attribute. For example, an

arrival called ARRIVAL-15 that is a PKP arrival from station ZOBO occurring at time 1234.56 and belonging to a related arrival group called RAG-12 would be represented as:

FRAME
arrival-15

SLOT	FACET	DATUM
AKO	value	arrival
time	value	1234.56
phase	value	pkp
station	value	zobo
rag	value	rag-12

The value of a slot can be another frame, such as ARRIVAL, PKP, ZOBO, and RAG-12 here. The AKO (A Kind Of) slot shows that ARRIVAL-15 is a kind of ARRIVAL. The ARRIVAL frame looks something like this:

FRAME
arrival

SLOT	FACET	DATUM
AKO	value	thing
time		
phase	required	(valid-phase :value)
station	required	(valid-station :value)
amplitude		
rag		
slowness		
azimuth		
to-db	value	(to-db-arrival :frame)

Most slots have their obvious seismological meaning. The TO-DB slot describes how information in an arrival frame is to be communicated to the parameter database. The AKO slot allows frames to be organized into an inheritance hierarchy. Properties of a frame are inherited from frames higher in the inheritance tree. The THING frame is at the top of the inheritance hierarchy. Thus, an ARRIVAL is a kind of THING, and ARRIVAL-15 is a kind of ARRIVAL.

In addition to the value facet, FRL has several facets that work in combination with it:

DEFAULT	A default value, to be used if no value is available.
IF-ADDED	A procedure executed if a value is added to a slot.
IF-REMOVED	A procedure executed if a value is removed from a slot.
IF-NEEDED	A procedure executed if a value is needed but unavailable.
REQUIRED	A check on the validity of a value added to a slot.

Such procedures work with the inheritance hierarchy to keep the frame database consistent, and make deductions. For example, when ARRIVAL-15 was created, checks, inherited from the ARRIVAL frame, were made to insure that the phase and station name were valid.

The frames representing seismic parameters have an inheritance hierarchy as shown in Fig. II-15. The EVENT, RAG, ARRIVAL, and STATION frames have their obvious seismic interpretation. H-ARRIVALS are hypothetical arrivals created by AX in an attempt to correct common arrival errors. They will be described further below.

Seismic waves are divided into their own inheritance hierarchy below the WAVE frame as shown in Fig. II-16.

2. Sentinels

A sentinel[22] is a procedure that waits for a triggering condition to occur in the database, and then does some action. Sentinels may vanish after they complete their action, or remain indefinitely. For example, the following sentinel propagates information about the distance range of an arrival to its related arrival group:

WHENEVER:
An arrival has a range estimate and is assigned to a rag.

ACTION:
Assign its range estimate to the rag.

Sentinels can create other sentinels or groups of sentinels. For example:

WHENEVER:
A rag comes from a station that has neighboring stations.

ACTION:
Create an event hypothesis and create sentinels that add incoming rags from neighboring stations to the event. After all arrivals that could be associated with the event have been read in, remove all the sentinels.

Thus, with sentinels one can create expectations of what should happen to the database in the future, based on its current state of knowledge.

3. Rules

Typically, programs are specified in terms of if – then – else decision trees. Rather than representing its control structure explicitly, AX represents much of its control structure in terms of rules. A rule is a chunk of knowledge (frame) that has two parts – a condition and an action. If the rule's condition is true, then its action can be executed. For example, the following rule suggests when a P-arrival might really be a Pg-arrival.

RULE-1
CONDITION:
A P arrival is less than 1° from an event

ACTION:
Hypothesize that its phase should be Pg.

In carrying out the action part of a rule, other rules may be executed. More than one rule may have its condition satisfied at any one time, and the order in which rules are executed is controlled by a rule interpreter. Related sets of rules may be organized into rule-domains that compartmentalize knowledge about different aspects of the problem. Each rule-domain can have its own rule format and its own style of rule interpreter.

The advantage of using rules, rather than explicit control structures, in complicated systems is that rules are modular and relatively independent.[23] Additional capability can be added by adding new rules to the appropriate rule-domains, with little regard for what the rest of the system does.

AX currently has about 20 rules for organizing incoming arrival and event information and hypothesizing and verifying events. About 30 other rules have been designed for reasoning about related arrival groups, hypothetical arrivals, and arrival-time residuals. To give an idea of how a rule-based approach works, the following section discusses reasoning about residuals.

4. Reasoning About Residuals

During the association process, arrival residuals provide evidence for the existence of events and for deciding which arrivals belong to which events. A fair amount of seismological knowledge must be used to reason about residuals. Although theoretical travel-time curves are available for only certain distance and depth ranges, arrivals are observed outside these ranges. Seismic knowledge must be used to decide if a travel-time curve can be extended. Also, arrivals have both arrival-time errors and phase-identification errors that can often be identified by seismologists. As an example of how AX might accomplish similar reasoning, consider the following situation: there is an event and a P-arrival from a station that could be associated with the event, but it is beyond the distance range for which P can be computed. There are several possibilities to consider:

(a) The event has not been located well enough.
(b) The arrival could belong to another event.
(c) The arrival could really be a PKP or a diffracted P (PDIF) arrival.
(d) The arrival time could be wrong.

The following set of rules could be used to consider whether the arrival could be PDIF or not:

RULE-2

CONDITION:
1) Phase of arrival is P, and
2) arrival doesn't match event, and
3) arrival could be PDIF from event, and
4) the event is large

ACTION:
Hypothesize phase of arrival is PDIF.

RULE-3

CONDITION:
Magnitude of event is > 5.5

ACTION:
Event is large.

RULE-4

CONDITION:
1) Event has arrivals from more than 15 stations, and
2) At least 2 of these stations are at least 50 degrees away

ACTION:
Event is large.

RULE-5

CONDITION:
1) Distance of station of arrivals to event is in PDIF range, and
2) Travel time matches PDIF

ACTION:
Arrival could be PDIF from event.

These rules form the structure as shown in Fig. II-17.

The first rule, RULE-2, states the conditions necessary to hypothesize that a P-arrival is really a PDIF. The other rules show how the subgoals of RULE-2 can be accomplished. RULE-2 uses more than just the size of the residual to decide if the arrival could be PDIF, it also checks that the event is large enough to make observing a PDIF likely. There are two ways to decide if the event is large enough. This allows the rule to work even if there are no amplitude data for the event.

Once we have hypothesized that the arrival is PDIF, we must still verify that this is true, which is not easy since we have not ruled out the other possibilities mentioned above. This is handled by creating a hypothetical arrival frame for this hypothesis:

FRAME
h-arrival-32

SLOT	FACET	DATUM	COMMENT
AKO	value	arrival-16	
phase	value	pdif	(:why reason-52)
	previous	p	

The hypothesis derives most of its information from the arrival it was derived from. The phase slot is tagged with a comment that contains the name of a frame describing the reasoning behind the hypothesis.

Once a hypothetical arrival is created, it is treated by the rest of the system as a normal arrival. Both the original and the hypothetical arrivals exist together, each treated independently by the system. The correct decision is made during the final event verification stage. Several rules are used to decide which arrival is correct. If the system can't decide, an analyst is asked to make the decision. It could even explain the reasoning behind the hypothesis.

This type of reasoning goes well beyond existing AA programs. They either make no adjustments to phase identification, in which case the arrival may remain unassociated forever, or they make adjustments based only on residuals from one event. Nothing is done to verify the adjustment.

K. R. Anderson
S. T. Rosenberg
D. Lanan

E. AN ENTROPY SCRAMBLED HASH FUNCTION

Hash functions that require only one probe per lookup and a minimum-sized table are called minimum perfect hash functions.[24,25] Although minimum perfect hash functions can be designed, they require a static set of keys, and only work for small sets. Thus, their application is limited.

This report describes a new method of computing a hash function from a subset of keys that produces evenly distributed hash addresses based on the entropy of individual bit positions of the keys. Although the method does not produce a perfect hash function, primary clustering is significantly reduced. Thus it can improve any hashing method, and it is attractive for retrieval from secondary storage.

1. Entropy

As the concept of entropy[26] is important in the analysis of the hash functions presented here, it will be briefly described. Entropy is a measure of information content. Suppose we had a source X of discrete messages x_i ($i = 1, \ldots, N$), each with an independent probability of occurring $p(x_i)$. Then, the entropy of the information source X is:

$$H = -\sum_{i=1}^{N} p(x_i) \log_2[p(x_i)] \quad \text{bits} \quad .$$

This is the average number of bits per message needed to encode the messages from X.

Entropy can also be thought of as a measure of the shape of the function p(x). The more uniformly distributed p(x) is, the higher the entropy.

For example, if X produces only two messages, 0 (with probability p_0) and 1 (with probability $p_1 = 1 - p_0$), then the entropy is:

$$H = -p_0 \log_2(p_0) - (1 - p_0) \log_2(1 - p_0) \quad . \tag{II-3}$$

When p_0 is very different from p_1, then H is near zero. When p_0 is approximately equal to p_1, then H is near its maximum value of 1.

Entropy can be used in several ways to measure the performance of hash functions. For example, given a hash function h(k) that returns an address in a table given a key k, its address entropy H_a is given by

$$H_a = -\sum_{k} p[h(k)] \log_2\{p[h(k)]\}$$

where p[h(k)] is the fraction of the keys that hash into address h(k). A perfect hash function would distribute its keys uniformly with one key per address. Then, p[h(k)] = 1/K, where K is the number of keys, and

$$H_a = \sum_{k} \frac{1}{K} \log_2(1/K) = \log_2(K) \quad .$$

If a hash function extracts less than $\log_2(K)$ bits of information from the keys, then it will not be able to distinguish between certain keys, and some keys will have the same initial hash address.

2. Hash Functions

As our attention focuses on the initial hash address, and not on methods of resolving collisions, a simple hashing algorithm is considered. It is similar to algorithm L of Knuth[27] and looks something like this when written in C (see Ref. 28):

```
search(k, keys)
{
    for(i = h(k); keys[i] != EMPTY; i = i + 1)
       if (keys[i] == k) return(i);
    return(FAIL);
}
```

Given a key k and a table of keys, keys[] , search(k, keys) returns the address in the table with a key corresponding to k. The hash function h(k) returns an address in the table given a key. The algorithm searches consecutive table elements starting at the hash address. A similar algorithm can be used to insert elements into the table. Although this method is effected by primary

clustering, it is convenient for searching secondary storage. However, to make this method effective, h(k) must be designed to minimize primary clustering.

To see the effect of primary clustering, consider a commonly used hash function that treats the key as an integer and uses it as the table address modulo the table size[27]:

```
H1(k)
{
    return(k%TABLESIZE);
}
```

The first line of Table II-3 summarizes the results of retrieving the 3553 seismic station codes from a table of size 8191 using the search method described above. The address entropy of H1 is relatively high since the maximum is $\log_2(3553) = 11.79$. However, H1 is strongly affected by primary clustering. Although the table is only 43-percent full, on the average it takes over 10 comparisons to find a match, and in the worst case 427 comparisons are made. This is significantly worse than the number of comparisons predicted theoretically by Knuth,[27] which is 1.37. He shows that given the fraction of the table that is full A, the number of comparisons in a successful search C is:

$$C = \frac{1 + [1/(1 - A)]}{2} \quad . \tag{II-4}$$

The theory assumes that the hash function distributes the keys evenly over the table. Clearly, this is not true here.

TABLE II-3
COMPARISON OF HASH FUNCTIONS

Method	Table Size	Unique Addresses	Address Entropy	No. Comparisons	
				Average	Worst Case
H1	8191	2617	11.23	10.49	427
H2	8192	2346	11.03	2.17	47
H3	8191	2766	11.32	1.65	27
H4	8191	2918	11.42	1.35	10
H4	4093	2359	11.04	3.61	112

This can be avoided by using the entropy of the individual bits of the keys to produce a more even distribution of hash addresses. The bit entropy H_i gives the amount of information gained about a key by knowing its i^{th} bit. It can be determined from Eq. (II-3) where p_0 is the percentage of the keys with that bit set to zero. Table II-4 shows the bit entropies for the bit positions in the 4-byte station codes. Figure II-18 shows the same information in histogram form. From Table II-4 and Fig. II-18, several things can be observed:

(a) Several bits provide no information about the keys. Since the ASCII character code is used, bit 7 of each character is always 0. Also, since the first two characters of the codes are always capital letters, their sixth bit is always 1.

TABLE II-4

BIT ENTROPIES FOR EACH BIT OF THE 4-BYTE STATION CODES

	Byte	Bit	P_0	Bit Entropy
1	2	2	0.4903	0.9997
2	1	2	0.5156	0.9993
3	0	1	0.4821	0.9991
4	1	1	0.5325	0.9969
5	1	0	0.4675	0.9969
6	2	1	0.5364	0.9962
7	0	2	0.5463	0.9938
8	0	0	0.4489	0.9925
9	2	3	0.5640	0.9881
10	2	0	0.4264	0.9843
11	1	3	0.6116	0.9638
12	2	4	0.6276	0.9525
13	1	4	0.6569	0.9277
14	0	3	0.6569	0.9277
15	0	4	0.6693	0.9156
16	2	6	0.1711	0.6603
17	2	5	0.8289	0.6603
18	3	0	0.9848	0.1136
19	1	6	0.9865	0.1033
20	1	5	0.0135	0.1033
21	3	1	0.9879	0.0944
22	3	6	0.9882	0.0926
23	3	5	0.0118	0.0926
24	3	3	0.9893	0.0854
25	3	2	0.9899	0.0817
26	3	4	0.9910	0.0741
27	0	6	0.0000	0.0000
28	1	6	0.0000	0.0000
29	0	7	1.0000	0.0000
30	1	7	1.0000	0.0000
31	2	7	1.0000	0.0000
32	3	7	1.0000	0.0000

(b) Most of the information about the keys comes from the low-order 3 or 4 bits of the first three characters.

(c) Almost no information is contained in the fourth character. This is because many of the codes are only three letters long.

This suggests that a reasonable hash function could be made by taking only the first 13 bits of Table II-4:

```
H2(k)
{
    h = 0;
    for (i = 1; i <= 13; i = i + 1)
       h = h <<1 | bit(i, k);
    return(h);
}
```

where bit(i, k) returns the bit of the key k mentioned in the i^{th} line of Table II-4. The effect of the for-loop is to rearrange the bits of the key so that the bits with the highest bit entropy appear at the high-order end of the key. The resulting scrambled keys are more evenly distributed over the address space than are the original keys.

The results of this hash function are summarized in the second line of Table II-3. The address entropy is not as good as that of hash function H1, because only 13 bits of information are used to compute the hash function. These 13 bits contain only 11.025 bits of independent information about the keys. On the other hand, the primary clustering has been significantly reduced.

An obvious improvement can be made to the hash function by using all the bits of a key that have any information about the keys, but scrambled by their bit entropy:

```
H3(k)
{
    h = 0;
    for (i = 1; i <= 26; i = i + 1)
       h = h << 1 | bit(i, k);
    return(h%TABLESIZE);
}
```

The corresponding line in Table II-3 shows that we get more than 5-percent increase in the number of unique addresses over H1 and a corresponding increase in the address entropy. The average number of comparisons and the worst-case number of comparisons have been significantly reduced.

A final improvement provides an 11-percent improvement, over H1, in the number of unique hash addresses, and an average number of comparisons that agrees well with Eq. (II-4):

```
H4(k)
{
    h = 0;
    right = 1.0;
    left = 0.0;

    for (i = 0; i <= 26; i = i + 1) {
       b = bit(i, k);
       if (b == 0) right = left + (right-left)*p0[i];
       else        left = left + (right - left)*(1.0 - p0[i]);
    }
    h = (left+right)*0.5*67108864;
    return(h%TABLESIZE);
}
```

where p0[i] is the probability that bit i is zero, taken from Table II-4, and 67108864 is 2^{26}. Hash function H4 is similar to a binary search. The position of the key in the table is bounded by LEFT and RIGHT. If p0[i] was allowed to be a function of the other bits in the key, a binary search would result and a unique hash address would be found for every key. However, this would replace a hash search with a binary search.

The last line of Table II-3 shows the effect of reducing the table size in half on hash function H4. The total number of unique addresses is still 80 percent of the value of the larger table, and the average number of comparisons agrees well with that predicted by Eq. (II-4). Even with over 80 percent of the table full, its performance is almost three times better than hash function H1.

In conclusion, the entropy concept provides several measures of hash function performance. Using bit entropy to scramble the bits can provide hash functions that have well-distributed hash addresses. The method is not limited to static sets. Usually, the application can provide some information about how to scramble the bits. For example, for most programming applications, ordering the bits so that the low-order bits of each character appear in the high-order bits of the scrambled key should be better than an unscrambled hash function such as H1.

K. R. Anderson
K. A. Huber

F. THREE-COMPONENT POWER-DETECTION STUDY

Three-component power detection has been tested on 24 h of data from seven stations. Data used in the study were from 2 October 1980, which was the second day of the IESD experiment. The detector used was our in-house Z-statistic detector which has been described in detail in the previous SATS.[2] Information pertaining to the stations is presented in Table II-5.

TABLE II-5
DATA AVAILABLE FOR THIS STUDY

Code	Type	Location	Outages
ANMO	SRO	Albuquerque, New Mexico	Negligible
BCAO	SRO	Bangui, Central African Republic	12.5 h starting at 6:00
BOCO	SRO	Bogota, Colombia	Various small dropouts
CPO	RSTN	Cumberland Plateau, Tennessee	Negligible
HN-	SDCS	Houlton, Maine	1 h starting 15:00
PI-	SDCS	Pinedale, Wyoming	Various small dropouts
PMR	USSN	Palmer, Alaska	Various small dropouts

Analyst picks from different sources were available for the data. Some of the analysts reported only teleseismic arrivals; others reported everything. Most of the picking was done on analog records. No records were available for PI-, so the picks from nearby BDW were used; also, no picks for HN- were available, so 23 h of digital data were picked by hand. Our AA algorithm produced 23 preliminary events which, in turn, were used to generate potential arrival times

at the stations. Analyst picks, along with potential arrival times generated from our PEL, provided a means to test the detector. Detection logs from the three components were merged and tested against the Z-component alone. Table II-6 shows the results.

TABLE II-6
EXPERIMENTAL RESULTS

Station	Z Dets	Extra H Dets	Analyst Picks	Z Det Picks	3 Det Picks	PEL Assc	Z Det Assc	3 Det Assc
ANMO	24	9	42	31	33	23	7	9
BCAO	10	11	11	6	6	23	5	6
BOCO	5	11	6	3	5	23	1	1
CPO	83	35	2	1	1	23	6	7
HN-	5	10	7	6	6	23	2	3
PI-	51	28	81	55	58	23	13	13
PMR	58	35	35	34	35	23	7	7

The second column (Z Dets) in Table II-6 is the number of times the detector triggered on the Z-component; the third column is the number of unique arrivals added by the horizontals. Clearly, adding H-components can increase the total number of arrivals anywhere from 37 to 200 percent. Column 4 contains the number of analyst picks, while column 5 contains the number of those picks that were within the detector on and off times on the Z-component. The sixth column contains similar information for all three components. At three of the stations, adding horizontals made no difference as far as the number of analyst picks detected; at the other four, the difference varied from one more detected at PMR to three more detected at PI-. Column 7 shows the number of potential arrivals generated from the PEL. The number of associated arrivals detected on the Z-component are shown in the eighth column, while the ninth column shows the corresponding information for all three components. Adding the detections from the horizontals increased the number of associated arrivals detected at four of the stations.

Certainly 3-component detection seems to provide us with more significant arrivals, but unfortunately there is also a three-fold increase in false alarms. One would expect this from a Gaussian distributed detection statistic (log of the average power). Figure II-19 shows the distribution of the Z-statistic (0 mean, S.D. = 1).

Figure II-20(a-c) shows some unassociated arrivals that were only detected on the H-components. Figure II-20(a) shows a short-period Love wave.

Figures II-21 to II-23 show the associated waveforms for three events which had some associations made from H-component detections. Figure II-21(a-b) shows event 1108, which is a split-off from a Fiji event. The split would have occurred with or without the H-component detections. Both the ANMO and PMR arrivals were detected on the horizontals alone. A split-off from an Eastern USSR event also occurred; however, this split could not have been formed without the horizontals (this event is not shown). Figure II-22(a-b) shows event 1109, located

in Colorado, which was not reported by USGS or Sweden. Without the detections on the horizontals at ANMO, there would have been insufficient arrivals to associate or locate this event. Event 1113, located in Western Idaho, is shown in Fig. II-23(a-b); this event is another original produced during the first pass of our AA. If not for the detections on the horizontals at BCAO, this event could not have been associated or located. It is interesting to note that the detector missed the detection on the Z-component, while it did manage to detect it on the horizontals.

Thus, we find that adding the detections from the horizontals can increase the number of significant arrivals for a given period of time. And, while one can argue that adding two marginal events and one split event to an event list is questionable given the requirement to process three times as many false alarms, it seems that with additional refinement 3-component detection can become a significant enhancement to the Automatic Signal Processor.

M. A. Tiberio

G. COMPARISON OF ANALYST AND AUTOMATIC TECHNIQUES FOR PICKING FIRST ARRIVALS

As part of the U.S. contribution to the International Data Collection Experiment, several methods of picking first arrivals were compared for the number of associated arrivals generated and accuracy of picks. The database used consists of all the digital and analog data collected on 2 and 4 October 1980 from the Global Digital Seismograph Network (GDSN), as well as reported readings from selected WWSSN stations. The NEIS monthly summary provides a check of each method by identifying which generated arrivals are associated with known events. The criteria for association of an arrival with a given event are very broad – an arrival is considered associated if its time agrees to within 1 min. with that predicted by the Jeffreys-Bullen travel-time tables. Such a range of acceptability is, of course, far from being tolerable for event location, but was found necessary to associate arrivals from particular events, which for some stations had large residuals no matter which method was used to make the arrival-time pick. The difference between the time pick and the arrival time predicted by the Jeffreys-Bullen time tables provides a measure of the accuracy of each method.

The four methods compared, ranging from completely manual to fully automatic detection and analysis, are listed below.

(1) Analyst ASL Detector – Analyst review of digital detections made by the Albuquerque Seismological Laboratory (ASL) or SRO detector. The digital data are plotted on a large scale, and time and amplitude measurements made by very precisely using a hardware cursor.

(2) Automatic LL Detector – Results of automatic processing as described in Sec. I-D of this SATS. In cases where the automatic time picker failed even though the "Z"-detector had identified a signal which was in fact associated, the time is that at which the detector triggered. No analyst review or interaction.

(3) Analyst SRO Analog – Analyst scanning film records of SRO/ASRO data, performing detection and measurements manually.

(4) Analyst Station (ALQ) – Analyst measurements made as (3) but on an alternate station (e.g., ALQ WWSSN station as alternative to ANMO). A conceivable advantage to such picks is that they are made at the station itself

by an analyst with considerable experience in recognizing signals particular to both the site and specific source regions.

One advantage of the automatic processor is in the speed with which the data can be analyzed. Detection, windowing, timing, and amplitude/period measurement on 24 h of continuous short-period (20 samples/s) data requires less than 15 min. of computer time on a moderate-sized computer. This is considerably faster than a human analyst processing the same number of arrivals (~30/day) from analog records.

Techniques (1) through (4) above generated 98, 111, 89, and 69 associated arrivals, respectively. Of these, 66, 70, 63, and 52 (67, 63, 71, and 75 percent), respectively, had travel-time residuals of less than 2 s. The distributions of the residuals by each technique are given in Table II-7. It can be seen that none of the four methods appears to produce picks which are either consistently late or early. The automatic technique is slightly more prone to generating picks with residuals greater than 10 s, which is, of course, unacceptable for the purposes of accurate location.

Moderate travel-time residuals (e.g., <3 to 4 s) do not necessarily indicate a poor arrival-time pick but can be due to regional variations in the travel-time pick. In order to attempt to cancel out such path-specific bias, the difference between the times determined by methods (2) through (4) above and that produced by (1) has been calculated for the associated picks only.

TABLE II-7

DISTRIBUTION OF TRAVEL-TIME RESIDUALS FOR ASSOCIATED ARRIVALS BY EACH METHOD

Residual R (s)	Analyst ASL Detector	Automatic LL Detector	Analyst SRO Analog	Analyst STA Analog
$R < -20$		1		
$-20 < R < -10$	2	2	1	
$-10 < R < -5$	1	1	2	1
$-5 < R < -4$	3	0	3	0
$-4 < R < -3$	2	2	2	0
$-3 < R < -2$	6	9	3	3
$-2 < R < -1$	12	16	9	8
$-1 < R < 0$	22	29	19	17
$0 < R < 1$	20	13	28	15
$1 < R < 2$	12	12	7	12
$2 < R < 3$	8	8	5	2
$3 < R < 4$	2	3	1	1
$4 < R < 5$	2	4	3	2
$5 < R < 10$	3	3	4	5
$10 < R < 20$	1	5	2	2
$R > 20$	2	3	0	1

TABLE II-8

DISTRIBUTION OF DIFFERENCES BETWEEN TIME PICKS MADE BY METHODS (2), (3), AND (4) AND METHOD (1)

Difference D (s)	Methods		
	(2) and (1)	(3) and (1)	(4) and (1)
$D < -10$	2	1	0
$-10 < D < -5$	2	0	0
$-5 < D < -2$	3	1	0
$-2 < D < -1.5$	2	1	1
$-1.5 < D < -1.0$	6	2	1
$-1.0 < D < -0.5$	12	2	3
$-0.5 < D < 0$	22	12	4
$0 < D < 0.5$	26	15	21
$0.5 < D < 1.0$	1	2	4
$1.0 < D < 1.5$	3	1	1
$1.5 < D < 2.0$	3	0	0
$2.5 < D < 5.0$	4	0	3
$5.0 < D < 10.0$	1	1	1
$D > 10.0$	4	1	2

(1) = Analyst pick, ASL detection

(2) = Automatic pick, LL detection

(3) = Analyst pick, SRO analog

(4) = Analyst pick, alternate station (9 stations only of total 17)

Technique (1) was chosen as the standard since it is reasonable to assume that the ability to plot the seismogram on a very large scale from the digital data will enable the most-accurate onset time picks to be made by the analyst. The results are shown in Table II-8. The tendency of automatic technique (2) to produce more erroneous picks than (3) or (4) is still apparent, as is its ability to produce more total picks than method (3) which uses analog data from the same seismometer. Perhaps the most surprising result is the occasional large difference between the times picked by the various human analysts. Even for arrivals designated by various analysts as impulsive, denoting an accuracy which the analyst believed to be ±0.2 s, differences of 1 s or larger are quite common.

The GDSN studied here consisted of 17 stations at the time of the data-collection experiment. For the 32 events on the monthly summary, 9 were recorded to minimum distances of less than 10°. Of the remaining 23, only 10 were detected at 5 or more stations of the GDSN network and could conceivably be located by data from these stations if the azimuthal coverage were adequate. Addition of data from the 7 other stations within the Continental U.S. and Alaska may improve this situation slightly.

R. G. North
M. W. Shields

REFERENCES

1. J. W. Tukey, Exploratory Data Analysis (Addison-Wesley, Reading, Massachusetts, 1977), pp. 205-236.
2. Seismic Discrimination SATS, Lincoln Laboratory, M.I.T. (31 March 1981), DTIC AD-A109184.
3. K. R. Anderson, "Syntactic Analysis of Seismic Waveforms using Augmented Transition Network Grammars," in Proceedings of the Second International Symposium on Computer-aided Seismic Analysis and Discrimination, IEEE Catalog No. 81CH1687-3 (1981), pp. 54-65.
4. H. H. Liu and K. S. Fu, "An Application of Syntactic Pattern Recognition to Seismic Discrimination," in Proceedings of the Second International Symposium on Computer Aided Seismic Analysis and Discrimination, IEEE Catalog No.81CH1687-3 (1981), pp. 49-53.
5. K. S. Fu, "Error-correcting for Syntactic Pattern Recognition," in Data Structure, Computer Graphics and Pattern Recognition, Klinger et al., Eds. (Academic Press, New York, 1976).
6. R. A. Wagner, "Order-n Correction of Regular Languages," Commun. ACM 17, 265-268 (1974).
7. K. S. Fu and T. L. Booth, "Grammatical Inference – Introduction and Survey," IEEE Trans. Syst. Man Cybern. SMC-5, 409-423 (1975).
8. C. S. Myers, "A Comparative Study of Several Dynamic Time Warping Algorithms for Speech Recognition," Master's Thesis, Department of Electrical Engineering and Computer Science, M.I.T. (May 1980).
9. R. Bellman and S. Dreyfus, Applied Dynamic Programming (Princeton University Press, New Jersey, 1962).
10. R. O. Duda and P. E. Hart, Pattern Classification and Scene Analysis (Wiley, New York, 1973), p. 229.
11. E. C. Freuder, "Affinity: A Relative Approach to Region Finding," Computer Graphics and Image Processing 5, 254-264 (1976).
12. J. H. Goncz, "Present Status and Dynamic Planning for Automatic Association Programs," SDAC-TR-80-2, Seismic Data Analysis Center, Teledyne Geotech, Alexandria, Virginia (1980).
13. Seismic Discrimination SATS, Lincoln Laboratory, M.I.T. (31 March 1980), DTIC AD-A091107/3.
14. E. H. Shortliffe, Computer-Based Medical Consultations: MYCIN (Elsevier, New York, 1976).
15. R. O. Duda, "The Prospector System for Mineral Exploration," SRI International, Menlo Park, California (1980).
16. R. Davis, H. Austin, I. Carlbom, B. Frawley, P. Pruchnik, R. Sneiderman, and A. Gilreath, "The DIPMETER ADVISOR: Interpretation of Geological Signals," Proc. 7th Int. Joint Conf. on Artificial Intelligence, Vancouver, 1981.
17. B. G. Buchanan and E. A. Feigenbaum, "DENDRAL and Meta-DENDRAL," Art. Intel. 11, 5-24 (1978).
18. E. Charniak, C. K. Riesbech, and D. V. McDermott, Artificial Intelligence Programming (Lawrence Erlbaum Associates, Hillsdale, New Jersey, 1980).
19. R. B. Roberts and I. P. Goldstein, "The FRL Primer," Memo 408, Artificial Intelligence Laboratory, M.I.T. (1977).
20. _____, "The FRL Manual," Memo 409, Artificial Intelligence Laboratory, M.I.T. (1977).
21. M. Minsky, "A Framework for Representing Knowledge," in The Psychology of Computer Vision, P. H. Winston, Ed. (McGraw-Hill, New York, 1975).
22. S. Rosenberg, "Understanding in Incomplete Worlds," Memo 475, Artificial Intelligence Laboratory, M.I.T. (1978).

23. R. Davis and J. J. King, "An Overview of Production Systems," in MI 8: Machine Representations of Knowledge, Elcock and Michie, Eds. (Wiley, New York, 1977).

24. R. Sprugnoli, "Perfect Hashing Functions: A Single Probe Retrieving Method for Static Sets," Commun. ACM 20, 841-850 (1977).

25. R. J. Cichelli, "Minimal Perfect Hash Functions Made Simple," Commun. ACM 23, 17-19 (1980).

26. C. E. Shannon and W. Weaver, The Mathematical Theory of Communication (University of Illinois Press, Urbana, Illinois, 1972).

27. D. E. Knuth, The Art of Computer Programming: Volume 3, Sorting and Searching (Addison-Wesley, Reading, Massachusetts, 1973).

28. B. W. Kernighan and D. M. Ritchie, The C Programming Language (Prentice-Hall, Englewood Cliffs, New Jersey, 1978).

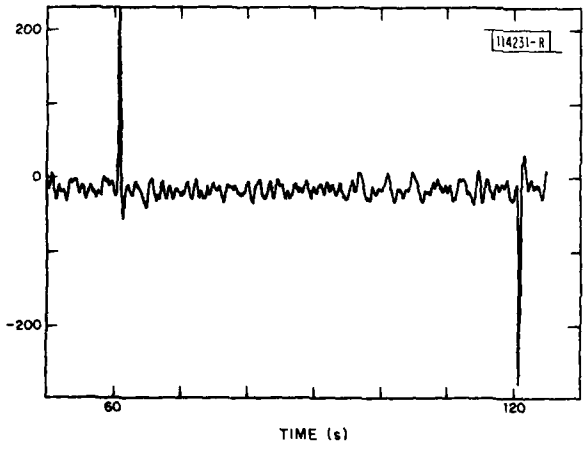

Fig. II-1. Typical calibration sequence. Computer description: 60.55 s of noise, a calibration sequence beginning at 60.55, and 54.3 s of noise.

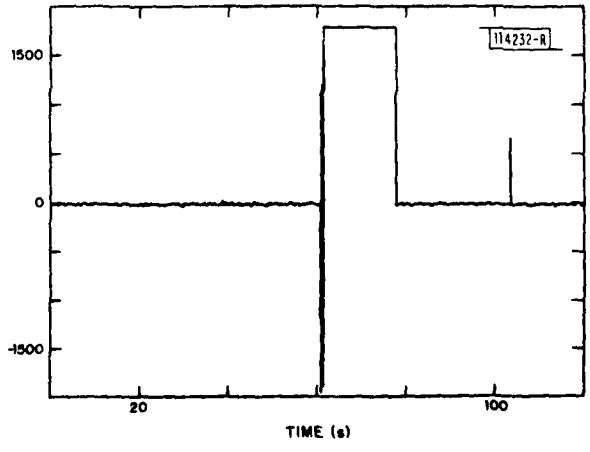

Fig. II-2. Computer description: 60.55 s of noise, a box with a height of 1789 beginning with a buzz, 25.65 s of noise, a glitch 0.1 s wide and 651 units high, and 90.1 s of noise.

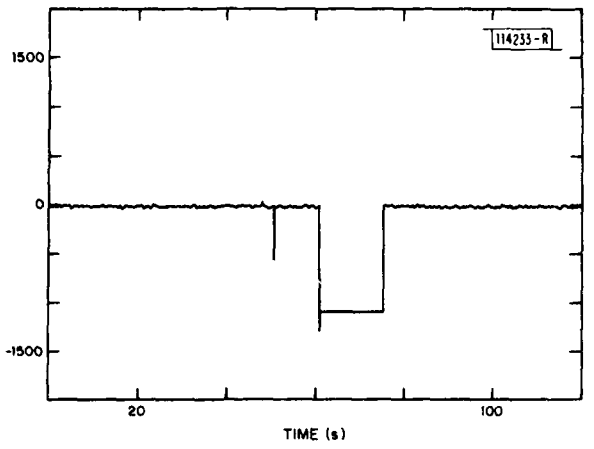

Fig. II-3. Computer description: 50.55 s of noise, a glitch 0.1 s wide and −560 units high, 10.1 s of noise, a box with a height of −1091 beginning with a glitch, and 115.25 s of noise.

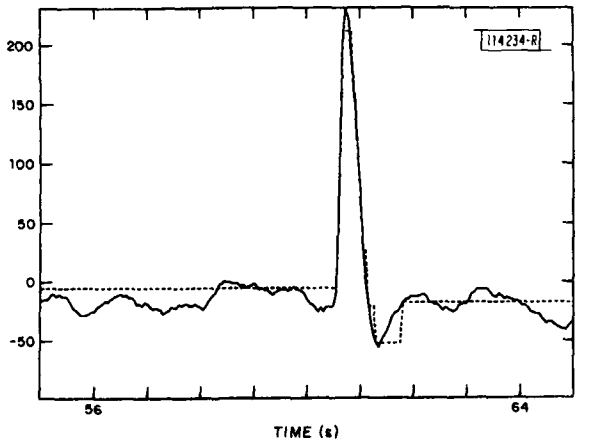

Fig. II-4. Detail of a calibration pulse (solid line) and its hysteresis filtered version (dotted line).

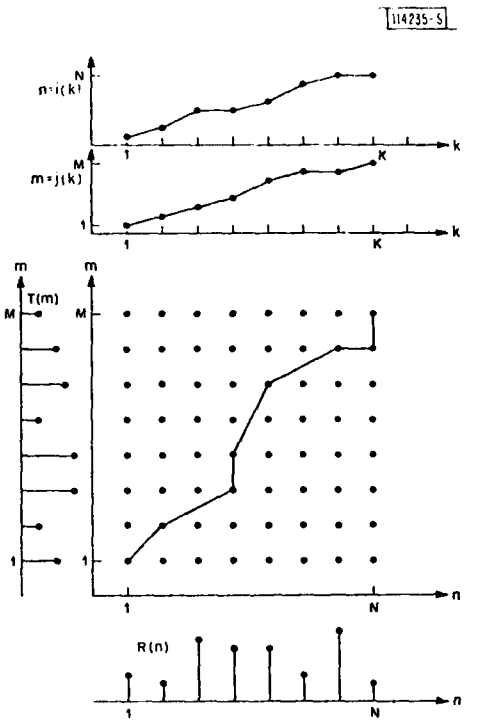

C22-6000

Fig. II-5. Dynamic Time Warping as path finding (after Myers[8]).

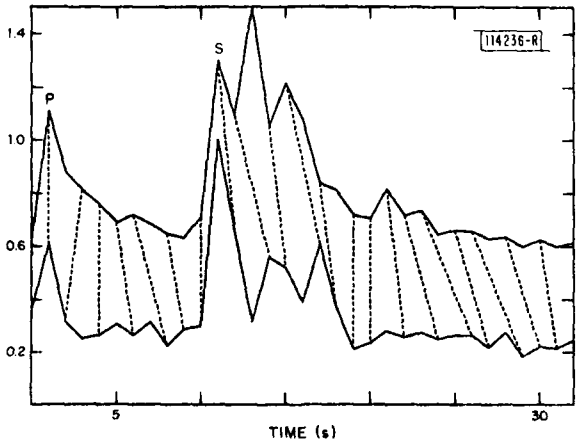

C22-6001

Fig. II-6. Dynamic match between envelopes of two local seismograms. Dotted lines are drawn between a point in each waveform that corresponds in match.

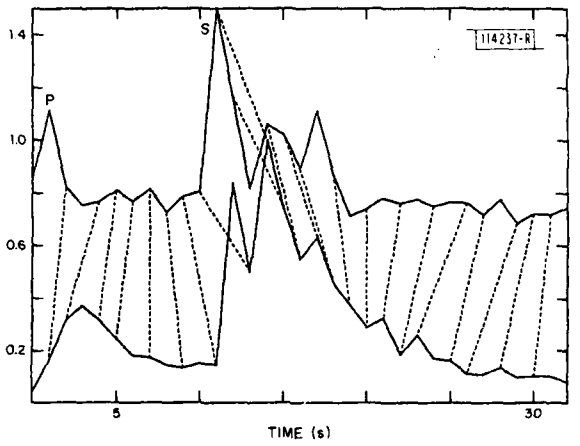

Fig. II-7. Dynamic match between two dissimilar waveforms.

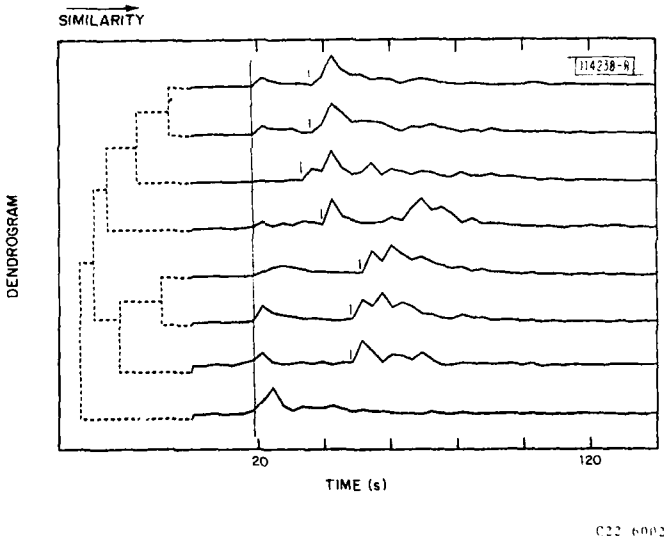

Fig. II-8. Cluster analysis of envelopes of eight local seismograms recorded at BDW. A dendrogram indicating hierarchical clustering of waveforms is shown by dotted lines to left of envelopes.

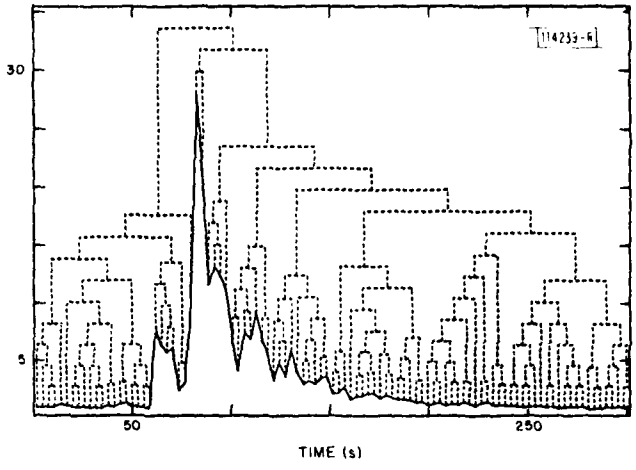

Fig. II-9. Tree structure of affinity based on average magnitude criteria.

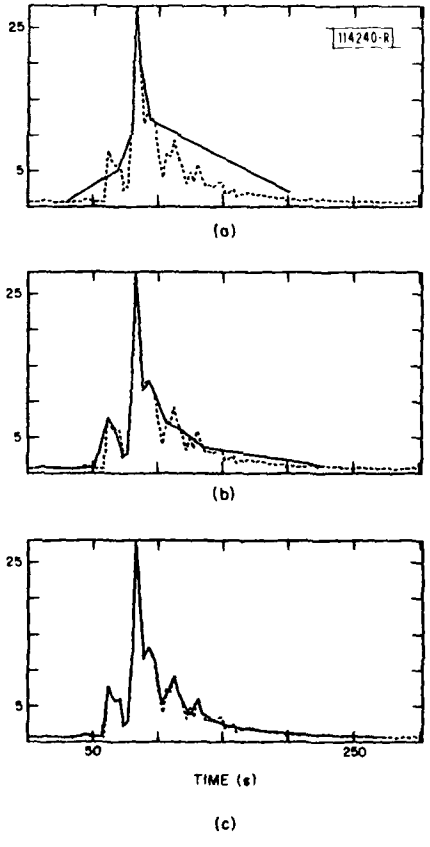

Fig. II-10. Representation of waveform at different levels down tree based on average amplitude criteria: (a) level 3, (b) level 5, and (c) level 7.

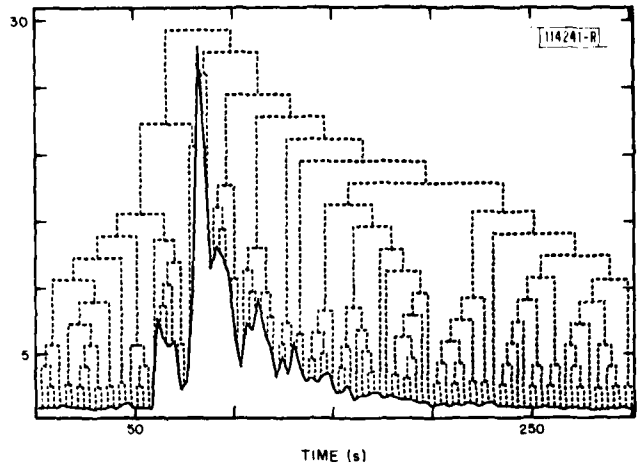

Fig. II-11. Tree structure of affinity based on slope criteria.

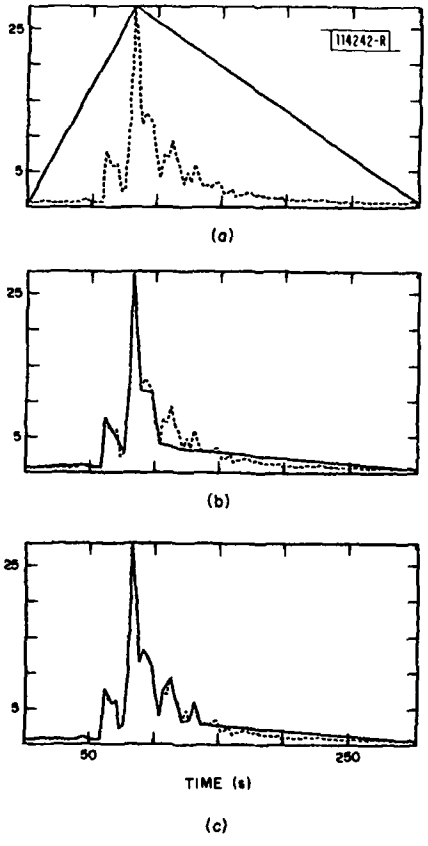

Fig. II-12. Representation of waveform at different levels down tree based on slope criteria: (a) level 1, (b) level 4, and (c) level 6.

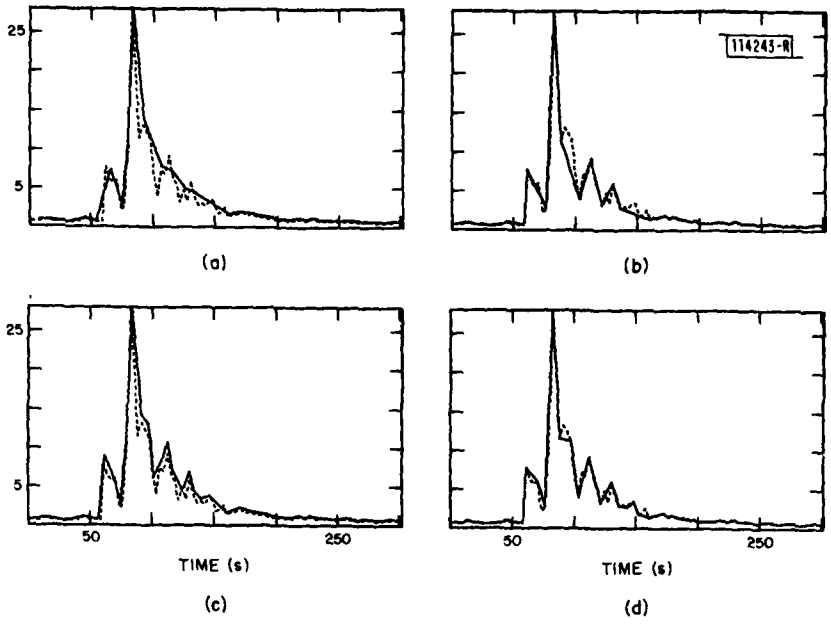

Fig. II-13. Example of versatility of tree format. Sequence of words can be obtained by definitions other than tree depth. Amplitude criteria on segments of (a) length 18 and (c) length 12; slope criteria on segments of (b) length 18 and (d) length 12.

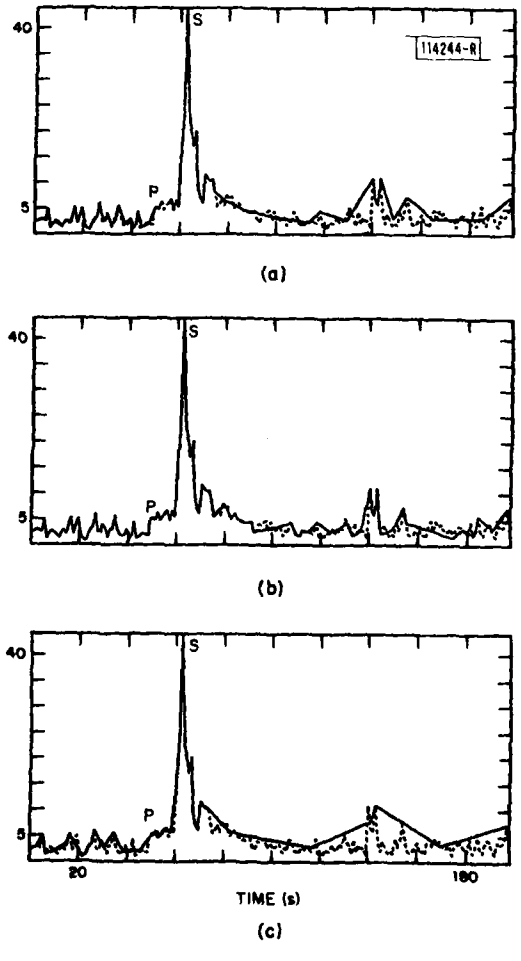

Fig. II-14. A problem with uneven distribution of resolution: (a) level 7, (b) level 9, and (c) level 11.

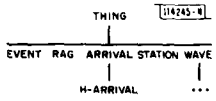

Fig. II-15. Inheritance hierarchy of frames representing seismic parameters.

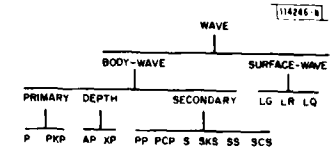

Fig. II-16. Inheritance hierarchy of frames representing seismic waves.

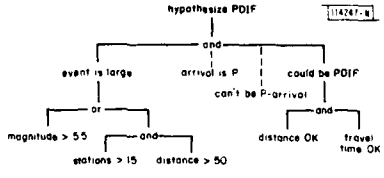

Fig. II-17. Structure formed by set of five rules used to determine whether or not an arrival could be PDIF.

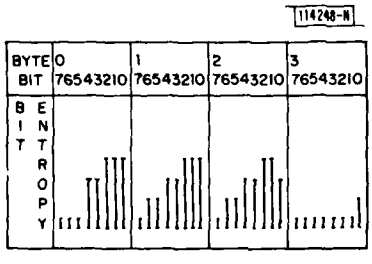

Fig. II-18. Bar graph showing relative entropies of each bit of 4-byte keys. Height of bars corresponds to divisions of Table II-4.

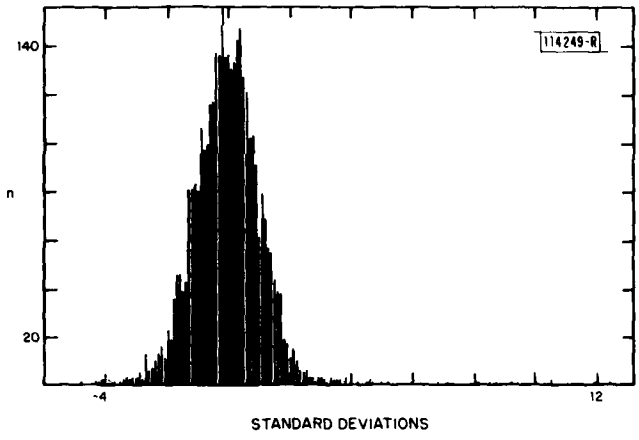

Fig. II-19. Z-statistic distribution.

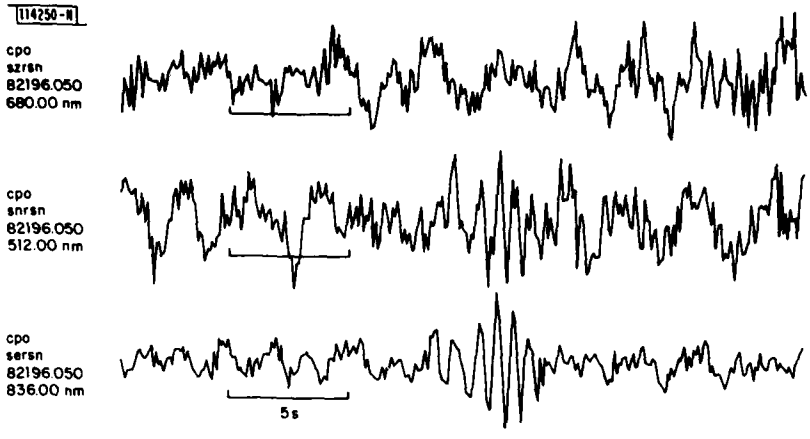

(a)

Fig. II-20(a-c). Unassociated arrival located on horizontal components.

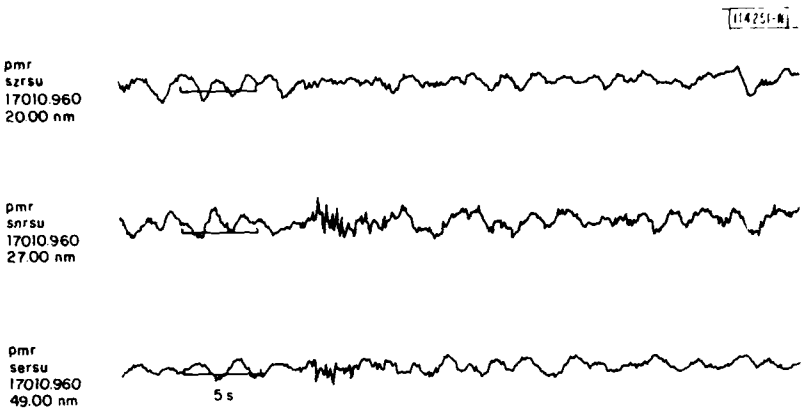

(b)

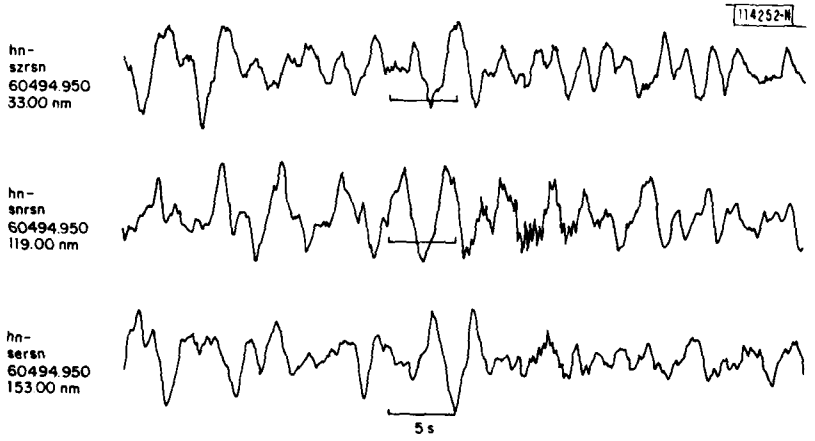

(c)

Fig. II-20(a-c). Continued.

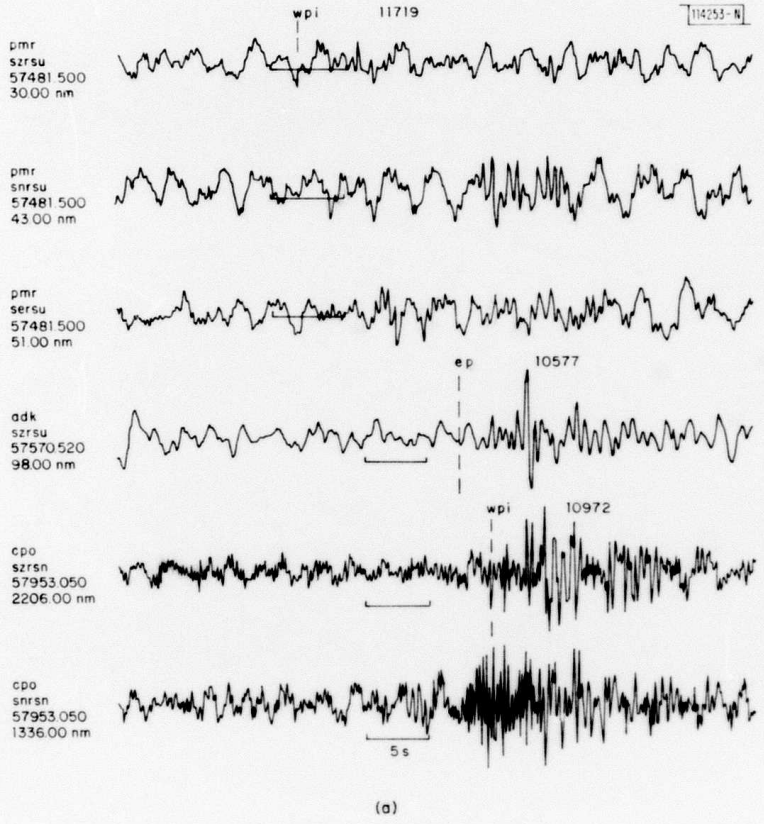

(a)

Fig. II-21(a-b). Bogus Alaskan event split from Fiji event.

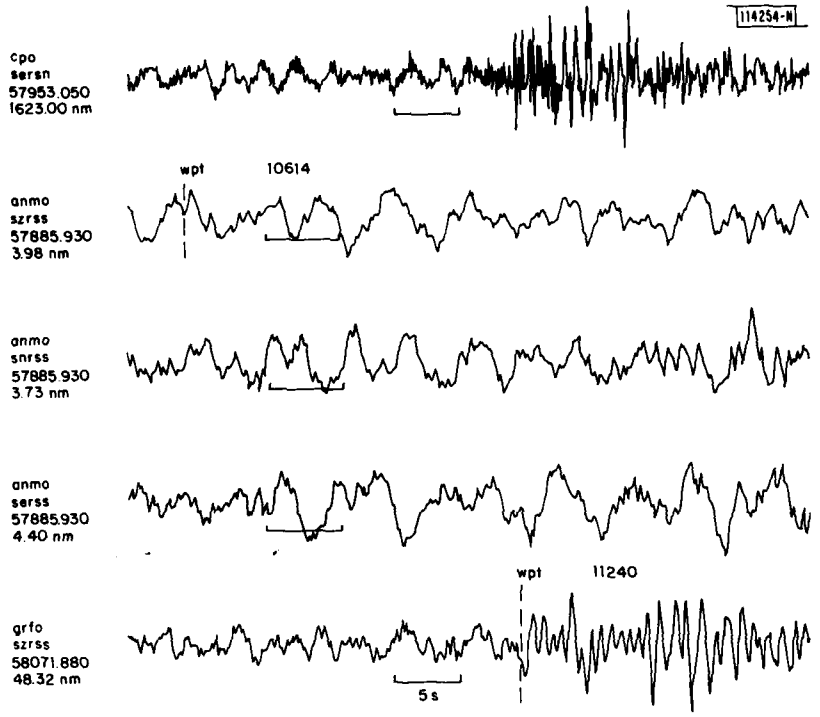

(b)

Fig. II-21(a-b). Continued.

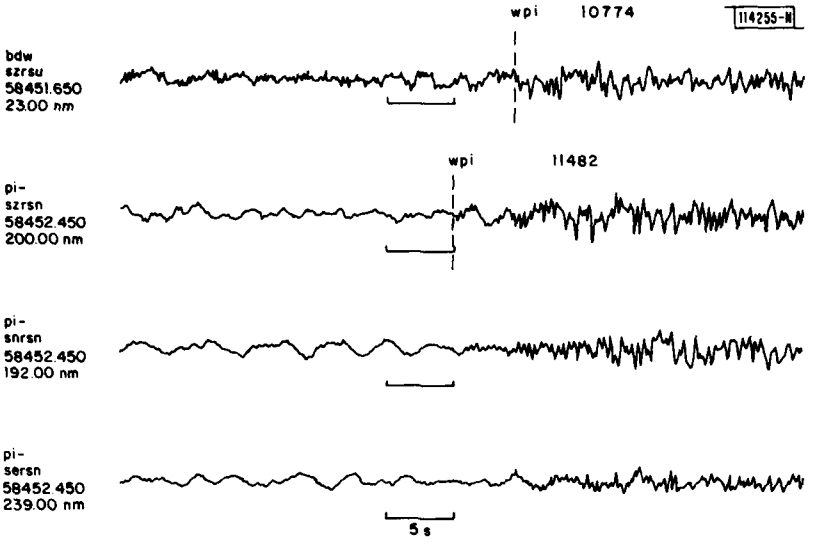

(a)

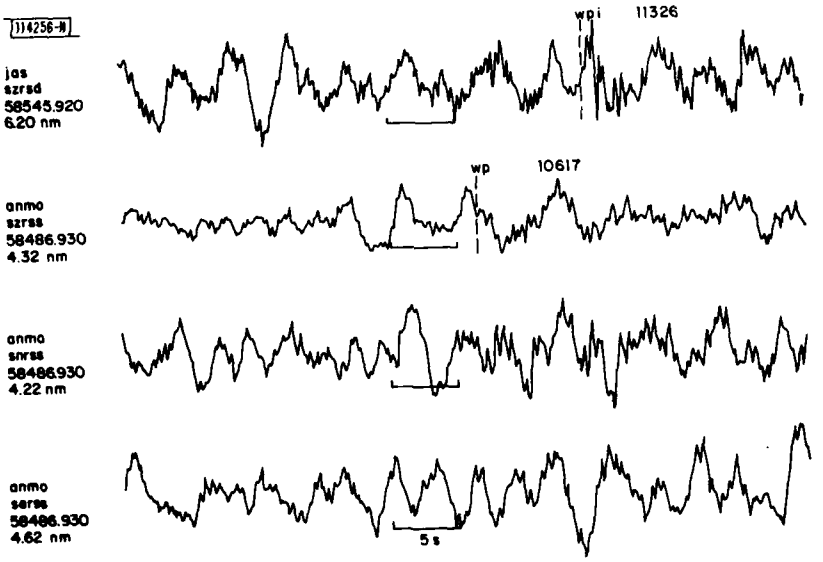

(b)

Fig. II-22(a-b). Hypothetical Colorado event.

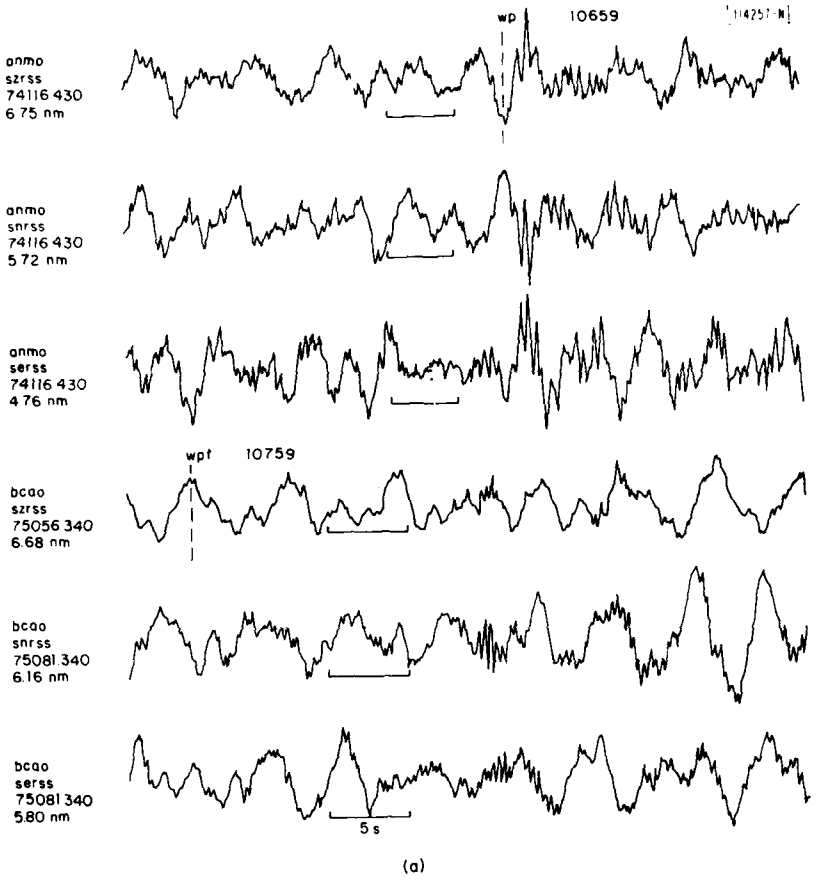

Fig. II-23(a-b). Hypothetical Western Idaho event.

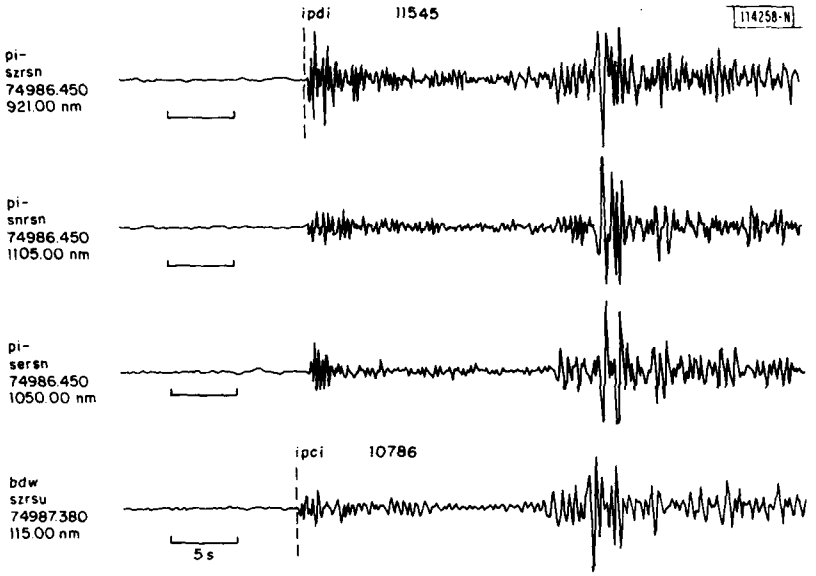

(b)

Fig. II-23(a-b). Continued.

III. GENERAL SEISMOLOGY

A. A REVIEW OF FREQUENCY-DEPENDENT ANELASTICITY

1. Frequency-Dependent Anelasticity from Spectral Measurements

Many studies have shown that the frequency content of body waves in the band 0.5 to 10 Hz is too high to be consistent with the intrinsic anelasticities Q_α and Q_β determined from observations of seismic waves in the band 0.005 to 0.1 Hz (see Refs. 1 and 2). The results of these studies are confirmed by the spectra of short-period P-waves observed at SRO/ASRO stations from deep focus events. The body-wave spectra of deep events are desirable in attenuation studies because they are uncontaminated by near-surface multiples, and they do not include the effects of anomalous elastic and anelastic structures that may be present in the source region. Eight events were chosen for study having foci from 350 to 650 km depth and body-wave magnitudes from m_b 5.5 to m_b 6.0. Spectral studies by Wyss and Molnar[3] of deep focus events of this size found the P-wave corner frequency to range from 0.1 to 0.6 Hz. This corner frequency is generally less than the frequency band of short-period SRO/ASRO stations in which the signal-to-noise ratio (SNR) is high for teleseismic body waves. A common practice is to assume an ω^{-2} rolloff above the corner frequency and to attribute the additional decay of the observed spectra to the effects of intrinsic anelasticity. The spectra of eight events were computed by correcting for the instrument response and applying a series of narrowband Gaussian filters equivalent to the MARS analysis described by Savino et al.[4] Filter outputs that were less than half the long-term average of the time-domain output of the filter or that lay outside of an acceptance window for group arrival time were rejected as noise. Figure III-1 shows the spectra and anelastic interpretations computed for a deep focus event in Peru recorded at ANMO. For a spectral rolloff of ω^{-2}, a $t^* = 0.2$ is inferred. (t^* is the path integrated effect of anelasticity on a body wave and is commonly defined by $t^* = \int Q^{-1} dt$, where the travel-time integral is taken along the ray path.)

Assuming double t^* for an equivalent surface focus event gives $t^*_\alpha = 0.4$. Figure III-2 shows the spectra for a shield station NWAO. Here, the interpretation with an ω^{-2} rolloff gives $t^* = 0.05$ (0.1 for an equivalent surface focus event). All the events required a $t^*_\alpha \leq 0.2$, confirming the results of Der et al.[5] that anelasticity must increase with frequency in order to account for the observed spectra of short-period body waves.

2. ScS/ScP Synthetics: Implications for a High-Frequency Cutoff in the Seismic Relaxation Spectrum

Burdick[6] determined the time-domain operator needed to convert an ScP phase into an ScS phase recorded at the same receiver site, and inferred from these results the high-frequency limit $1/2\pi\tau_m$ of the relaxation spectrum of the mantle. A fundamental observation to match in his data set of short-period WWSSN records is that the apparent period of ScS is nearly always at least twice that of ScP. Since both phases leave the source as S-waves at a takeoff angle that differs by less than 9°, the difference in frequency content can be primarily attributed to attenuation in the mantle rather than to source directivity. Burdick tested a model in which the frequency dependence was assumed to be constant with depth. With this model he concluded that strong frequency dependence in the mantle does not occur until frequency exceeds 1 Hz. This result would imply that anelastic models giving $t^*_\alpha = 1$ are still appropriate for body waves

observed on short-period WWSSN records having dominant energy at 1 Hz. Using this result and assuming an absorption-band model that allows Q to increase linearly with frequency above 1 Hz, it is impossible to match the high-frequency content of the ScS phases observed by Sipkin and Jordan[7] and the body waves that bottom in the mid-mantle observed by Der et al.[5]

Experiments with synthetic ScS and ScP phases in both the time and frequency domains were conducted in order to confirm Burdick's results and to investigate the effects on ScS and ScP of source pulse width, instrument band width, and the effects of anelastic models that vary with depth as well as frequency. Spectra and seismograms were synthesized by the methods described in Lundquist and Cormier[8] for models of the relaxation spectrum of the mantle. All calculations were performed in the isotropic PREM model[9] referenced at 1 Hz, the attenuation model of which gives $t^*_\alpha = 1$ for a teleseismic P-wave of an event having a surface focus. The lower time constant of a mantle-wide absorption band was varied from $\tau_m = 0.01$ to 0.9 s/rad. The frequency-independent Q model of PREM was reproduced at frequencies below 16 Hz for $\tau_m = 0.01$, and below 0.06 Hz for $\tau_m = 0.9$ s/rad. Time-domain pulses were synthesized for a 600-km-deep event using a triangle source pulse with a width that varied between 0.25 to 2 s. Figure III-3 shows the results for ScS and ScP phases observed with a WWSSN short-period instrument for a 1-s source pulse. For all source pulse widths, it was impossible to obtain the observed shift in frequency of ScS relative to ScP without having $\tau_m \leq 0.1$, which corresponds to a $t^*_\alpha \geq 0.7$ at 1 Hz for a surface focus P-wave observed at 60°. This test essentially confirms the results of Burdick for a mantle-wide absorption band.

Another series of tests was performed for a mantle-wide relaxation band that possessed a high attenuation zone at the base of the mantle of the type suggested by Mitchell and Helmberger,[10] which has $Q_\beta = 100$ and $Q_\alpha = 300$ in a 150-km zone above the core-mantle boundary. Figure III-4 compares the results for the synthetic spectral ratio ScS/ScP for this model (dotted lines) with the results of a model having small attenuation at the base of the mantle (solid lines). The effect of a low Q zone of this magnitude is not sufficient to move the models having small attenuation at high frequencies ($\tau_m > 0.1$) into the domain of ScS/ScP observations.

A third type of relaxation model was tested in which the relaxation band was assumed to lie in the high-frequency band in the upper 400 km and lowermost 150 km of the mantle, but shifts to frequencies less than 0.06 Hz in the mid-mantle. In the upper mantle, this model resembles the double absorption band proposed by Lundquist and Cormier[8] to satisfy the waveforms of short-period body waves. The additional absorption band at high frequencies at the base of the mantle follows the model used by Anderson and Given[11] to simultaneously satisfy free-oscillation and body-wave data. They justify the depth dependence of a seismic absorption band, in which attenuation is shifted to low frequencies in the mid-mantle, by the effects that the pressure and homologous temperature profiles are expected to have on physical mechanisms of anelasticity. With this type of triple absorption-band model, it is possible to satisfy the relative frequency content of ScS and ScP phases (dashed lines in Fig. III-4) while obtaining a $t^*_\alpha = 0.5$ Hz for a surface focus P-wave bottoming in the mid-mantle. A more intense or thicker zone of attenuation at the base of the mantle than that proposed by Mitchell and Helmberger,[10] however, is required in order to bring a curve having $\tau_m = 0.4$ into the domain of ScS/ScP observations.

An experiment similar to ScS/ScP in eliminating the source spectrum is that of sS/sP. For sS, sP phases bottoming in the upper 700 km of the mantle, Burdick[12] needed to satisfy an observed shift to lower frequency in the unconverted sS phase. Even though these observations were made on narrowband instruments, it would be difficult to satisfy the observed frequency

shift without placing the absorption band in the instrument band. These results demonstrate the difficulty in simultaneously satisfying the spectral content of body waves bottoming in the mid-mantle, and the ratios ScS^{n+1}/ScS^{n}, ScS/ScP, and sS/sP, without allowing the limits of the seismic relaxation band to strongly vary as a function of depth. The simplest model that can satisfy all data is one having absorption in the high-frequency band of seismic body waves in the upper and lowermost mantles, but shifted to frequencies less than 0.1 Hz in the mid-mantle. Regional variation of ScS^{n+1}/ScS^{n} observed by Sipkin and Jordan[13] and amplitude variations in core grazing PKP waves observed by Sacks et al.[14] suggest regional variation in the absorption bands in both the upper and lowermost mantles.

Experiments that eliminate the source function can provide additional constraints on the interpretation of body-wave spectra in terms of absorption-band models. These experiments can now be repeated with greater precision using digital data recorded over a broader band. The combined interpretation of source-canceling experiments and spectra of short-period body waves should include the type of depth dependence of an absorption band that may be expected for the temperature and pressure profile of the mantle. Quite different depth dependences of the absorption bands can satisfy the spectral ratios of a source-canceling experiment. It may be possible, however, to show that for a given seismic moment and source time function a particular absorption-band model that satisfies spectral-ratio data would produce a body pulse that is too small to be observed.[15] It is thus essential for time-domain modeling to model absolute as well as relative amplitudes.

V. F. Cormier

B. THE CALCULATION OF $d\Delta/dp$ AND OF PARTIAL DERIVATIVES FOR TRAVEL-TIME INVERSION IN TRANSVERSELY ISOTROPIC SPHERICAL EARTH MODELS

The increasing evidence for anisotropy in the Earth's upper mantle and the fact that the recent Preliminary Reference Earth Model (PREM)[16] incorporates a transversely isotropic region make it necessary to take into account anisotropy in ray theoretic calculations, such as the calculation of travel-time curves, geometrical spreading factors, and in the inversion of travel times. The most general kind of anisotropy which can exist in a spherically symmetric Earth model, corresponding to the spherically averaged Earth, is transverse isotropy, in which the tensor of elastic parameters is invariant under rotations about any radius vector and is characterized by the five elastic parameters N, L, A, C, and F, each functions of radius r. It is the purpose of this contribution to give formulas for the calculation of $d\Delta/dp$ for such a model, and also to present results for the partial derivatives of travel times with respect to model parameters which are needed in linearized travel-time inversion.

Results for travel time T and distance Δ as functions of ray parameter p have been given by Woodhouse[17] and are repeated here. The one-way intercept time may be written:

$$\tau(p) = \int q_{\tau}(p, r)\, dr \qquad \text{(III-1)}$$

and

$$T(p) = \int q_{T}(p, r)\, dr$$

$$\Delta(p) = \int q_{\Delta}(p, r)\, dr \qquad \text{(III-2)}$$

where

$$q_\Delta = -\partial q_\tau / \partial p$$

$$q_T = q_\tau + p q_\Delta \quad . \tag{III-3}$$

In the above, and in later integrals, it is understood that the integration is over intervals of radius for which q_τ is real, and that for rays with multiple legs the appropriate multiple contributions to the integrals should be taken. The integrands are given by[17]:

For SH

$$q_\tau = \left(\frac{\rho}{L} - \frac{N}{L}\frac{p^2}{r^2}\right)^{1/2}$$

$$q_T = \frac{1}{q_\tau} \cdot \frac{\rho}{L}$$

$$q_\Delta = \frac{p}{r^2 q_\tau} \cdot \frac{N}{L} \tag{III-4}$$

and for P-SV (upper and lower signs, respectively)

$$q_\tau = \left(s_1 - s_3\frac{p^2}{r^2} \mp R\right)^{1/2}$$

$$q_\Delta = \frac{p}{r^2 q_\tau}\left[s_3 \pm \frac{1}{R}\left(s_4\frac{p^2}{r^2} + s_5\right)\right]$$

$$q_T = \frac{1}{q_\tau}\left[s_1 \mp \frac{1}{R}\left(s_5\frac{p^2}{r^2} + s_2^2\right)\right] \tag{III-5}$$

with

$$R \equiv \left(s_4\frac{p^4}{r^4} + 2s_5\frac{p^2}{r^2} + s_2^2\right)^{1/2} \tag{III-6}$$

and

$$s_1 = \frac{1}{2}\left(\frac{\rho}{L} + \frac{\rho}{C}\right)$$

$$s_2 = \frac{1}{2}\left(\frac{\rho}{L} - \frac{\rho}{C}\right)$$

$$s_3 = \frac{1}{2LC}(AC - F^2 - 2LF)$$

$$s_4 = s_3^2 - \frac{A}{C}$$

$$s_5 = \frac{1}{2}\frac{\rho}{C}\left(1 + \frac{A}{L}\right) - s_1 s_3 \tag{III-7}$$

where ρ is density (it may be noted that the integrands depend only upon the ratios L/ρ, N/ρ, A/ρ, C/ρ, and F/ρ which have the attributes of squared wave velocities).

1. The Calculation of $d\Delta/dp$

A turning radius b(p) for a ray with ray parameter p is determined by

$$q_\tau(p, r)\Big|_{r=b(p)} = 0 \qquad \text{(III-8)}$$

and it will be assumed that

$$q_\tau > 0 \qquad \text{for } r > b \quad .$$

For the sake of definiteness and simplicity, we shall restrict our attention here to a single smoothly varying region of a spherical model ($c < r < a$) in which a turning radius b(p) exists ($c < b < a$). The integrands q_Δ, q_T are singular at $r = b$, and in order to evaluate the integrals numerically the integrands must be made regular there. A simple way to regularize them is to define a new independent variable

$$u = (r - b)^{1/2} \quad , \quad \text{i.e., } r = b(p) + u^2 \quad . \qquad \text{(III-9)}$$

Then,

$$\Delta(p) = \int_0^{(a-b)^{1/2}} 2G(p, b + u^2)\, du \qquad \text{(III-10)}$$

where

$$G(p, r) \equiv (r - b)^{1/2}\, q_\Delta(p, r) \qquad \text{(III-11)}$$

and similarly for T(p). The singularity in the integrand has been eliminated and the integral may be evaluated numerically by any suitable method (e.g., Romberg or Gaussian integration).

To evaluate $d\Delta/dp$, we write

$$\Delta(p) = \int_{b(p)}^{a} \frac{G(p, r)}{[r - b(p)]^{1/2}}\, dr \quad . \qquad \text{(III-12)}$$

Differentiation under the integral sign is not admissible directly because of the singularity at the turning radius; however, we may write

$$\Delta(p) = \int_b^a \frac{G(p, r) - G(p, b)}{(r - b)^{1/2}}\, dr + 2(a - b)^{1/2}\, G(p, b) \qquad \text{(III-13)}$$

where the second term arises from explicit integration of the term subtracted from the integrand. The new integrand vanishes at the turning point, and differentiating under the integral and simplifying we find:

$$\frac{\partial \Delta}{\partial p} = \int_b^a \frac{1}{(r - b)^{1/2}} \left[G_p(p, r) + \tfrac{1}{2} b'(p)\, \frac{G(p, r) - G(p, b)}{r - b}\right] dr - \frac{b'(p)\, G(p, b)}{(a - b)^{1/2}} \qquad \text{(III-14)}$$

where subscript p indicates partial differentiation. The integrand here has an integrable singularity which may be regularized by the transformation (III-9). It may be shown that the quantities b'(p) and G(p, b) in Eq.(III-14) are given by

$$b'(p) = \left. \frac{-\partial q_\tau^2/\partial p}{\partial q_\tau^2/\partial r} \right|_{r=b}$$

$$G(p,b) = \frac{1}{2} b'(p) (\partial q_\tau^2/\partial r)^{1/2} \Big|_{r=b} \quad . \tag{III-15}$$

It is straightforward to obtain expressions for the various quantities appearing in Eqs. (III-14) and (III-15) from Eqs. (III-11), (III-4), (III-5), (III-6), and (III-7); since they are lengthy, we will not list them explicitly. It may be noted that the derivatives of the model parameters with respect to radius are required at the turning point, and should be evaluated (preferably analytically) in terms of the interpolants used to define the model. With a model, such as PREM, specified in terms of low-order polynomials in radius this is a simple matter, but for a model specified pointwise a suitable interpolation scheme (e.g., cubic splines) must be chosen.

2. Partial Derivatives with Respect to Model Parameters

Let us suppose that the Earth model is specified by a number of parameters η_i. These may be, for example, polynomial coefficients or values of wave velocities at specific radii. Having specified an interpolation scheme, we have

$$A(r) = A(r, \eta_i)$$

$$C(r) = C(r, \eta_i) \quad \text{etc.}$$

and

$$q_\tau = q_\tau(p, r, \eta_i)$$

$$q_T = q_T(p, r, \eta_i)$$

$$q_\Delta = q_\Delta(p, r, \eta_i) \quad . \tag{III-16}$$

In order to incorporate travel-time data into a linearized inversion technique for the estimation of the model parameters η_i, it is necessary to find expressions for $(\partial T/\partial \eta)_\Delta$, where the subscript indicates the variable to be held constant in the partial differentiation and where η denotes any one of the parameters η_i. Julian and Anderson[18] have shown in the case of isotropy that

$$\left(\frac{\partial T}{\partial \eta}\right)_\Delta = \left(\frac{\partial \tau}{\partial \eta}\right)_p \tag{III-17}$$

where τ is the intercept time [Eq. (III-1)], and this result can be immediately extended to the present case; we have

$$dT = \left(\frac{\partial T}{\partial p}\right)_\eta dp + \left(\frac{\partial T}{\partial \eta}\right)_p d\eta$$

$$= p\left(\frac{\partial \Delta}{\partial p}\right)_\eta \left[\left(\frac{\partial p}{\partial \Delta}\right)_\eta d\Delta + \left(\frac{\partial p}{\partial \eta}\right)_\Delta d\eta\right] + \left(\frac{\partial T}{\partial \eta}\right)_p d\eta \tag{III-18}$$

using $p = dT/d\Delta$. Thus,

$$\left(\frac{\partial T}{\partial \eta}\right)_\Delta = \left(\frac{\partial T}{\partial \eta}\right)_p + p\left(\frac{\partial \Delta}{\partial p}\right)_\eta \left(\frac{\partial p}{\partial \eta}\right)_\Delta \quad .$$

But,

$$d\Delta = \left(\frac{\partial \Delta}{\partial p}\right)_\eta \, dp + \left(\frac{\partial \Delta}{\partial \eta}\right)_p \, d\eta$$

so that

$$\left(\frac{\partial p}{\partial \eta}\right)_\Delta = - \frac{\left(\frac{\partial \Delta}{\partial \eta}\right)_p}{\left(\frac{\partial \Delta}{\partial p}\right)_\eta}$$

whence

$$\left(\frac{\partial T}{\partial \eta}\right)_\Delta = \left(\frac{\partial T}{\partial \eta}\right)_p - p\left(\frac{\partial \Delta}{\partial \eta}\right)_p = \left(\frac{\partial \tau}{\partial \eta}\right)_p \qquad \text{(III-19)}$$

as stated in Eq. (III-17).

Using Eq. (III-17) it is straightforward, but again algebraically involved, to calculate the partial derivatives of travel times with respect to a model parameter η. We have simply:

$$\left(\frac{\partial T}{\partial \eta}\right)_\Delta = \int \left(\frac{\partial q_\tau}{\partial \eta}\right)_p dr \quad ;$$

the integrand is singular but integrable, and the integrals may be evaluated using the transformation Eq. (III-9). This causes no difficulty if it is desired simply to estimate the model parameters η_i as implicitly assumed here. Since the integrands are not square integrable, however, it is not possible to apply directly the apparatus of Backus-Gilbert inverse theory. The solution to this difficulty has been given by Johnson and Gilbert[19] who have shown that integration by parts may be used to recast the problem in terms of square integrable kernels – a technique which could also be applied in the present case.

A computer program has been developed to perform the calculations outlined here, for an arbitrary seismic phase and source depth, under the assumption that the model is parameterized in the same way as the PREM model of Dziewonski and Anderson.[16]

J. H. Woodhouse
T. P. Girnius

C. THE EXCITATION OF SEISMIC WAVES BY A SOURCE POSSESSING NON-NEGLIGIBLE SECOND GLUT MOMENTS

The technique of Dziewonski, Chou, and Woodhouse[20,21] for the routine estimation of seismic moment tensors, centroid locations, and centroid times, using long-period SRO data has been extended in several ways in order to gain more information about seismic sources not adequately modeled by point sources in space and time. These extensions, described here and in previous SATSs,[20,22] have included the estimation of source duration and rupture velocity, the simultaneous inversion for a number of point sources, and the "mapping" of complex events. It is the purpose of this contribution to give results for the excitation of seismic waves by sources possessing non-negligible glut moments which, it is hoped, will enable certain properties of these second-moment tensors to be estimated from the data. This development is appealing, in that the second-moment tensors contain, in a unified way, information on the spatial extent, duration, and propagation velocity of a seismic source. Backus[23] has considered in detail the properties of these moment tensors which are theoretically determinable under a number of different sets of assumptions. Our numerical experiments, which will not be discussed fully

here, suggest that in practice there are other indeterminacies which remain to be investigated. Nevertheless, we feel that to pose questions about the spatial and temporal extent of a seismic source in terms of its second-moment tensors is a useful exercise, in that if the inner-product matrix and corresponding right-hand vector are once calculated for the estimation of the second-moment tensor components from a given set of seismograms, they represent (in a highly condensed form) the sum of information in the data about the size and duration properties of the event. It is then possible to use the calculated inner-product matrix to test various models of or assumptions about the earthquake, or to invert the data under different assumptions.

The seismic displacement of a spherically asymmetric Earth model due to any indigenous source may be written

$$\underline{u}(x, t) = \sum_k \underline{s}_k(x) \int_{-\infty}^{t} dt' \int_{V_s} d^3x' h_k(t - t') \, \underline{\bar{e}}^{(k)}(\underline{x}') : \dot{\Gamma}(\underline{x}', t) \tag{III-20}$$

(for notation, see Ref. 21). Expanding $h_k(t - t') \, \underline{\bar{e}}^{(k)}(\underline{x}')$ about a fiducial point $\underline{x}' = \underline{x}_s$ in the source region and a fiducial time $t' = t_s$ close to the origin time, we obtain[24]

$$\begin{aligned} \underline{u}(x, t) = \sum_k \underline{s}_k(x) \Big\{ & h_k(t - t_s) \, [M_{ij}^{(0,0)} \bar{e}_{ij}^{(k)} + M_{ijp}^{(1,0)} \bar{e}_{ij,p}^{(k)} + \tfrac{1}{2} M_{ijpq}^{(2,0)} \bar{e}_{ij,pq}^{(k)}] \\ & - \dot{h}_k(t - t_s) \, [M_{ij}^{(0,1)} \bar{e}_{ij}^{(k)} + M_{ijp}^{(1,1)} \bar{e}_{ij,p}^{(k)}] \\ & + \ddot{h}_k(t - t_s) \cdot \tfrac{1}{2} M^{(0,2)} \bar{e}_{ij}^{(k)} \Big\} \end{aligned} \tag{III-21}$$

where the modal strains $\bar{e}_{ij}^{(k)}$ and strain gradients $\bar{e}_{ij,p}^{(k)}, \bar{e}_{ij,pq}^{(k)}$ are those evaluated at the fiducial point. The superscripts on the various glut moment tensors indicate, respectively, the spatial and temporal degrees of the moments,[23,24] e.g.,

$$\begin{aligned} M_{ij}^{(0,0)} &= \int_{-\infty}^{\infty} dt \int_{V_s} d^3x \dot{\Gamma}_{ij}(\underline{x}, t) \\ M_{ijpq}^{(2,0)} &= \int_{-\infty}^{\infty} dt \int_{V_s} d^3x (x_p - x_{sp}) \, (x_q - x_{sq}) \, \dot{\Gamma}_{ij}(\underline{x}, t) \\ M_{ijp}^{(1,1)} &= \int_{-\infty}^{\infty} dt \int_{V_s} d^3x (t - t_s) \, (x_p - x_{sp}) \, \dot{\Gamma}_{ij}(\underline{x}, t) \end{aligned} \tag{III-22}$$

and others similarly. Following Gilbert and Dziewonski[25] and Dziewonski et al.,[21] Eq.(III-21) leads to a straightforward evaluation of synthetic seismograms in terms of the spherical components of the moment tensors, when the spherical components of the strains and strain gradients are known. The calculation is most economical if performed in a coordinate system in which the source is at the pole ($\Theta = 0$). The relevant formulas for $\bar{e}_{ij}, \bar{e}_{ij,p}$ have been given in Refs. 25 and 21. It remains to list the corresponding formulas for the second derivatives $\bar{e}_{ij,pq}$, and the spherical components of this fourth-rank tensor are listed in Table III-1. They have been obtained using the formalism of Phinney and Burridge.[26]

TABLE III-1

SPHERICAL COMPONENTS OF THE SECOND-STRAIN GRADIENT TENSOR

	Spheroidal					Toroidal				
	$m = 0$	$m = \pm 1$	$m = \pm 2$	$m = \pm 3$	$m = \pm 4$	$m = 0$	$m = \pm 1$	$m = \pm 2$	$m = \pm 3$	$m = \pm 4$
$E_{11} = \bar{e}_{rrrr}$	$k_o{}^s1$									
$E_{21} = \bar{e}_{\theta\theta rr}$	$-k_o{}^s17$		$k_2{}^s5$					$\mp ik_2{}^t5$		
$E_{31} = \bar{e}_{\phi\phi rr}$	$-k_o{}^s17$		$-k_2{}^s5$					$\pm ik_2{}^t5$		
$E_{41} = 2\bar{e}_{r\theta rr}$		$-2k_1{}^s11$					$\pm 2ik_1{}^t11$			
$E_{51} = 2\bar{e}_{r\phi rr}$		$\pm 2ik_1{}^s11$					$2k_1{}^t11$			
$E_{61} = 2\bar{e}_{\theta\phi rr}$			$\mp 2ik_2{}^s5$					$-2k_2{}^t5$		
$E_{12} = \bar{e}_{rr\theta\theta}$	$-k_o{}^s4$		$k_2{}^s3$					$\mp ik_2{}^t3$		
$E_{22} = \bar{e}_{\theta\theta\theta\theta}$	$k_o(\frac{1}{2}{}^s10 + {}^s20)$		$-k_2({}^s9 + {}^s19)$		$k_4{}^s8$			$\pm ik_2({}^t9 + {}^t19)$		$\mp ik_4{}^t8$
$E_{32} = \bar{e}_{\phi\phi\theta\theta}$	$k_o(-\frac{1}{2}{}^s10 + {}^s20)$		$k_2({}^s9 - {}^s19)$		$-k_4{}^s8$			$\mp ik_2({}^t9 - {}^t19)$		$\pm ik_4{}^t8$
$E_{42} = 2\bar{e}_{r\theta\theta\theta}$		$k_1({}^s16 + 2{}^s15)$		$-2k_3{}^s14$			$\mp ik_1({}^t16 + 2{}^t15)$		$\pm 2ik_3{}^t14$	
$E_{52} = 2\bar{e}_{r\phi\theta\theta}$		$\pm ik_1({}^s16 - 2{}^s15)$		$\pm 2ik_3{}^s14$			$k_1({}^t16 - 2{}^t15)$		$2k_3{}^t14$	
$E_{62} = 2\bar{e}_{\theta\phi\theta\theta}$			$\pm 2ik_2{}^s9$		$\mp 2ik_4{}^s8$	$-k_o{}^t10$		$2k_2{}^t9$		$-2k_4{}^t8$
$E_{13} = \bar{e}_{rr\phi\phi}$	$-k_o{}^s4$		$-k_2{}^s3$					$\pm ik_2{}^t3$		
$E_{23} = \bar{e}_{\theta\theta\phi\phi}$	$k_o(-\frac{1}{2}{}^s10 + {}^s20)$		$k_2(-{}^s9 + {}^s19)$		$-k_4{}^s8$			$\mp ik_2(-{}^t9 + {}^t19)$		$\pm ik_4{}^t8$
$E_{33} = \bar{e}_{\phi\phi\phi\phi}$	$k_o(\frac{1}{2}{}^s10 + {}^s20)$		$k_2({}^s9 + {}^s19)$		$k_4{}^s8$			$\mp ik_2({}^t9 + {}^t19)$		$\mp ik_4{}^t8$
$E_{43} = 2\bar{e}_{r\theta\phi\phi}$		$k_1(-{}^s16 + 2{}^s15)$		$2k_3{}^s14$			$\pm ik_1({}^t16 - 2{}^t15)$		$\mp 2ik_3{}^t14$	
$E_{53} = 2\bar{e}_{r\phi\phi\phi}$		$\mp ik_1({}^s16 + 2{}^s15)$		$\mp 2ik_3{}^s14$			$-k_1({}^t16 + 2{}^t15)$		$-2k_3{}^t14$	
$E_{63} = 2\bar{e}_{\theta\phi\phi\phi}$			$\pm 2ik_2{}^s9$		$\pm 2ik_4{}^s8$	$k_o{}^t10$		$2k_2{}^t9$		$2k_4{}^t8$
$E_{14} = 2\bar{e}_{rrr\theta}$		$-2k_1{}^s2$					$\pm 2ik_1{}^t2$			
$E_{24} = 2\bar{e}_{\theta\theta r\theta}$		$k_1({}^s7 + 2{}^s18)$		$-2k_3{}^s6$			$\mp ik_1({}^t7 + 2{}^t18)$		$\pm 2ik_3{}^t6$	
$E_{34} = 2\bar{e}_{\phi\phi r\theta}$		$k_1(-{}^s7 + 2{}^s18)$		$2k_3{}^s6$			$\pm ik_1({}^t7 - 2{}^t18)$		$\mp 2ik_3{}^t6$	
$E_{44} = 4\bar{e}_{r\theta r\theta}$	$-4k_o{}^s13$		$4k_2{}^s12$					$\mp 4ik_2{}^t12$		
$E_{54} = 4\bar{e}_{r\phi r\theta}$			$\mp 4ik_2{}^s12$			$4k_o{}^t13$		$-4k_2{}^t12$		
$E_{64} = 4\bar{e}_{\theta\phi r\theta}$		$\mp 2ik_1{}^s7$		$\pm 4ik_3{}^s6$			$-2k_1{}^t7$		$4k_3{}^t6$	
$E_{15} = 2\bar{e}_{rrr\phi}$		$\pm 2ik_1{}^s2$					$2k_1{}^t2$			
$E_{25} = 2\bar{e}_{\theta\theta r\phi}$		$\pm ik_1({}^s7 - 2{}^s18)$		$\pm 2ik_3{}^s6$			$k_1({}^t7 - 2{}^t18)$		$2k_3{}^t6$	
$E_{35} = 2\bar{e}_{\phi\phi r\phi}$		$\mp ik_1({}^s7 + 2{}^s18)$		$\mp 2ik_3{}^s6$			$-k_1({}^t7 + 2{}^t18)$		$-2k_3{}^t6$	
$E_{45} = 4\bar{e}_{r\theta r\phi}$			$\mp 4ik_2{}^s12$			$-4k_o{}^t13$		$-4k_2{}^t12$		
$E_{55} = 4\bar{e}_{r\phi r\phi}$	$-4k_o{}^s13$		$-4k_2{}^s12$					$\pm 4ik_2{}^t12$		
$E_{65} = 4\bar{e}_{\theta\phi r\phi}$		$2k_1{}^s7$		$4k_3{}^s6$			$\mp 2ik_1{}^t7$		$\mp 4ik_3{}^t6$	
$E_{16} = 2\bar{e}_{rr\theta\phi}$			$\mp 2ik_2{}^s3$					$-2k_2{}^t3$		
$E_{26} = 2\bar{e}_{\theta\theta\theta\phi}$			$\pm 2ik_2{}^s19$		$\mp 2ik_4{}^s8$	$k_o{}^t10$		$2k_2{}^t19$		$-2k_4{}^t8$
$E_{36} = 2\bar{e}_{\phi\phi\theta\phi}$			$\pm 2ik_2{}^s19$		$\pm 2ik_4{}^s8$	$-k_o{}^t10$		$2k_2{}^t19$		$2k_4{}^t8$
$E_{46} = 4\bar{e}_{r\theta\theta\phi}$		$\mp 2ik_1{}^s16$		$\pm 4ik_3{}^s14$			$-2k_1{}^t16$		$4k_3{}^t14$	
$E_{56} = 4\bar{e}_{r\phi\theta\phi}$		$2k_1{}^s16$		$4k_3{}^s14$			$\mp 2ik_1{}^t16$		$\mp 4ik_3{}^t14$	
$E_{66} = 4\bar{e}_{\theta\phi\theta\phi}$	$2k_o{}^s10$				$-4k_4{}^s8$					$\pm 4ik_4{}^t8$

The constants k_n are[21]

$$k_n = \frac{1}{2^n} \left\{ \frac{2\ell + 1}{4\pi} \cdot \frac{(\ell + n)!}{(\ell - n)!} \right\}^{1/2} \quad . \tag{III-23}$$

The quantities s_i for spheroidal modes and t_i for toroidal modes are of the form

$$s_i = a_1 \dddot{U} + a_2 r^{-1} \ddot{U} + a_3 r^{-2} \dot{U} + a_4 r^{-3} U$$

$$+ a_5 \ddot{V} + a_6 r^{-1} \dot{V} + a_2 r^{-2} \dot{V} + a_8 r^{-3} V$$

$$t_i = a_1 \dddot{W} + a_2 r^{-1} \ddot{W} + a_3 r^{-2} \dot{W} + a_4 r^{-3} W \tag{III-24}$$

etc., where U, V, and W are scalar eigenfunctions evaluated at the source depth. The coefficients a_i are listed for spheroidal modes in Table III-2 and for toroidal modes in Table III-3. It may be noted that, as a result of the compatibility relations,

$$e_{ij,k\ell} + e_{k\ell,ij} = e_{ik,j\ell} + e_{j\ell,ik} \quad . \tag{III-25}$$

We have

$$s_{17} + s_4 = 2s_{13} \qquad t_3 + t_5 = 2t_{12}$$

$$s_3 + s_5 = 2s_{12} \qquad t_{16} + t_7 = t_{18} + t_{15}$$

$$s_{10} = s_{20}$$

$$s_{16} + s_7 = s_{18} + s_{15}$$

In Tables III-2 and III-3

$$L \equiv \ell(\ell + 1)$$

where ℓ is angular order.

J. H. Woodhouse

D. INTERMEDIATE- AND LONG-PERIOD SOURCE MECHANISMS OF SEVERAL RECENT EARTHQUAKES

In the last SATS,[22] we described how the approach of Dziewonski, Chou, and Woodhouse[21] can be extended to incorporate, in the search for the earthquake source mechanism, information on excitation at very long periods. In the original application,[21] only the intermediate-period data (~60 s) on excitation of the minor arc body waves were used. Here, we wish to show solutions for two major earthquakes ($M_s > 7$) and also for a cluster of events in southern Greece, which gives an opportunity to examine our location procedure.

One of the important features of the centroid method is that, in addition to yielding a moment-tensor solution, it also provides information on the epicentral location, depth, and origin time of the best point source. Because we view the earthquakes through, as if, a somewhat distorting lens – lateral heterogeneities – the apparent position of the source may not coincide with its true location. Functionals of the Earth's structure employed to locate earthquakes using arrival times of P-waves and using the centroid method are quite different. Therefore, the answers may be biased in a different way. Because the centroid method is primarily used to obtain

TABLE III-2

SPHEROIDAL-MODE PARAMETERS USED IN TABLE III-1

Mode	$\ddot{U}$	$r^{-1}\ddot{U}$	$r^{-2}\dot{U}$	$r^{-3}U$	$\ddot{V}$	$r^{-1}\ddot{V}$	$r^{-2}\dot{V}$	$r^{-3}V$
s_1	1							
s_2		1	−2	2		−1	2	−2
s_3			1	−2			−2	4
s_4		−1	$\frac{1}{2}L + 2$	$-(L + 2)$			$-L$	$2L$
s_5						1	−2	2
s_6							1	−2
s_7			−1	2		−1	$\frac{1}{2}L + 1$	$-L$
s_8								1
s_9				−1			−2	$\frac{1}{2}L + 1$
s_{10}			2	$-(L + 2)$			$-L$	$\frac{1}{4}L(L + 6)$
s_{11}		$\frac{1}{2}$	−1	1	$\frac{1}{2}$	$-\frac{1}{2}$	1	−1
s_{12}			$\frac{1}{2}$	−1		$\frac{1}{2}$	−2	3
s_{13}		−1	$\frac{1}{4}L + 2$	$-\frac{1}{2}L - 2$		$+\frac{1}{4}L$	$-L$	$\frac{3}{2}L$
s_{14}				$\frac{1}{2}$			$\frac{1}{2}$	$-\frac{5}{2}$
s_{15}			$-\frac{3}{2}$	$\frac{1}{4}L + \frac{5}{2}$		$-\frac{1}{2}$	$\frac{1}{4}L + \frac{3}{2}$	$-\frac{5}{4}L - \frac{1}{2}$
s_{16}			−2	$\frac{1}{4}L + \frac{7}{2}$			$\frac{1}{4}L + \frac{3}{2}$	$-\frac{5}{4}L - \frac{3}{2}$
s_{17}		−1	2	−2		$\frac{1}{2}L$	$-L$	L
s_{18}			$-\frac{3}{2}$	3		$-\frac{1}{2}$	$\frac{1}{2}L + 1$	$-(L + 1)$
s_{19}				−2			−1	$+\frac{1}{2}L + 2$
s_{20}			2	$-L - 2$			$-L$	$\frac{1}{4}L(L + 6)$

TABLE III-3

TOROIDAL-MODE PARAMETERS USED IN TABLE III-1

Mode	$\ddot{W}$	$r^{-1}\ddot{W}$	$r^{-2}\dot{W}$	$r^{-3}W$
t_2		-1	2	-2
t_3			-2	4
t_5		1	-2	2
t_6			1	-2
t_7		-1	$\frac{1}{2}L + 1$	$-L$
t_8				1
t_9			-2	$\frac{1}{2}L + 1$
t_{10}			$-L$	$\frac{1}{4}L(L + 2)$
t_{11}	$\frac{1}{2}$	$-\frac{1}{2}$	1	-1
t_{12}		$\frac{1}{2}$	-2	3
t_{13}		$\frac{1}{4}L$	$-\frac{1}{2}L$	$\frac{1}{2}L$
t_{14}			$\frac{1}{2}$	$-\frac{5}{2}$
t_{15}		$-\frac{1}{2}$	$\frac{1}{4}(L + 6)$	$-\frac{3}{4}L - \frac{1}{2}$
t_{16}			$-\frac{1}{4}L + \frac{3}{2}$	$+\frac{1}{4}L - \frac{3}{2}$
t_{18}		$-\frac{1}{2}$	1	-1
t_{19}			-1	2

information on the source mechanism and the answers depend on the assumed position of the source (see synthetic example in Ref. 21), it is possible to think of the role of our relocation procedure as the means to minimize in the least-square sense the first moment of the stress glut.[23,24] This, regardless of the physical meaning of the spatio-temporal shift in the apparent position of the source, leads to better estimates of the zeroth moment, commonly referred to as the seismic moment tensor. Without providing a rigorous proof of this statement, we shall show an example that illustrates its apparent validity.

1. The El Asnam, Algeria Earthquake of 10 October 1980

This event, with a surface-wave magnitude of 7.3, caused the death of at least 5000 people. The reported length of the surface rupture was 42 km. Our solution, obtained using both GDSN (Global Digital Seismograph Network) and IDA (International Deployment of Accelerometers) data, is summarized in Table III-4 and the nodal plane solution corresponding to the major double-couple is shown in Fig. III-5. The seismic moment, for the focal depth of 10 km, is about 4.5×10^{26} dyn-cm, substantially less than the 1.4×10^{27} reported by Baranowski et al.[27] Although our moment could be doubled, if a sub-Moho depth were to be assumed,[28] there is no reason to expect that much of the radiation was due to the fracture at sub-crustal depths.

Table III-4 shows the moment-tensor solution obtained using the starting coordinates (NEIS, 10 s added to allow for the finite duration) and the final centroid location. There is not much difference between the two, because the position of the epicenter changed very little (depth was held at 10 km) – less than 20 km. The similarity of the two solutions can also be appreciated in Fig. III-5.

Figures III-6(a) through (c) and III-7 show comparison of the observed and synthetic seismograms for the GDSN and IDA data, respectively. The match for the GDSN data is highly satisfactory, and it is difficult to imagine that our estimate of the moment could be grossly wrong. In Fig. III-7, the match for station ERM (Japan) is poor, but this station is close to the nodal plane for Rayleigh waves. When the observed amplitudes are large (TWO, RAR, CMO), the agreement between the observed and computed seismograms is highly satisfactory.

2. The Eureka, California Earthquake of 8 November 1980

This event, given an M_S of 7.2 by the NEIS, occurred offshore and caused very little damage, considering its magnitude. It is probably the largest earthquake in California since the Kern County series of 1952.

Figure III-8 shows the distribution of the stations used to study this event. Table III-5 gives the numerical details of the solution, and Fig. III-9 shows the nodal plane solutions for the major double-couple for the starting (NEIS) and final (centroid) locations of the source. Unlike for the El Asnam earthquake, the difference between the two solutions is significant. The position of the centroid is shifted nearly 80 km due West, and this change in location has significant impact on the source geometry derived in inversion. The final solution is a nearly perfect strike-slip, in accordance with the tectonic evidence. The starting solution, on the other hand, has a very large dip-slip component. Our final solution agrees very closely with that obtained for this earthquake by Lay et al.[29]

It is quite clear that the NEIS location was not wrong by 80 km. Also, there is an indication from the distribution of aftershocks that the fault was bilateral. Thus, the apparent change in

TABLE III-4

ALGERIAN EARTHQUAKE OF 10 OCTOBER 1980†

		Starting	Final
Origin Time		12:25:23.5+10	12:25:33.5
Latitude (°N)		36.20	36.20
Longitude (°E)		1.35	1.58
Depth (km)		10	(10)
M_{rr}		3.74 ± 0.08	3.41 ± 0.05
$M_{\theta\theta}$		−2.65 ± 0.13	−2.48 ± 0.09
$M_{\phi\phi}$		−1.09 ± 0.21	−0.85 ± 0.07
$M_{r\theta}$		−1.10 ± 0.21	−0.85 ± 0.17
$M_{r\phi}$		−1.16 ± 0.20	−1.58 ± 0.17
$M_{\theta\phi}$		−2.53 ± 0.08	−2.51 ± 0.06
Principal Axes T-Axis	Moment	4.24	3.92
	Plunge/AZM	74°/102°	72°/91°
N-Axis	Moment	0.68	0.74
	Plunge/AZM	10°/230°	13°/229°
P-Axis	Moment	−4.92	−4.67
	Plunge/AZM	12°/322°	11°/322°

† Scale factor is 10^{26} dyn-cm.

TABLE III-5

EUREKA EARTHQUAKE OF 8 NOVEMBER 1980†

		Starting	Final
	Origin Time	10:27:33.4+10	10:27:45.6
	Latitude (°N)	41.16	41.21
	Longitude (°W)	124.34	125.40
	Depth (km)	14	(14)
	M_{rr}	2.78 ± 0.14	−1.27 ± 0.14
	$M_{\theta\theta}$	−5.90 ± 0.21	−8.61 ± 0.20
	$M_{\phi\phi}$	5.62 ± 0.19	9.87 ± 0.18
	$M_{r\theta}$	5.46 ± 0.28	0.22 ± 0.38
	$M_{r\phi}$	6.97 ± 0.28	0.19 ± 0.46
	$M_{\theta\phi}$	2.58 ± 0.16	4.30 ± 0.17
Principal Axes T-Axis	Moment	11.99	10.84
	Plunge/AZM	36°/290°	1°/282°
Principal Axes N-Axis	Moment	−2.76	−1.27
	Plunge/AZM	36°/52°	88°/55°
Principal Axes P-Axis	Moment	−9.23	−9.57
	Plunge/AZM	34°/172°	1°/192°

† Scale factor is 10^{26} dyn-cm.

position is an artifact of lateral heterogeneity. Yet, shifting the epicenter to this location helps derive the correct moment tensor. In particular, the anomalously large elements $M_{r\phi}$ and $M_{r\theta}$ become zero, for all practical purposes. This is important, because these two elements yield notoriously unstable values for shallow earthquakes.[30] It has been thought that the small values of the tangential strain near the surface are the cause of this instability. In a way this is true, because the tangential stress must vanish at the free surface. But our result indicates that lateral heterogeneity seriously compounds the problem. The explanation of this effect follows.

In the epicentral coordinate system, excitation of seismic waves due to the elements $M_{r\theta}$ and $M_{r\phi}$ (dip-slip components) is governed by the spherical harmonic Y_ℓ^1 or $(\partial/\partial\theta)\, Y_\ell^1$. In the asymptotic limit, these are shifted in phase by 90° with respect to Y_ℓ^0, Y_ℓ^2 or their derivatives, which enter into the expressions for excitation due to the remaining four independent components of the moment tensor. Thus, introduction of a finite (dip-slip) fault motion may mimic a phase shift. Because the amplitude due to these terms varies as $\cos\phi$ or $\sin\phi$, the amount of the phase shift will vary like $\cos(\phi + \epsilon)$. This is similar to the phase shift introduced by a change in the epicentral coordinates of the point source,[22] or the equivalent velocity anomaly. Yet, the latter effect does not produce the amplitude effects that introduction of $M_{r\theta}$ and $M_{r\phi}$ does. Therefore, in inversion which allows for shift in locations of the source, the effect of a true or apparent shift of the epicenter can be separated from the excitation pattern due to the dip-slip elements of the moment tensor. On the other hand, in inversion in which epicentral coordinates are fixed, as they are in all other inversion techniques and in the starting iteration of our method, the effect of lateral heterogeneity may be readily absorbed by an artificial contribution to $M_{r\theta}$ and $M_{r\phi}$.

The large apparent westward shift of the epicenter of the Eureka earthquake is not an exception; a nearly identical shift is obtained for the Mexicale earthquake of 15 October 1979. It may be possible, therefore, to anticipate this correction for the strike-slip earthquakes in this region of the west coast of North America.

Figures III-10(a) through (c) and III-11 show comparison between the observed and synthetic seismograms for the Eureka earthquake.

3. Three Earthquakes in Southern Greece

An earthquake of magnitude M_S = 6.7 on 24 February 1981 was followed by two other large shocks: M_S = 6.4 on 25 February, and 6.5 on 4 March. The PDE locations indicate that all these events are within 20 to 30 km of each other, and it occurred to us that this may represent an opportunity to test the relative accuracy of our relocation procedure. Because these events were so closely spaced in time, the network coverage was essentially constant for all three earthquakes. Only the GDSN network was used; IDA data are not yet available. Table III-6 lists the results of inversion and Fig. III-12 shows the fault-plane solution, indicating that all three events were associated with normal faulting.

Figure III-13 is a comparison of PDE locations (crosses) with the relocation result (solid circles). There is an overall shift of locations toward the southwest; this may well be a large-scale effect of the lateral heterogeneity: the Yugoslavian earthquake of 15 April 1979 and the Italian event of 23 November 1980 showed westward and southwestward shifts, respectively.[22] In addition, however, the relative positions of individual events have changed after inversion. While the PDE locations do not show any consistent pattern with respect to the strike of the

TABLE III-6

RELOCATION PARAMETERS AND THE ELEMENTS OF THE MOMENT TENSOR FOR THREE RECENT EARTHQUAKES IN SOUTHERN GREECE†

		24 February 1981	25 February 1981	4 March 1981
NEIS	Origin Time	20:53:38.7	2:35:53.3	21:58:07.5
	Latitude (°N)	38.24	38.11	38.31
	Longitude (°E)	23.02	23.11	23.18
Relocation	δt_0	7.9	5.4	6.3
	Latitude (°N)	37.91	37.93	38.01
	Longitude (°E)	22.60	23.00	22.98
	M_{rr}	−1.21 ± 0.03	−0.39 ± 0.01	−0.33 ± 0.01
	$M_{\theta\theta}$	1.40 ± 0.04	0.40 ± 0.01	0.32 ± 0.02
	$M_{\phi\phi}$	−0.20 ± 0.03	−0.01 ± 0.01	0.01 ± 0.01
	$M_{r\theta}$	0.00 ± 0.06	−0.06 ± 0.02	0.00 ± 0.03
	$M_{r\phi}$	−0.45 ± 0.04	−0.05 ± 0.02	−0.11 ± 0.02
	$M_{\theta\phi}$	−0.06 ± 0.03	0.16 ± 0.01	0.12 ± 0.01
Principal Axes T-Axis	Moment	1.41	0.46	0.36
	Plunge/AZM	0°/2°	5°/160°	3°/160°
Principal Axes N-Axis	Moment	−0.03	−0.07	0.01
	Plunge/AZM	21°/93°	4°/70°	17°/69°
Principal Axes P-Axis	Moment	−1.38	−0.39	−0.37
	Plunge/AZM	69°/271°	84°/301°	73°/261°

† The hypocentral depth has been held fixed at 15 km. The scale factor of 10^{26} dyn-cm is common for all moment values.

fault, the events of 25 February and 4 March are located along the strike axis of the initial earthquake. Unless this is a coincidence, the conclusion should be that one may obtain quite precise relative locations by matching the waveforms of GDSN recordings; data from fourteen SRO, ASRO, and DWWSSN stations were used in inversion.

A. M. Dziewonski

E. PARAMETER SPACE SEARCH FOR THE LOCATION OF THE BEST POINT SOURCE

Dziewonski, Chou, and Woodhouse[21] have developed a procedure that allows simultaneous determination of the moment tensor and estimation of the location of the best point source using long-period (~60 s) waveform data from the GDSN. Because their method, like all other location algorithms, involves linearization of the problem, the convergence of the solution depends on the condition that the starting hypocentral coordinates be linearly close to the true position of the source in space and time. After having obtained satisfactory results for numerous sources (see Ref. 21), we have encountered an earthquake for which it seemed impossible, starting with the NEIS hypocentral coordinates, to obtain a solution that would give a good fit to the data and yield a moment tensor consistent with the geological and geophysical evidence. This was the St. Elias earthquake of 28 February 1979.

The inference was that this must have been a complex event of considerable spatio-temporal dimensions. As the hypocentral coordinates determined from the times of the P-wave arrivals led to unrealistic answers, the alternative was to perform a parameter space search. Such a search, if the procedure of Ref. 21 were to be applied to each starting solution, could be extremely time consuming. The subject here is an algorithm that allows us to speed up this process by a factor of 100 or more.

Given the origin time, epicentral coordinates, and depth, the inverse problem for the moment tensor of a point source is derived from the following equations of condition:

$$u_k(\underline{r}, t) = \sum_{i=1}^{6} \psi_{ki}(\underline{r}, r_s, t) \cdot f_i \qquad \text{(III-26)}$$

where u_k is the k^{th} record in the set of seismograms used in inversion, ψ_{ki} are the excitation kernels, and f_i are the elements of the moment tensor.

The least-squares condition leads to normal equations of the following form:

$$\underline{\underline{A}} \cdot \underline{f} = \underline{b} \qquad \text{(III-27)}$$

where an element of the inner product matrix $\underline{\underline{A}}$ is:

$$A_{ij} = \sum_k \int_{t_{1_k}}^{t_{2_k}} \psi_{ki}(t)\, \psi_{kj}(t)\, dt \qquad \text{(III-28)}$$

and an element of the $\underline{b}$ vector is:

$$b_j = \sum_k \int_{t_{1_k}}^{t_{2_k}} u_k(t) \cdot \psi_{kj}(t)\, dt \quad . \qquad \text{(III-29)}$$

There is an important difference between the changes of the matrix $\underline{\underline{A}}$ and vector $\underline{b}$ with respect to perturbations in the location and the origin time: the matrix $\underline{\underline{A}}$ changes slowly, or is relatively insensitive to moderate changes in hypocentral parameters; the vector $\underline{b}$, on the other hand, changes rapidly.

The general proof of the statement above may be difficult, but the following example seems convincing. Assume that we consider an isolated P-wave with the accompanying pP and sP pulses with a dominant period of 1 s. Let us say that our station is at a distance 80° from the epicenter. If we now change the distance to 81°, the integrals (III-28) will change very little, because the synthetic pulses will be shifted by the same amount of time, and amplitudes of P-waves at 80° change very slowly with distance. At the same time, there will be a very significant change in the result of calculation of the elements of the $\underline{b}$ vector, as the observed and synthetic pulses will be shifted with respect to each other by more than 5 s. It is possible, therefore, to think of a scheme in which we could calculate the matrix $\underline{\underline{A}}$ only once and assume that its value remains constant with respect to moderate changes in location of the source, but $\underline{b}$ would have to be calculated exactly.

Let us consider what enters into the calculation of $\underline{b}$. The excitation functions ψ can be written [see Eqs. (A15) through (A17) in Ref. 21]:

$$\psi_{ik} = \sum_{\ell} \sum_{j} \sigma_j^{(\ell)}(t, r_s)\, c_j^{ki}(\Theta, \phi, \ell) \qquad \text{(III-30)}$$

where r_s is the source radius; the quantities σ represent contributions of the appropriate combinations of eigenfunctions and their derivatives for all overtones of a particular angular order number ℓ.

The vector $\underline{b}$ is therefore:

$$b_i = \sum_{\ell} \sum_{k} \sum_{j} c_j^{ki}(\Theta, \phi, \ell)\, \gamma_{jk}^{(\ell)} \qquad \text{(III-31)}$$

where

$$\gamma_{jk}^{(\ell)} = \int_{t_{1_k}}^{t_{2_k}} u_k \cdot \sigma_j^{(\ell)}(t, r_s)\, dt \quad . \qquad \text{(III-32)}$$

The important property of expression (III-32) is that it does not depend on the epicentral coordinates. It is possible, therefore, to calculate $\gamma_{jk}^{(\ell)}$ only once for a given depth and origin time and then evaluate Eq. (III-31) very rapidly for any position of the source, as only a sum of scalar values is involved, while in evaluation of Eq. (III-32) one must consider 100 to 200 samples, on average. Such a transformation is not possible in the case of matrix $\underline{\underline{A}}$, which is quadratic in functions that depend on the position of the source.

The procedure is as follows. We establish a grid system in the geographical coordinates, calculate $\gamma_{jk}^{(\ell)}$ and $\underline{\underline{A}}$ for the center of the grid ($\underline{r}_c$) and then, very rapidly, find $\underline{b}(\underline{r})$ for each grid point. The solution is then found:

$$\underline{f}(\underline{r}) = \underline{b}(\underline{r}) \cdot \underline{\underline{A}}^{-1}(\underline{r}_c) \quad . \qquad \text{(III-33)}$$

The goodness of fit is approximated by the relative variance:

$$\epsilon = 1 - \sum_{i=1}^{6} \frac{f_i b_i}{\sum_k y_k^2} \qquad \text{(III-34)}$$

where

$$y_k^2 = \int_{t_{1_k}}^{t_{2_k}} u_k^2 dt \quad .$$

It is important to remember that the vector $\underline{f}(\underline{r})$ represents only an approximate solution; thus, it is possible that this estimate of the variance may become negative.

Figure III-14 shows a result of application of the method to a synthetic case, in which a point source (normal fault) has been placed at the center of the grid; the grid spacing is 0.2° of arc. The network coverage is realistic: the same as that used in the investigation of the Irpinia earthquake of 23 November 1980.[22,31] The value of ϵ (the figures indicate $100 \times \epsilon$) indeed reaches a minimum at the location of the point source (cross). The noticeable distortion of contours is the result of uneven network coverage.

In the second synthetic example, we move the source by 1° of longitude and 1° of latitude from the center of the grid. Figure III-15 shows the result. The center of the minimum value of ϵ is only a fraction of the grid spacing away from the "true" position (cross), even though this point is some 150 km away from the grid center (plus sign). However, ϵ assumes negative values; this is the result of the approximation implied by Eq. (III-33). This means that the elements of the moment tensor are somewhat incorrect. But the important result is that the location of the source has been found correctly. Having this location, we can initiate the procedure of Ref. 21, and the exact result will be obtained in one or two iterations.

Shifting the source in time may also produce rather dramatic effects. Because we deal with signals in which energy is concentrated within the range of periods from 50 to 60 s, shifting the origin time by 25 to 30 s may lead to an apparent convergence of the solution but with a wrong sign of the moment tensor; these secondary minima are quite well defined.

Thus, for complex earthquakes of significant duration we produce a series of contour maps, each for different offset in the origin time; a step between 5 and 10 s is reasonable for the frequency band of our analysis. Application of this procedure to the recordings of the St. Elias earthquake by the SRO/ASRO network allows us to locate the position of the best point source some 100 km east of the epicenter and 37.5 s after the origin time determined from the first breaks of the P-waves. This is shown in Fig. III-16.

Having determined the position and time for the best point source, we can now apply the procedure of Dziewonski[22] for the analysis of multiple sources. Since the St. Elias earthquake generated P-waves of significant amplitude, it is reasonable to assume for the first source the origin time and location of the NEIS epicenter, and for the second source the result shown in Fig. III-16. These times and locations change surprisingly little during the inversion. Figure III-17 is a map taken from Stephens et al.[32] The fault-plane solutions corresponding to the "major double-couple" derived from the analysis of the moment tensor are shown at the bottom of the figure.

The first source is a very shallow thrust, in agreement with the nodal-plane solution of Perez and Jacob[33] based on the signs of the P-wave arrivals. The steeply dipping nodal plane of these authors coincides with that of Fig. III-17 within a few degrees; the dip direction of the shallow dipping plane is usually poorly determined. But the second source with the centroid time of 37 s after the origin has a substantially different mechanism. It is a reverse fault, with the fault planes dipping at roughly 45° and a substantial strike-slip component. The sense of slip is consistent with the north-south compression. Thus, our result implies that the source mechanism of the St. Elias earthquake underwent a major change during the faulting process.

Using our procedure, we have also analyzed the Tabas-e-Golshan (Iran) earthquake of 16 September 1978. The best point source was located northeast of the epicenter and some 20 s later. Unfortunately, the network coverage for this event is very uneven, and there are major trade-offs between the geographical coordinates and the origin time. We have fixed the locations of times of three sources, as shown in Fig. III-18, and simply solved for their source mechanism. Again, for the first source we obtain an essentially dip-slip solution, while the second and third sources are reverse faults. As in the case of the St. Elias event, a significant strike-slip component develops near the end of the faulting process. The initial solution is essentially consistent with that obtained by Berberian et al.[34] from the P-wave polarities.

The techniques described in this report provide a tool for resolving very rapidly the essential complexities of large earthquakes. If the data were transmitted in real time, the results for the February 1979 or September 1978 events could be obtained within 3 h after the earthquakes occurred. This could be important for rapid assessment of the damage, as well as for determining the strategy of post-seismic geophysical and geodetic measurements.

A. M. Dziewonski
J. H. Woodhouse

F. PURE-PATH MODELS FROM RAYLEIGH-WAVE DISPERSION IN A FREQUENCY RANGE FROM 1.5 TO 6 mHz

Dziewonski[35] and Dziewonski and Steim[36] have described a new technique of analysis of mantle waves which allows one to extract directly information on the Earth's structure from waveform data. An iterative procedure was designed to perturb the structural elements (both velocity and Q) to improve the transfer function for Rayleigh waves traveling around the world. We have presented examples of application of this technique in the analysis of synthetic as well as real data. We have named this method the "waveform inversion technique (WIT)."

This report describes application of the method to a "pure-path" decomposition of the phase-velocity and Q data. Numerous analyses of this type have been performed in the past.[37-45] The results obtained in these studies have been used to infer the depth to which lateral variations in the elastic and anelastic parameters are correlated with the surficial tectonic nature of a given region. Implications of these inferences can be of fundamental importance to our understanding of the dynamics of the Earth. The results presented in this section might be understood as a test of WIT in application to this type of analysis. Also, there is an indication that extension of measurements to frequencies as low as 1.5 mHz provides important structural constraints.

From a large number of visually examined recordings of the IDA[46] network, we have selected 37 recordings that showed the best SNR. Their northern hemisphere poles are shown in Fig. III-19. The poles have a fairly uniform distribution in longitude, but nearly equatorial

latitudes (corresponding to nearly polar paths) are poorly represented. In the future, particular effort should be made to assure even geographical coverage.

The matching of transfer functions for individual paths was achieved by perturbation of three parameters in shear velocity (constant perturbations in the depth ranges 80 to 220, 220 to 400, and 400 to 670 km) and two in Q (perturbations in the depth ranges from 80 to 400 and 400 to 670 km). The experiments, such as those discussed in our previous reports,[35,36] demonstrated that this parametrization is sufficient to obtain good transfer functions. Clearly, other parametrization schemes, including transverse anisotropy,[16] are feasible. The range of frequencies (angular order numbers) used in inversion was determined through visual examination of the spectra: the total span of the order numbers used is from 7 to 60 (from 800 to 150 s, roughly), but it varied appreciably from record to record. For this reason, one should not anticipate full correspondence between the results of regionalization using either the model or data space.

The regionalization adopted here is based on the work of Mauk[47] who divided the world into 20 types of regions, using a 5° × 5° grid, and considered fractional contributions (with a precision of one-tenth) of individual regions to a given cell. We have combined Mauk's regions into four types: (1) stable continents, including continental shelves, for which tectonic activity ceased at least 400 m.y. ago; (2) tectonic, including island arcs; (3) ocean floors younger than 38 m.y.; and (4) ocean floors older than 38 m.y. Perhaps a more detailed regionalization will be warranted in the future, when the number of paths increases significantly. Figure III-20 is a map of the world schematically showing our regionalization. Fractional contributions for each cell were considered in actual calculation of path compositions.

After the data obtained through application of WIT to individual paths were corrected for ellipticity,[48,49] the pure-path decomposition was calculated using the approach of Toksöz and Anderson.[37] The results for periods of normal modes, group velocities, and Q are presented in Table III-7 for the range of angular order numbers from 9 to 55. The differences of pure-path phase and group velocities from those computed for PREM[16] are shown in Fig. III-21(a-b). Roughness of the curves at frequencies lower than 3 mHz and, in particular, higher than 5 mHz is the result of the fact that data were not available for all paths outside the 3- to 5-mHz range. Except for roughness, there is no overall change in the trend due to variations in path coverage; this indicates the stability of the inverse problem and internal consistency of the data set.

At frequencies higher than 4 mHz, the major differences are between young oceans and tectonic regions on one hand and stable continents and old oceans on the other. This is qualitatively consistent with the results of previous studies of this kind. Phase velocities become very close to each other at the lower frequency range of analysis (1.57 mHz), but then begin to diverge in a rather distinct manner: for stable continents and tectonic regions the phase velocities follow the global average and are very close to each other up to a 3-mHz frequency, while the values for young oceans begin to diverge much earlier. A similar trend can be inferred from the results of Silver and Jordan[44] for the end members of their regionalization of continental and oceanic areas. An intuitive interpretation would imply deep-seated differences in structure beneath the young and old oceans.

The results for pure-path Q indicate that the derived differences are not statistically significant; there is some indication, however, that Q for the continental regions may be higher than for the oceanic ones. We test this hypothesis by decreasing the resolution of the regionalization and distinguish only between continents and oceans. The results are shown in Table III-8 which also contains the properly weighted global average and comparison with the appropriate

TABLE III-7

RESULTS OF PURE-PATH ANALYSIS FOR PERIODS OF NORMAL MODES, GROUP VELOCITIES, AND ATTENUATION

MODE	NORMAL MODE PERIODS								GROUP VELOCITY								ATTENUATION							
	STABLE CONT		TECTONIC		YOUNG OCEAN		OLD OCEAN		STABLE CONT		TECTONIC		YOUNG OCEAN		OLD OCEAN		STABLE CONT		TECTONIC		YOUNG OCEAN		OLD OCEAN	
	PERIOD	S.D. %	PERIOD	S.D. %	PERIOD	S.D. %	PERIOD	S.D. %	GR VEL	S.D. %	GR VEL	S.D. %	GR VEL	S.D. %	GR VEL	S.D. %	Q	S.D. %	Q	S.D. %	Q	S.D. %	Q	S.D. %
9	633.62	0.05	634.22	0.09	634.24	0.06	633.66	0.03	6.228	0.19	6.247	0.38	6.242	0.24	6.253	0.11	319.6	8.4	395.4	20.9	327.9	10.9	319.5	5.1
10	579.32	0.04	579.56	0.06	579.78	0.05	579.31	0.02	5.641	0.15	5.665	0.22	5.649	0.16	5.664	0.07	318.5	7.1	359.3	12.0	341.4	8.4	301.3	3.0
11	537.21	0.05	537.30	0.07	537.44	0.05	536.89	0.02	5.240	0.19	5.262	0.27	5.242	0.21	5.272	0.08	321.3	7.7	325.7	11.1	321.0	8.4	304.9	3.1
12	502.77	0.06	502.67	0.08	502.97	0.06	502.26	0.02	4.982	0.22	5.009	0.31	4.982	0.23	5.023	0.09	317.7	7.6	314.9	10.5	314.0	8.0	297.2	3.0
13	473.67	0.06	473.45	0.09	473.90	0.07	472.99	0.03	4.801	0.25	4.826	0.36	4.790	0.27	4.846	0.11	309.6	7.6	310.8	11.0	307.3	8.1	290.6	3.1
14	448.46	0.06	448.22	0.10	448.98	0.07	447.71	0.03	4.660	0.23	4.678	0.39	4.627	0.27	4.704	0.12	308.7	7.0	303.1	11.2	290.7	7.4	284.0	3.2
15	426.49	0.07	426.20	0.11	427.14	0.08	425.61	0.04	4.532	0.26	4.545	0.43	4.489	0.30	4.578	0.13	304.7	8.0	295.1	12.7	278.0	8.2	275.2	3.6
16	407.08	0.07	406.77	0.13	407.87	0.09	406.09	0.04	4.415	0.27	4.420	0.45	4.360	0.31	4.461	0.14	300.1	9.2	286.6	14.5	265.3	9.2	265.9	4.1
17	389.79	0.08	389.49	0.14	390.72	0.09	388.70	0.04	4.305	0.28	4.306	0.47	4.244	0.33	4.351	0.15	294.8	10.7	277.9	16.6	253.0	10.3	256.5	4.6
18	374.27	0.09	374.01	0.15	375.37	0.10	373.12	0.05	4.204	0.29	4.198	0.48	4.134	0.34	4.246	0.15	288.9	12.2	269.0	18.6	241.3	11.4	247.0	5.2
19	360.21	0.10	360.11	0.16	361.40	0.11	359.12	0.05	4.113	0.28	4.095	0.48	4.038	0.33	4.150	0.15	283.8	13.4	259.3	20.2	232.7	12.2	236.4	5.4
20	347.47	0.10	347.44	0.17	348.82	0.11	346.34	0.05	4.034	0.29	4.001	0.48	3.945	0.33	4.063	0.15	277.1	14.7	250.9	21.9	222.6	13.0	227.6	5.8
21	335.81	0.10	335.88	0.17	337.32	0.12	334.68	0.05	3.958	0.30	3.918	0.51	3.865	0.35	3.986	0.15	270.2	15.8	242.8	23.4	213.6	13.8	219.1	6.2
22	325.09	0.11	325.27	0.18	326.76	0.12	323.98	0.05	3.895	0.32	3.841	0.54	3.796	0.37	3.917	0.16	263.2	16.7	235.2	24.5	205.5	14.4	211.2	6.5
23	315.18	0.11	315.49	0.18	317.00	0.12	314.10	0.06	3.842	0.31	3.779	0.53	3.734	0.36	3.855	0.16	256.2	17.4	228.0	25.5	198.3	14.9	203.9	6.7
24	305.98	0.11	306.42	0.18	307.94	0.12	304.93	0.06	3.796	0.31	3.726	0.53	3.688	0.36	3.799	0.16	249.3	18.0	221.3	26.3	191.9	15.3	197.1	6.9
25	297.39	0.11	297.96	0.18	299.48	0.12	296.40	0.06	3.758	0.33	3.677	0.57	3.646	0.39	3.754	0.17	242.6	18.3	215.0	26.7	186.3	15.6	190.8	7.0
26	289.34	0.11	290.06	0.19	291.56	0.13	288.41	0.06	3.726	0.34	3.638	0.59	3.610	0.40	3.717	0.18	236.0	18.5	209.3	27.0	181.4	15.7	185.1	7.1
27	281.77	0.11	282.64	0.19	284.11	0.13	280.91	0.06	3.700	0.36	3.607	0.63	3.583	0.43	3.686	0.19	229.7	18.6	204.0	27.1	177.1	15.9	179.8	7.1
28	274.64	0.11	275.64	0.19	277.09	0.13	273.85	0.06	3.681	0.38	3.572	0.66	3.557	0.44	3.660	0.20	223.6	18.6	199.0	27.3	173.3	15.9	174.9	7.1
29	267.88	0.11	269.04	0.19	270.44	0.13	267.17	0.06	3.663	0.38	3.555	0.66	3.541	0.45	3.638	0.20	217.8	18.5	194.5	27.2	170.0	16.0	170.4	7.0
30	261.48	0.12	262.77	0.19	264.13	0.13	260.85	0.06	3.653	0.38	3.534	0.66	3.525	0.45	3.624	0.20	212.2	18.3	190.3	27.0	167.1	16.0	166.3	7.0
31	255.39	0.12	256.82	0.20	258.13	0.13	254.84	0.06	3.644	0.38	3.517	0.67	3.512	0.45	3.612	0.20	206.9	18.1	186.4	26.8	164.6	15.9	162.4	6.9
32	249.59	0.12	251.16	0.20	252.41	0.13	249.11	0.06	3.638	0.38	3.507	0.65	3.505	0.44	3.602	0.20	201.9	17.9	182.8	26.7	162.5	15.9	158.9	6.8
33	244.05	0.12	245.75	0.20	246.95	0.14	243.65	0.06	3.635	0.39	3.499	0.67	3.500	0.45	3.596	0.20	197.1	17.6	179.4	26.4	160.6	15.9	155.6	6.8
34	238.76	0.12	240.59	0.21	241.73	0.14	238.43	0.06	3.634	0.38	3.490	0.66	3.495	0.45	3.593	0.20	192.5	17.4	176.3	26.3	159.0	15.9	152.6	6.7
35	233.69	0.13	235.64	0.21	236.73	0.14	233.44	0.07	3.634	0.39	3.486	0.68	3.494	0.46	3.591	0.20	188.2	17.2	173.4	26.2	157.7	15.9	149.7	6.6
36	228.83	0.13	230.91	0.21	231.93	0.14	228.65	0.07	3.636	0.39	3.482	0.69	3.489	0.46	3.593	0.21	184.0	17.0	170.7	25.9	156.5	16.0	147.1	6.6
37	224.16	0.13	226.36	0.22	227.33	0.15	224.05	0.07	3.639	0.40	3.480	0.71	3.491	0.48	3.592	0.21	180.1	16.9	168.2	25.9	155.6	16.2	144.6	6.6
38	219.68	0.14	221.98	0.22	222.91	0.15	219.63	0.07	3.642	0.42	3.479	0.74	3.492	0.50	3.595	0.22	176.4	16.8	165.8	26.0	154.9	16.3	142.2	6.6
39	215.38	0.14	217.78	0.23	218.65	0.15	215.37	0.07	3.646	0.43	3.479	0.76	3.493	0.51	3.600	0.23	172.8	16.7	163.6	26.2	154.3	16.5	140.0	6.6
40	211.26	0.15	213.71	0.24	214.56	0.16	211.26	0.08	3.646	0.46	3.483	0.80	3.491	0.54	3.607	0.24	170.1	17.4	161.1	26.7	153.9	17.1	137.8	6.8
41	207.26	0.15	209.80	0.24	210.62	0.16	207.31	0.08	3.648	0.49	3.485	0.85	3.494	0.58	3.614	0.26	166.9	17.5	159.1	27.1	153.6	17.5	135.8	6.9
42	203.42	0.15	206.03	0.25	206.81	0.17	203.50	0.08	3.651	0.53	3.489	0.92	3.498	0.62	3.620	0.28	163.9	17.7	157.3	27.5	153.4	18.0	134.0	7.0
43	199.71	0.16	202.39	0.26	203.13	0.17	199.81	0.08	3.657	0.59	3.494	1.01	3.498	0.68	3.627	0.31	161.0	17.9	155.5	28.0	153.4	18.4	132.2	7.1
44	196.12	0.16	198.87	0.26	199.59	0.18	196.26	0.08	3.662	0.63	3.498	1.09	3.500	0.73	3.633	0.33	158.2	18.0	153.9	28.5	153.4	19.0	130.5	7.2
45	192.69	0.17	195.45	0.28	196.17	0.19	192.80	0.09	3.663	0.71	3.503	1.20	3.503	0.81	3.642	0.37	159.4	19.3	149.2	28.9	154.8	20.0	127.9	7.4
46	189.30	0.17	192.27	0.28	192.81	0.19	189.48	0.09	3.672	0.74	3.496	1.27	3.507	0.85	3.650	0.38	158.1	20.1	145.5	29.8	155.9	21.2	126.3	7.7
47	186.09	0.18	189.18	0.28	189.51	0.19	186.29	0.09	3.676	0.81	3.497	1.40	3.514	0.94	3.657	0.42	157.0	20.7	149.2	31.8	151.2	21.6	126.0	8.0
48	182.93	0.18	186.05	0.29	186.46	0.20	183.19	0.09	3.684	0.86	3.505	1.48	3.513	1.00	3.662	0.45	150.6	20.0	143.6	30.9	157.9	22.9	126.2	8.1
49	179.89	0.19	183.06	0.30	183.45	0.21	180.16	0.10	3.690	0.93	3.510	1.60	3.513	1.08	3.671	0.48	148.2	20.5	142.3	31.6	158.6	23.6	125.1	8.3
50	176.97	0.20	180.12	0.33	180.50	0.22	177.26	0.11	3.691	0.98	3.529	1.71	3.526	1.16	3.668	0.53	146.8	20.6	152.5	35.1	156.9	24.2	120.7	8.6
51	173.96	0.22	177.53	0.36	177.81	0.24	174.41	0.11	3.710	1.11	3.512	1.92	3.515	1.29	3.678	0.57	144.6	21.1	151.1	36.0	157.8	25.1	119.7	8.8
52	171.30	0.23	174.62	0.39	174.95	0.25	171.71	0.12	3.697	1.02	3.540	1.87	3.542	1.21	3.674	0.53	136.4	20.7	159.9	42.7	169.7	29.4	116.2	9.1
53	168.63	0.23	171.96	0.40	172.28	0.26	169.05	0.12	3.701	1.07	3.542	1.96	3.547	1.27	3.680	0.55	134.2	21.1	160.9	44.4	170.4	30.5	115.4	9.3
54	165.87	0.26	168.95	0.44	170.05	0.31	166.43	0.13	3.725	1.20	3.580	2.21	3.517	1.56	3.690	0.64	147.8	25.7	155.9	48.0	151.2	32.2	117.2	10.7
55	163.35	0.27	166.43	0.46	167.54	0.32	163.91	0.14	3.730	1.26	3.583	2.31	3.518	1.63	3.698	0.67	145.9	26.3	156.2	49.7	151.6	33.4	116.5	11.0

TABLE III-8

COMPARISON OF PERIODS OF NORMAL MODES, THEIR GROUP VELOCITIES, AND ATTENUATION WITH THE PROPERLY WEIGHTED AVERAGE OF ALL DATA AND VALUES COMPUTED FOR PREM

	NORMAL MODE PERIODS							GROUP VELOCITY							ATTENUATION							
MODE	CONTINENT		OCEAN		AVERAGE		PREM	CONTINENT		OCEAN		AVERAGE		PREM	CONTINENT		OCEAN		AVERAGE		PREM
	PERIOD	S.D. %	PERIOD	S.D. %	PERIOD	S.D. %	PERIOD	GR VEL	S.D. %	GR VEL	S.D. %	GR VEL	S.D. %	GR VEL	Q	S.D. %	Q	S.D. %	Q	S.D. %	Q
9	633.86	0.02	633.83	0.01	633.84	0.00	633.61	6.232	0.09	6.249	0.06	6.243	0.02	6.237	338.9	4.4	321.2	2.5	327.6	0.7	332.7
10	579.49	0.02	579.42	0.01	579.45	0.00	579.22	5.646	0.07	5.659	0.05	5.654	0.01	5.648	339.4	3.5	309.5	2.0	320.2	0.6	327.8
11	537.35	0.02	537.03	0.01	537.15	0.00	536.94	5.242	0.10	5.263	0.06	5.255	0.02	5.254	326.1	3.4	308.7	2.0	314.9	0.6	322.1
12	502.86	0.03	502.45	0.02	502.60	0.00	502.42	4.985	0.12	5.011	0.07	5.001	0.02	4.997	319.9	3.3	301.5	1.9	308.1	0.5	315.2
13	473.75	0.03	473.24	0.02	473.43	0.01	473.28	4.800	0.14	4.830	0.08	4.819	0.02	4.813	313.1	3.4	294.8	1.9	301.3	0.5	307.2
14	448.55	0.04	448.09	0.02	448.26	0.01	448.15	4.656	0.16	4.681	0.10	4.672	0.03	4.665	307.9	3.4	286.0	1.9	293.7	0.6	298.3
15	426.60	0.04	426.06	0.02	426.26	0.01	426.19	4.524	0.18	4.552	0.11	4.542	0.03	4.533	301.9	3.8	276.2	2.1	285.2	0.6	288.8
16	407.21	0.05	406.61	0.03	406.83	0.01	406.80	4.403	0.20	4.432	0.12	4.421	0.04	4.411	295.4	4.4	266.1	2.4	276.2	0.7	278.9
17	389.96	0.05	389.29	0.03	389.54	0.01	389.55	4.291	0.21	4.321	0.13	4.310	0.04	4.298	288.4	5.1	255.9	2.7	267.0	0.8	268.9
18	374.49	0.06	373.77	0.04	374.03	0.01	374.07	4.187	0.22	4.214	0.13	4.204	0.04	4.193	281.1	5.8	245.8	3.0	257.7	0.9	259.1
19	360.51	0.06	359.77	0.04	360.04	0.01	360.11	4.091	0.22	4.119	0.13	4.109	0.04	4.097	274.6	6.3	235.9	3.3	248.9	1.0	249.7
20	347.82	0.07	347.04	0.04	347.33	0.01	347.42	4.006	0.23	4.031	0.14	4.021	0.04	4.011	267.0	6.8	226.7	3.5	240.1	1.1	240.8
21	336.22	0.07	335.43	0.04	335.72	0.01	335.83	3.927	0.24	3.953	0.15	3.944	0.04	3.934	259.5	7.3	218.1	3.7	231.8	1.1	232.4
22	325.56	0.08	324.76	0.05	325.06	0.01	325.18	3.860	0.25	3.884	0.15	3.875	0.04	3.866	252.2	7.7	210.2	3.9	224.0	1.2	224.8
23	315.71	0.08	314.91	0.05	315.20	0.01	315.33	3.804	0.25	3.823	0.15	3.816	0.04	3.808	245.1	8.0	202.9	4.0	216.7	1.2	217.7
24	306.56	0.08	305.77	0.05	306.06	0.01	306.20	3.757	0.24	3.770	0.15	3.765	0.04	3.758	238.3	8.3	196.2	4.1	209.9	1.3	211.3
25	298.03	0.08	297.25	0.05	297.54	0.02	297.68	3.716	0.25	3.726	0.15	3.722	0.04	3.716	231.9	8.4	190.1	4.2	203.7	1.3	205.4
26	290.04	0.09	289.28	0.05	289.56	0.02	289.70	3.682	0.25	3.690	0.15	3.687	0.04	3.681	225.8	8.5	184.5	4.2	197.9	1.3	200.0
27	282.53	0.09	281.79	0.05	282.06	0.02	282.20	3.654	0.26	3.660	0.16	3.658	0.04	3.652	220.0	8.6	179.5	4.2	192.7	1.3	195.1
28	275.44	0.09	274.73	0.06	274.99	0.02	275.13	3.630	0.27	3.635	0.16	3.633	0.04	3.629	214.7	8.6	174.9	4.2	187.8	1.3	190.7
29	268.74	0.09	268.06	0.06	268.31	0.02	268.44	3.613	0.26	3.614	0.16	3.614	0.04	3.611	209.6	8.6	170.7	4.2	183.3	1.3	186.6
30	262.39	0.10	261.73	0.06	261.97	0.02	262.09	3.600	0.27	3.600	0.16	3.600	0.05	3.597	204.8	8.5	166.9	4.2	179.2	1.3	182.9
31	256.34	0.10	255.72	0.06	255.95	0.02	256.06	3.588	0.27	3.588	0.16	3.588	0.05	3.586	200.3	8.5	163.4	4.2	175.4	1.3	179.5
32	250.59	0.10	249.99	0.06	250.21	0.02	250.32	3.581	0.27	3.579	0.16	3.580	0.04	3.578	196.1	8.4	160.2	4.1	171.9	1.3	176.4
33	245.09	0.10	244.53	0.06	244.74	0.02	244.83	3.577	0.27	3.573	0.17	3.574	0.05	3.573	192.1	8.3	157.3	4.1	168.6	1.3	173.4
34	239.84	0.10	239.30	0.06	239.50	0.02	239.59	3.573	0.28	3.569	0.17	3.571	0.05	3.569	188.4	8.2	154.6	4.1	165.6	1.3	170.7
35	234.81	0.11	234.30	0.06	234.49	0.02	234.57	3.572	0.28	3.568	0.17	3.569	0.05	3.568	184.9	8.2	152.1	4.1	162.8	1.3	168.2
36	229.99	0.11	229.51	0.07	229.69	0.02	229.76	3.570	0.29	3.568	0.18	3.569	0.05	3.568	181.5	8.1	149.8	4.0	160.2	1.2	165.9
37	225.36	0.11	224.90	0.07	225.08	0.02	225.14	3.572	0.30	3.568	0.18	3.570	0.05	3.569	178.4	8.1	147.7	4.0	157.8	1.2	163.6
38	220.92	0.11	220.48	0.07	220.64	0.02	220.70	3.574	0.31	3.571	0.19	3.572	0.05	3.571	175.5	8.1	145.7	4.1	155.5	1.2	161.6
39	216.64	0.12	216.22	0.07	216.38	0.02	216.43	3.576	0.32	3.574	0.19	3.575	0.05	3.573	172.7	8.1	143.9	4.1	153.3	1.2	159.6
40	212.53	0.12	212.12	0.07	212.27	0.02	212.32	3.576	0.34	3.579	0.20	3.578	0.06	3.577	170.1	8.5	142.1	4.2	151.3	1.3	157.7
41	208.56	0.13	208.17	0.08	208.31	0.02	208.35	3.577	0.36	3.585	0.21	3.582	0.06	3.580	167.6	8.5	140.5	4.3	149.4	1.3	156.0
42	204.74	0.13	204.36	0.08	204.50	0.02	204.53	3.581	0.37	3.590	0.22	3.586	0.06	3.584	165.2	8.6	139.0	4.3	147.6	1.3	154.3
43	201.06	0.13	200.67	0.08	200.81	0.02	200.85	3.585	0.40	3.595	0.24	3.591	0.07	3.588	162.9	8.8	137.6	4.4	146.0	1.3	152.7
44	197.50	0.14	197.12	0.08	197.26	0.02	197.28	3.589	0.42	3.600	0.25	3.596	0.07	3.593	160.8	8.9	136.3	4.5	144.4	1.4	151.2
45	194.06	0.14	193.68	0.09	193.82	0.02	193.84	3.591	0.47	3.607	0.27	3.601	0.08	3.597	160.2	9.4	134.8	4.7	143.1	1.4	149.7
46	190.73	0.15	190.34	0.09	190.48	0.03	190.51	3.594	0.49	3.615	0.29	3.607	0.08	3.602	158.4	9.8	133.8	4.9	141.8	1.5	148.3
47	187.57	0.15	187.11	0.09	187.27	0.03	187.29	3.596	0.52	3.621	0.31	3.612	0.09	3.606	158.8	10.2	132.4	5.0	140.9	1.6	146.9
48	184.43	0.16	184.01	0.09	184.17	0.03	184.18	3.603	0.56	3.625	0.33	3.617	0.10	3.611	153.3	10.1	133.8	5.2	140.4	1.6	145.7
49	181.41	0.16	180.99	0.10	181.15	0.03	181.16	3.608	0.60	3.631	0.35	3.623	0.10	3.615	151.5	10.3	133.0	5.4	139.3	1.6	144.4
50	178.43	0.17	178.12	0.11	178.24	0.03	178.24	3.619	0.62	3.631	0.38	3.626	0.11	3.620	154.6	10.9	129.0	5.6	137.5	1.7	143.2
51	175.60	0.18	175.28	0.11	175.40	0.03	175.40	3.622	0.65	3.637	0.40	3.631	0.11	3.624	152.8	11.2	128.4	5.8	136.5	1.7	142.1
52	172.87	0.18	172.54	0.11	172.66	0.03	172.65	3.626	0.60	3.641	0.36	3.635	0.10	3.629	152.7	12.1	126.9	6.0	135.4	1.9	140.9
53	170.20	0.19	169.87	0.11	169.99	0.03	169.98	3.629	0.62	3.647	0.37	3.640	0.11	3.633	151.5	12.4	126.2	6.2	134.5	1.9	139.9
54	167.54	0.22	167.35	0.13	167.42	0.04	167.39	3.646	0.75	3.646	0.44	3.646	0.12	3.637	159.6	15.0	124.5	6.8	135.3	2.1	138.8
55	165.02	0.22	164.83	0.13	164.90	0.04	164.88	3.649	0.79	3.652	0.46	3.651	0.13	3.641	158.6	15.4	123.9	7.0	134.5	2.2	137.8

functionals for PREM.[16] The standard errors in pure-path Q decrease substantially and could be considered statistically significant. The systematic trend of differences between the continental and oceanic Q values is illustrated in Fig. III-22. At a period of 250 s, the continental and oceanic Q's are 196 ± 16 and 160 ± 7, respectively – a difference of about 20 percent.

The comparison of the average data from 37 paths studied in this paper with the functionals of PREM, a model derived using a much broader data set, is a test of the overall performance of WIT. Even small systematic differences could be detected in this way. For periods of normal modes, the maximum difference is 0.05 percent with an average rms of 0.02 percent – an excellent agreement indeed! The differences between the group velocities do not significantly exceed 0.01 km/s, a remarkable result considering the fact that group velocities were not used in derivation of PREM and that there are substantial variations in group velocities estimated for individual paths: the maximum difference in pure-path group velocities approaches 5 percent. The average Q values are also very close to those for PREM. At all frequencies the difference is less than 5 percent, which is the estimated accuracy of the average Q data in the relevant range of frequencies (see Table V in Ref. 16).

Because of the inherent difficulty in the direct comparison of the results of measurements of Q with the original data (seismograms), we show in Fig. III-23 the average Q values obtained in this study together with the results of Sailor,[50] and Geller and Stein[51]; the Q-curve for PREM is included. Sailor obtained his results by using the traveling-wave approach and a refined spectral ratio method; thus, there should be no common source of bias between his result and ours. Sailor's data show small amplitude oscillations superimposed on a smooth curve that is essentially parallel to ours with, perhaps, a few-percent systematic difference at the short-period end. The results of Geller and Stein, obtained by measuring the time-domain decay of the envelope of individual modes, have very large scatter; this might be construed as an indication of the advantage of the traveling-wave approach for periods shorter than about 500 s.

Finally, we consider the results obtained in the model space. For each path we have a set of perturbations in velocities and Q that were introduced to improve the transfer function. We can thus solve the pure-path problem directly in the model space, without the need to invert the data. As stated above, the results need not be fully compatible with those obtained for the normal-mode functionals, because the frequency range of inversion differs from path to path, while the parametrization remains the same. Figure III-24 shows perturbations in shear velocity for the individual regions with respect to the reference model (IREM[52]). The most unusual feature of this plot is the large differences between the velocities for young and old oceans in a depth range from 400 to 670 km. At shallower depths, the results are compatible with those from other studies. The structures in the depth range from 80 to 220 km reflect the composite properties of the crust, lithosphere, and the low-velocity zone: fundamental Rayleigh-mode data with a short-period cutoff at 165 s have no resolving power to determine these separate elements of the structure.

The total spread of values is very large (0.34 km/s) in the depth range from 80 to 220 km. The relative slowness of the young oceans and tectonic regions is in good agreement with regional surface-wave studies. The total spread of shear velocities is relatively small in the depth range from 220 to 400 km. It is less than 0.1 km/s, and the error bars in Fig. III-24 indicate that the differences are not statistically significant. In a depth range from 400 to 670 km, the velocities for stable continents and tectonic regions are very close to each other

and, also, to the global average. The difference between the young and old oceans is large – nearly 0.2 km/s or 4 percent – and appears to be statistically significant. One cannot discount the possibility that it is an artifact of the errors introduced by the geometrical-ray-theory approximation, but in that case abnormal properties of the models for stable continents and tectonic regions could be expected: either of the two region types is smaller in the total area than the young oceans.

The matter should be satisfactorily resolved by application of the theory of Woodhouse and Girnius,[53] which avoids the approximation inherent in the geometrical ray theory. Also, improved path coverage should lead to higher resolution. The important result of this experiment is that the extended period range provides sufficient resolution below a depth of 400 km to infer structural differences in the region of the transition zone.

A. M. Dziewonski
J. M. Steim†

† Department of Geological Sciences, Harvard University.

REFERENCES

1. T. Kurita, "Attenuation of Short-Period P-Waves and Q in the Mantle," J. Phys. Earth 16, 61-78 (1968).
2. Z. A. Der and T. W. McElfresh, "The Relationship Between Anelastic Attenuation and Regional Amplitude Anomalies of Short-Period P Waves in North America," Bull. Seismol. Soc. Am. 67, 1303-1317 (1977).
3. M. Wyss and P. Molnar, "Source Parameters of Intermediate and Deep Focus Earthquakes in the Tonga Arc," Phys. Earth Planet. Inter. 6, 279-292 (1972).
4. J. F. Masso, C. B. Archambeau, and J. M. Savino, "Implementation, Testing and Specification of a Seismic Event Detection and Discrimination System," Final Report U.S. Arms Control and Disarmament Agency, Report SSS-R-79-3963, Systems, Science, and Software, La Jolla, California (March 1979).
5. Z. A. Der, T. A. McElfresh, and A. O'Donnell, "An Investigation of the Regional Variations and Frequency Dependence of Anelastic Attenuation in the Mantle under the United States in the .5-4 Hz Band," Geophys. J. Astr. Soc. (in press, 1981).
6. L. J. Burdick, "Waveform Studies of the Velocity and Q Structure of the Mantle," Annual Technical Report of AFOSR Contract #F 49620-79-C-0021, Columbia University-LDGO (1981).
7. S. A. Sipkin and T. H. Jordan, "Frequency Dependence of Q ScS," Bull. Seismol. Soc. Am. 69, 1055-1081 (1979).
8. G. M. Lundquist and V. F. Cormier, "Constraints on the Absorption Band Model of Q," J. Geophys. Res. 85, 5244-5256 (1980).
9. A. M. Dziewonski and D. L. Anderson, "Preliminary Reference Earth Model," Phys. Earth Planet. Inter. 25, 297-356 (1981).
10. B. J. Mitchell and D. V. Helmberger, "Shear Velocities at the Base of the Mantle from Observations of S and ScS," J. Geophys. Res. 78, 6009-6020 (1973).
11. D. L. Anderson and J. W. Given, "Absorption Band Q Model for the Earth" (to be published).
12. L. J. Burdick, "t* for S Waves with a Continental Ray Path," Bull. Seismol. Soc. Am. 68, 1013-1030 (1979).
13. S. A. Sipkin and T. H. Jordan, "Regional Variation of Q ScS," Bull. Seismol. Soc. Am. 70, 1071-1102 (1980).
14. I. S. Sacks, J. A. Snoke, and L. Beach, "Lateral Heterogeneity at the Base of the Mantle Revealed by Observations of Amplitudes of PKP Phases," Geophys. J. R. Astr. Soc. 59, 379-387 (1979).
15. G. L. Choy and J. Boatwright, "The Rupture Characteristics of Two Deep Earthquakes Inferred from Broadband GDSN Data," Bull. Seismol. Soc. Am. 71, 691-712 (1981).
16. A. M. Dziewonski and D. L. Anderson, "Preliminary Reference Earth Model," Phys. Earth Planet. Inter. 25, 297-356 (1981).
17. J. H. Woodhouse, "A Note on the Calculation of Travel Times in a Transversely Isotropic Earth Model," Phys. Earth Planet. Inter. 25, 357-359 (1981).
18. B. R. Julian and D. L. Anderson, "Travel Times, Apparent Velocities and Amplitudes of Body Waves," Bull. Seismol. Soc. Am. 58, 339-366 (1968).
19. L. E. Johnson and F. Gilbert, "Inversion and Inference for Teleseismic Ray Data," Meth. Comput. Phys. 12, 231-266 (1972).
20. Seismic Discrimination SATS, Lincoln Laboratory, M.I.T. (31 March 1980), DTIC AD-A091107/3.
21. A. M. Dziewonski, T.-A. Chou, and J. H. Woodhouse, "Determination of Earthquake Source Parameters from Waveform Data for Studies of Global and Regional Seismicity," J. Geophys. Res. 86, 2825-2852 (1981).
22. Seismic Discrimination SATS, Lincoln Laboratory, M.I.T. (31 March 1981), DTIC AD-A109184.

23. G. E. Backus, "Interpreting the Seismic Glut Moments of Total Degree Two or Less," Geophys. J. R. Astr. Soc. 51, 1-25 (1977).

24. G. E. Backus and M. Mulcahy, "Moment Tensors and Other Phenomenological Descriptions of Seismic Sources, I., Continuous Displacements," Geophys. J. R. Astr. Soc. 46, 341-361 (1976).

25. F. Gilbert and A. M. Dziewonski, "An Application of Normal Mode Theory to the Retrieval of Structural Parameters and Source Mechanisms from Seismic Spectra," Philos. Trans. R. Soc. London, Ser. A 278, 187-269 (1975).

26. R. A. Phinney and R. Burridge, "Representation of the Elastic-Gravitational Excitation of a Spherical Earth Model by Generalized Spherical Harmonics," Geophys. J. R. Astr. Soc. 34, 451-487 (1973).

27. J. M. Baranowski, J. Nabelek, and M. N. Toksöz, "Fault Parameters of the Algerian Earthquake of October 10, 1980" (abstract), EOS, Trans. Am. Geophys. Un. 62, 331 (1981).

28. J. H. Woodhouse, "The Excitation of Long Period Seismic Waves by a Source Spanning a Structural Discontinuity," Geophys. Res. Lett. 8, 1129-1131 (1981).

29. T. Lay, J. W. Given, and H. Kanamori, "Long Period Mechanism of the November 8, 1980 Eureka, California Earthquake," Bull. Seismol. Soc. Am. (in press).

30. H. Kanamori and H. H. Given, "Use of Long-Period Surface Waves for Fast Determination of Earthquake Source Parameters," Phys. Earth Planet. Inter. (in press).

31. E. Boschi, F. Mulargia, E. Mantovani, M. Bonafede, A. M. Dziewonski, and J. H. Woodhouse, "The Irpinia Earthquake of November 23, 1980" (abstract), EOS, Trans. Am. Geophys. Un. 62, 330 (1981).

32. C. D. Stephens, J. C. Lahr, K. A. Fogleman, and R. B. Horner, "The St. Elias, Alaska, Earthquake of February 28, 1979: Regional Recording of Aftershocks and Short-Term, Pre-earthquake Seismicity," Bull. Seismol. Soc. Am. 70, 1607-1633 (1980).

33. O. J. Perez and K. H. Jacob, "St. Elias, Alaska, Earthquake of February 28 1979: Tectonic Setting and Precursory Seismic Pattern," Bull. Seismol. Soc. Am. 70, 1595-1606 (1980).

34. M. Berberian, I. Asudeh, R. G. Bilham, C. H. Scholz, and C. Soufleris, "Mechanism of the Main Shock and the Aftershock Study of the Tabas-e-Golshan (Iran) Earthquake of September 16, 1978: A Preliminary Report," Bull. Seismol. Soc. Am. 69, 1851-1859 (1979).

35. Seismic Discrimination SATS, Lincoln Laboratory, M.I.T. (30 September 1980), DTIC AD-A097999/7.

36. A. M. Dziewonski and J. M. Steim, "Dispersion and Attenuation of Mantle Waves Through Waveform Inversion," Geophys. J. R. Astr. Soc. (in press, 1982).

37. M. N. Toksöz and D. L. Anderson, "Phase Velocities of Long Period Surface Waves and Structure of the Upper Mantle," J. Geophys. Res. 71, 1649-1658 (1966).

38. H. Kanamori, "Velocity and Q of Mantle Waves," Phys. Earth Planet. Inter. 2, 259-275 (1970).

39. A. M. Dziewonski, "On Regional Differences in Dispersion of Mantle Rayleigh Waves," Geophys. J. R. Astr. Soc. 22, 289-325 (1971).

40. F. T. Wu, "Mantle Rayleigh Wave Dispersion and Tectonic Provinces," J. Geophys. Res. 77, 6445-6453 (1972).

41. Seismic Discrimination SATS, Lincoln Laboratory, M.I.T. (31 March 1979), DDC AD-A073772/6.

42. I. Nakanishi, "Phase Velocity and Q of Mantle Waves," Geophys. J. R. Astr. Soc. 58, 35-59 (1979).

43. J. J. Leveque, "Regional Upper Mantle S-Velocity Models from Phase Velocities of Great-Circle Rayleigh Waves," Geophys. J. R. Astr. Soc. 63, 23-43 (1980).

44. P. G. Silver and T. H. Jordan, "Fundamental Spheroidal Mode Observations of Aspherical Heterogeneity," Geophys. J. R. Astr. Soc. 64, 605-634 (1981).

45. I. Nakanishi, "Shear Velocity and Shear Attenuation Models from World-Wide and Pure-Path Average Data of Mantle Rayleigh Waves ($_0S_{25}$ to $_0S_{80}$) and Fundamental Spheroidal Modes ($_0S_2$ to $_0S_{80}$)," Geophys. J. R. Astr. Soc. 66, 83-130 (1981).

46. D. Agnew, J. Berger, R. Buland, W. Farell, and F. Gilbert, "International Deployment of Accelerometers: A Network for Very Low Frequency Seismology," EOS, Trans. Am. Geophys. Un. 57, 180-188 (1976).

47. F. J. Mauk, "A Tectonic Based Rayleigh Wave Group Velocity Model for Production of Dispersion Character Through Ocean Basins," Ph. D. Thesis, University of Michigan (1977).

48. F. A. Dahlen, "The Correction of Great Circular Surface Wave Phase Velocity Measurements for Rotation and Ellipticity of the Earth," J. Geophys. Res. 80, 4895-4903 (1975).

49. A. M. Dziewonski and R. V. Sailor, "Comments on 'The Correction of Great Circular Surface Wave Phase Velocity for the Rotation and Ellipticity of the Earth' by F. A. Dahlen," J. Geophys. Res. 81, 4947-4950 (1976).

50. R. V. Sailor, "Attenuation of Low Frequency Seismic Energy," Ph. D. Thesis, Harvard University (1978).

51. R. J. Geller and S. Stein, "Time-Domain Attenuation Measurements for Fundamental Spheroidal Modes ($_0S_6$ to $_0S_{28}$) for the 1977 Indonesian Earthquake," Bull. Seismol. Soc. Am. 69, 1671-1691 (1979).

52. A. M. Dziewonski and D. L. Anderson, "A Proposal for an Interim Reference Earth Model," a report submitted to the Standard Earth Model Committee of the IUGG, Canberra, Australia (1979).

53. J. H. Woodhouse and T. P. Girnius, "Surface Waves and Free Oscillations in a Regionalized Earth Model," Geophys. J. R. Astr. Soc. (in press).

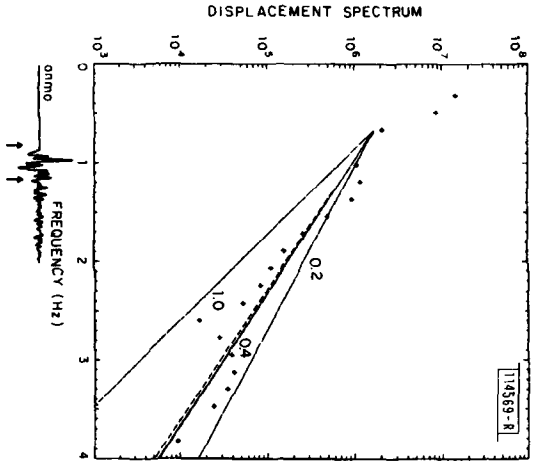

Fig. III-1. Spectrum of P-wave recorded by short-period SRO station ANMO for a deep focus earthquake in Banda Sea. Dotted line is least-squares line fit to spectrum for frequencies greater than 0.7 Hz. Solid lines are predicted spectral decay for t^*_α = 0.4, 0.2, and 0.1 for an equivalent event at surface. Arrows show "time acceptance window" of P-wave.

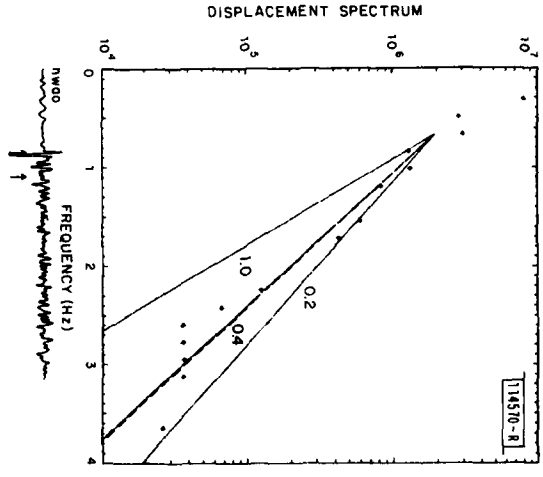

Fig. III-2. Spectrum of P-wave recorded by short-period SRO station NWAO for a deep focus earthquake in Peru. Lines and symbols defined in caption to Fig. III-1.

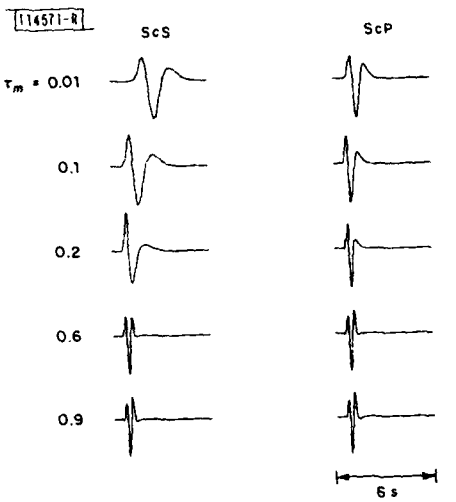

Fig. III-3. Synthetic ScS and ScP phases computed for varying values of the lower time constant τ_m of a mantle-wide absorption band. For frequencies less than $1/2\ \pi\tau_m$, the attenuation model converges to that of PREM; for frequencies greater than $1/2\ \pi\tau_m$ Hz, Q_α and Q_β decrease as ω^{-1}. Results shown are for a triangle source pulse of 1-s width convolved with a short-period WWSSN instrument response.

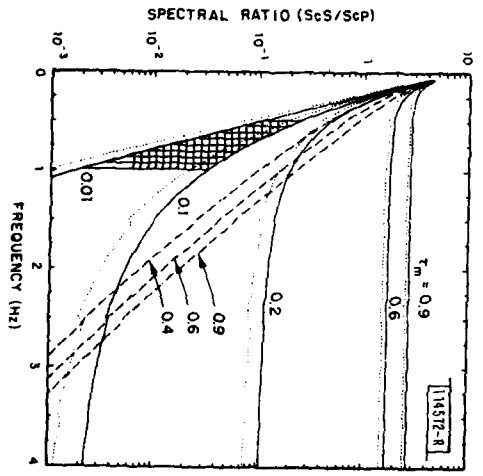

Fig. III-4. Synthetic spectral ratio of ScS/ScP vs frequency. Solid lines are for a mantle-wide absorption band that converges to PREM for frequencies less than $1/2\ \pi\tau_m$ Hz and has Q_α and Q_β decrease as ω^{-1} for frequencies greater than $1/2\ \pi\tau_m$. Dotted lines include a low Q zone in the lower 150 km of mantle with Q_α = 100 and Q_β = 50. Dashed lines are for an absorption band spanning the band of high-frequency body waves (τ_m = 0.01) in the upper 400 and lower 150 km of the mantle, but shifted to low frequencies in mid-mantle (τ_m = 0.6, 0.4). Shaded region is domain of frequencies and ScS/ScP observations found by Burdick.[6]

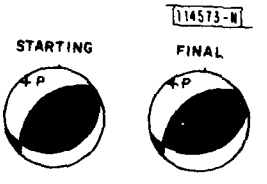

Fig. III-5. *Comparison* of fault-plane solutions (major double-couple) obtained using starting and final coordinates of El Asnam, Algeria earthquake of 10 October 1980.

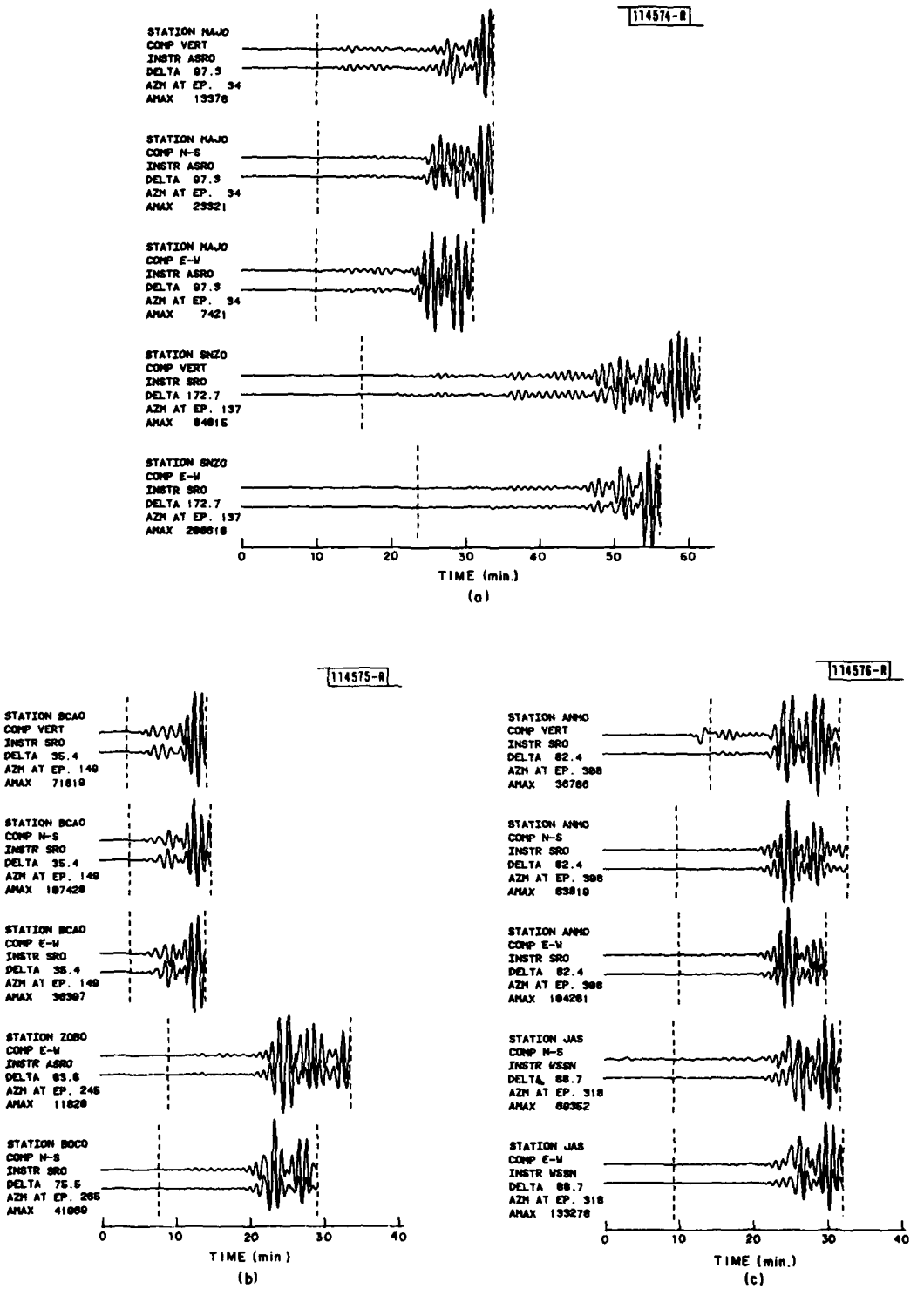

Fig. III-6(a-c). Comparison of observed (top) and synthetic GDSN seismograms for El Asnam, Algeria earthquake of 10 October 1980.

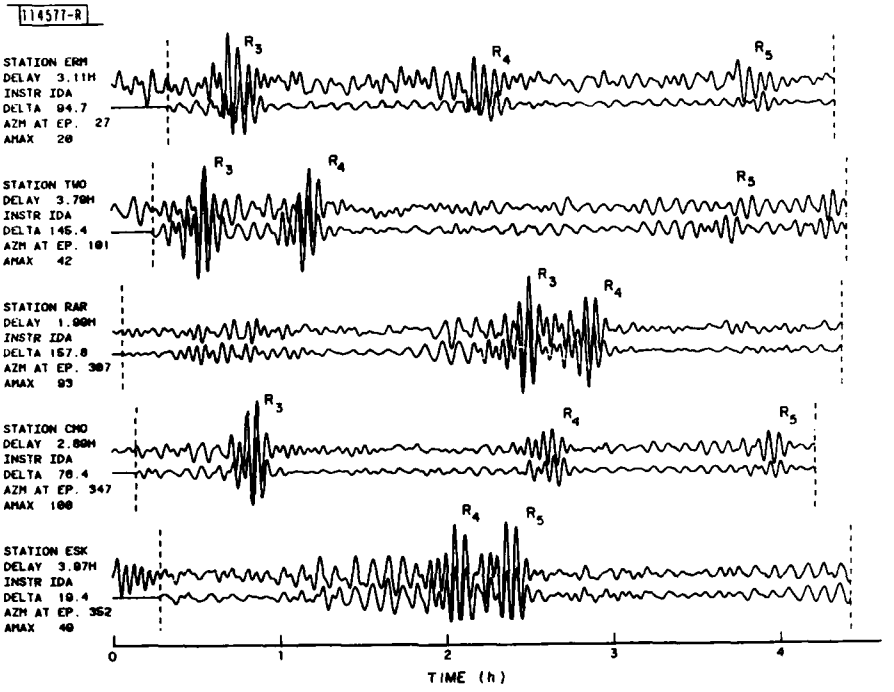

Fig. III-7. Comparison of observed (top) and synthetic IDA seismograms for El Asnam, Algeria earthquake of 10 October 1980.

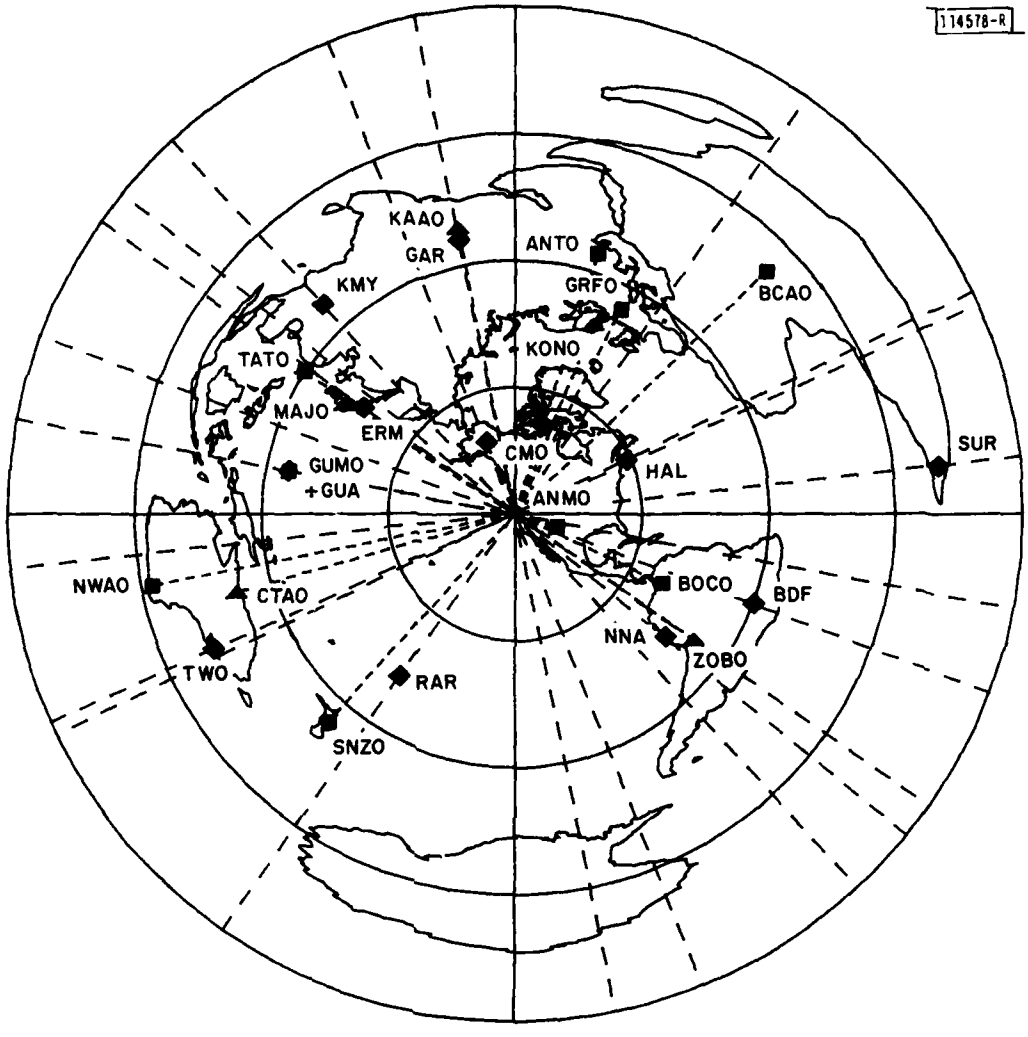

Fig. III-8. Coverage of Eureka earthquake of 8 November 1980 by instruments of GDSN (SRO – square; ASRO – upward-pointing triangle) and IDA (diamonds) networks.

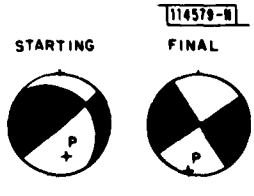

Fig. III-9. Comparison of fault-plane solutions (major double-couple) obtained using starting and final coordinates of Eureka earthquake of 8 November 1980.

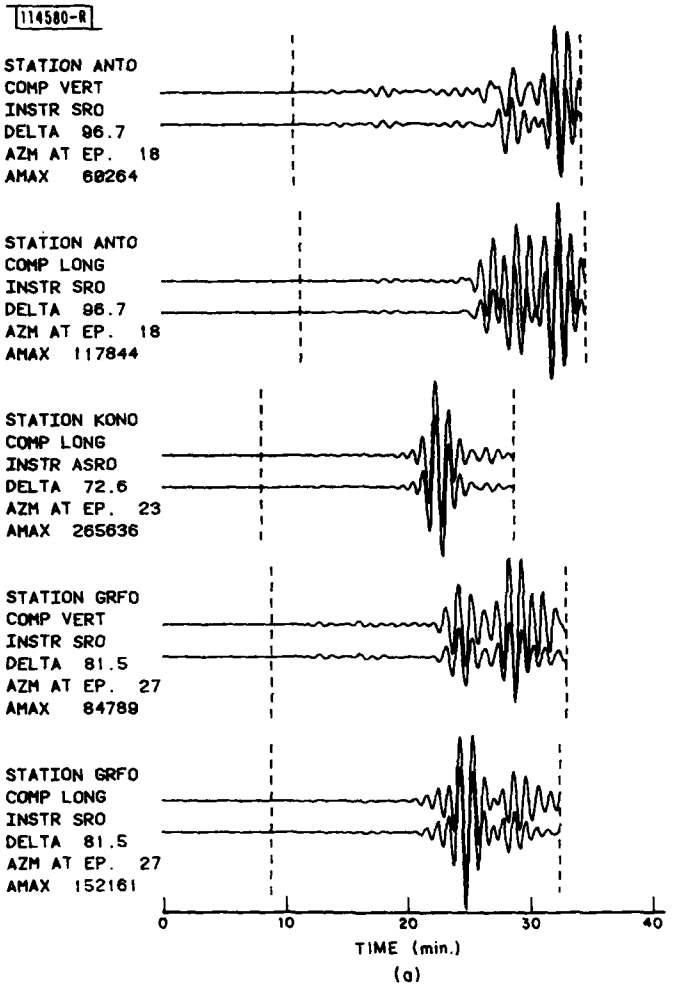

Fig. III-10(a-c). Comparison of observed (top) and synthetic GDSN seismograms for Eureka earthquake of 8 November 1980.

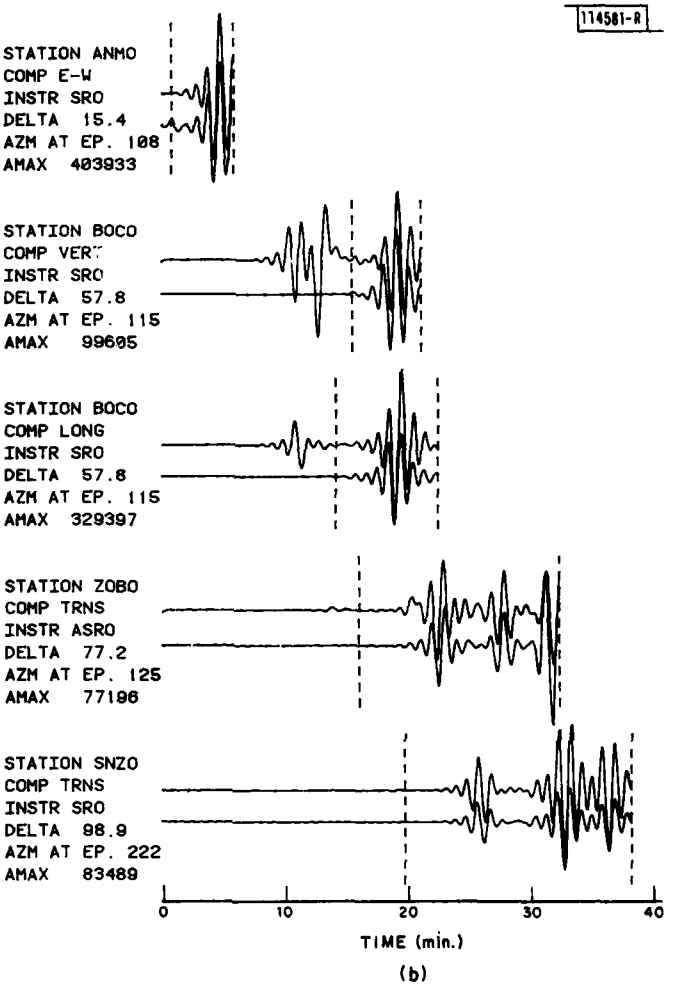

Fig. III-10(a-c). Continued.

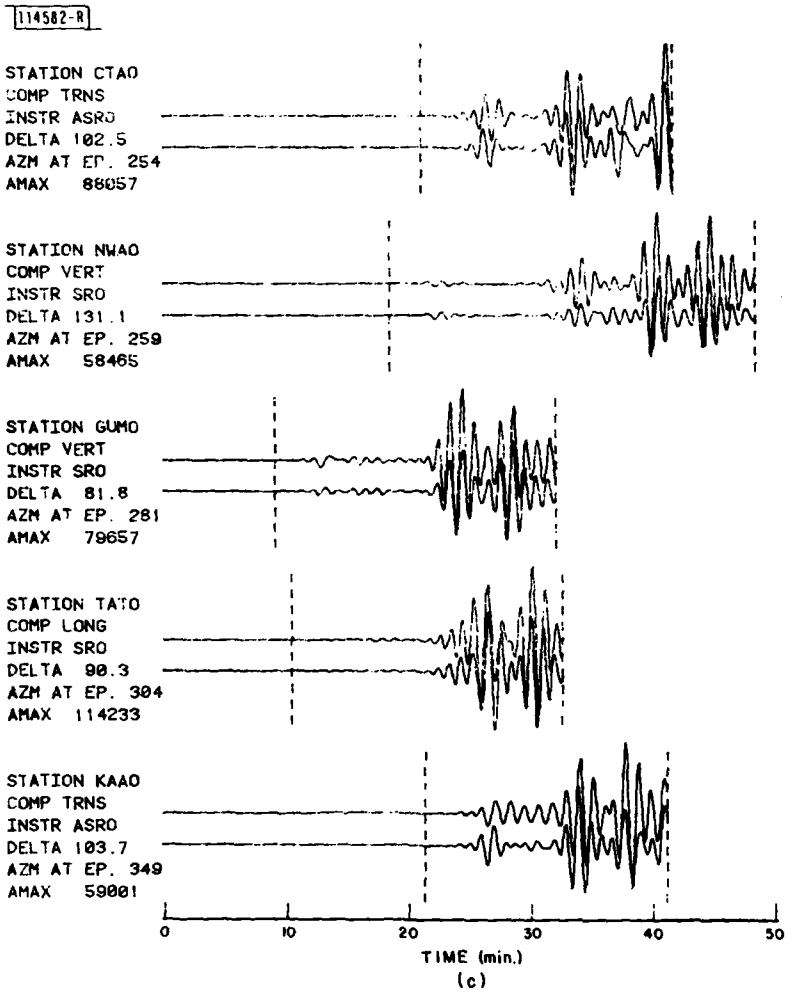

Fig. III-10(a-c). Continued.

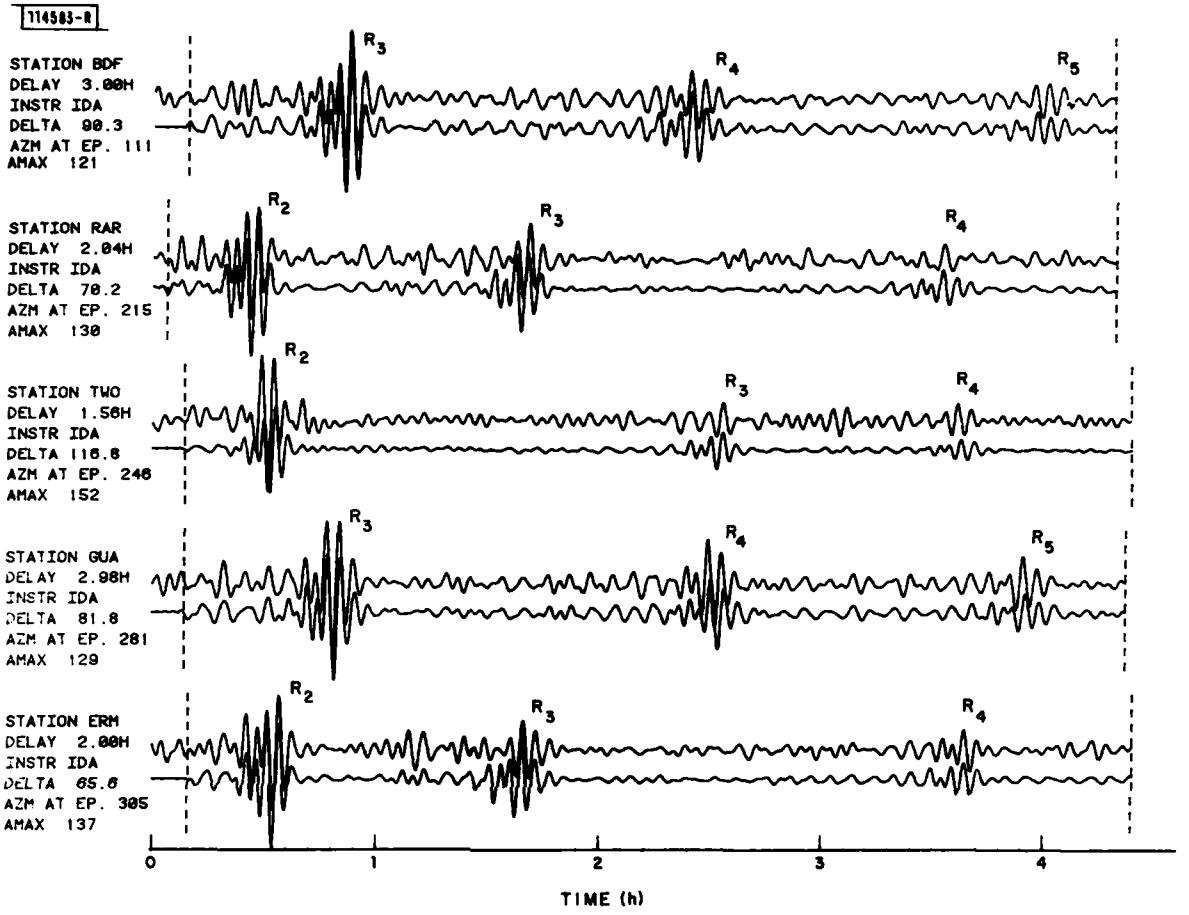

Fig. III-11. Comparison of observed (top) and synthetic IDA seismograms for Eureka earthquake of 8 November 1980.

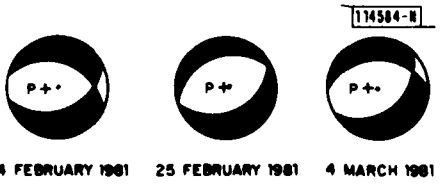

Fig. III-12. Fault-plane solutions (major double-couple) of three closely spaced earthquakes in Southern Greece.

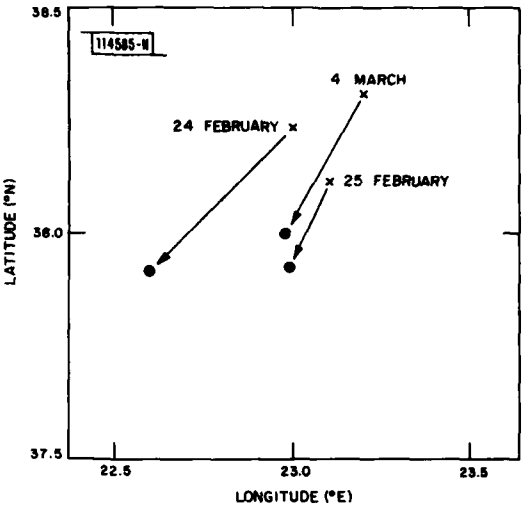

Fig. III-13. Relocation of epicenters of three earthquakes in Southern Greece. Crosses are NEIS locations, solid circles are centroid locations. Note that, after relocation, earthquakes lie on an axis parallel to strike direction (see Fig. III-12).

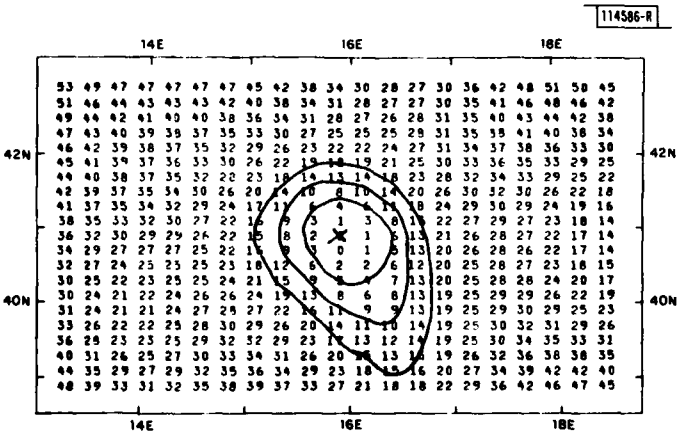

Fig. III-14. A contour map of $\epsilon \times 100$ [Eq. (III-34)]. Minimum value of ϵ indicates best location of point source for specific amount of shift in origin time. In this test with synthetic data, location of source coincided with center of grid system. Result is exact.

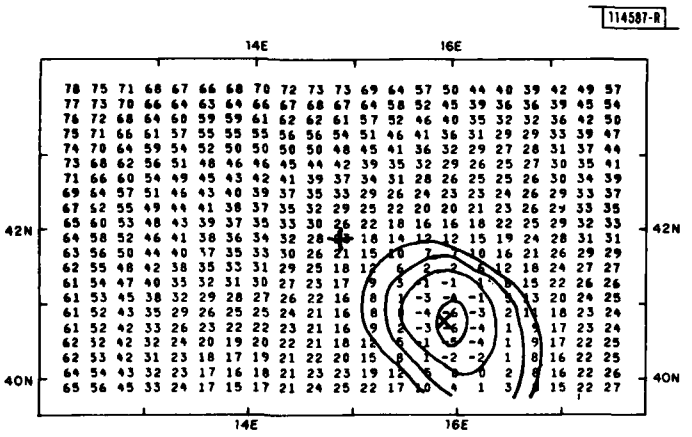

Fig. III-15. Same as Fig. III-14, but source is offset with respect to center of grid (plus sign). Parameter search allows locating of source satisfactorily even though offset is greater than 150 km.

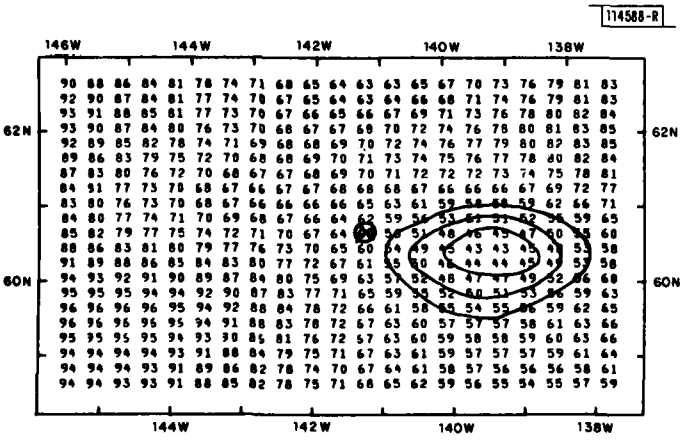

Fig. III-16. Application of parameter search procedure to analysis of St. Elias earthquake of 28 February 1979. Crossed circle is NEIS location of this event. We determine that best location of point source is about 100 km to east of NEIS location and 37 s after origin time.

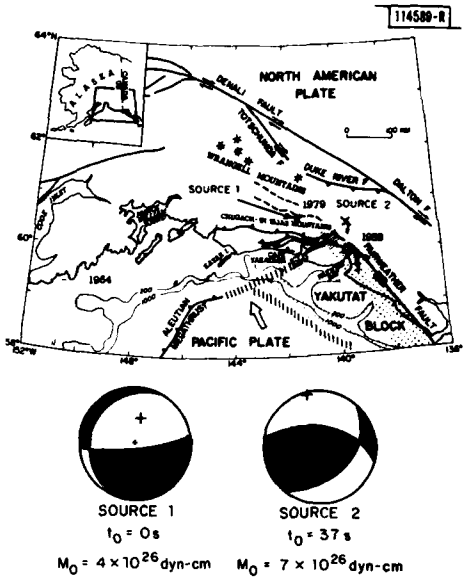

Fig. III-17. Result of inversion of SRO/ASRO from St. Elias earthquake for point sources: first one coincides with NEIS location (star), second source (cross) corresponds to location determined in Fig. III-16. Mechanism of source 1 closely corresponds to that obtained from P-wave polarities[32]; source 2 is markedly different. Tectonic map is from a paper by Stephens et al.[32] [Reprinted with permission from C. D. Stephens et al., Bull. Seismol. Soc. Am. 70, 1607-1634 (1980).]

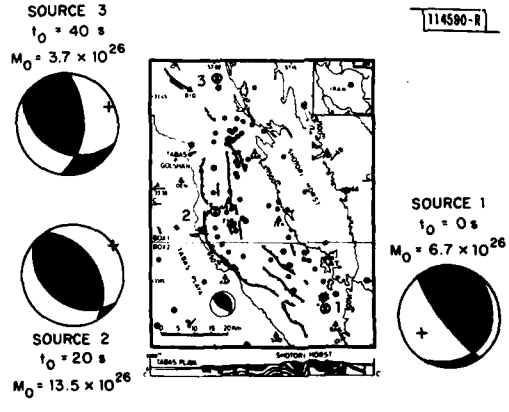

Fig. III-18. Result of inversion of SRO/ASRO data from Tabas-e-Golshan (Iran) earthquake for three point sources denoted by crossed circles (sequence is from lower right to upper left). Faulting progresses from dip-slip (or very shallow thrust) to reverse faulting, and last source develops significant strike-slip component. Note similarity between evolution of this event and that of St. Elias earthquake. Map is from Berberian et al.[34]; solution from P-wave polarities is superimposed on map. [Reprinted with permission from M. Berberian et al., Bull. Seismol. Soc. Am. 69, 1851-1860 (1979).]

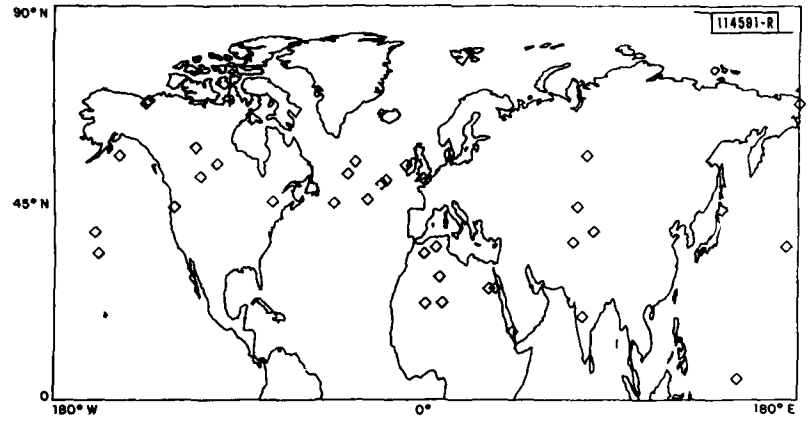

Fig. III-19. Location of northern hemisphere poles of 37 great-circle paths analyzed in this report.

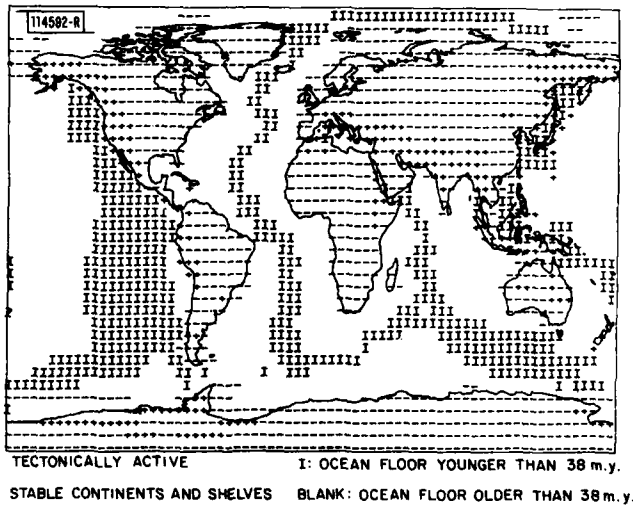

Fig. III-20. Schematic representation of regionalization adopted in our pure-path analysis. This regionalization has been obtained by combining several regions of similar tectonic nature as defined by Mauk.[4]

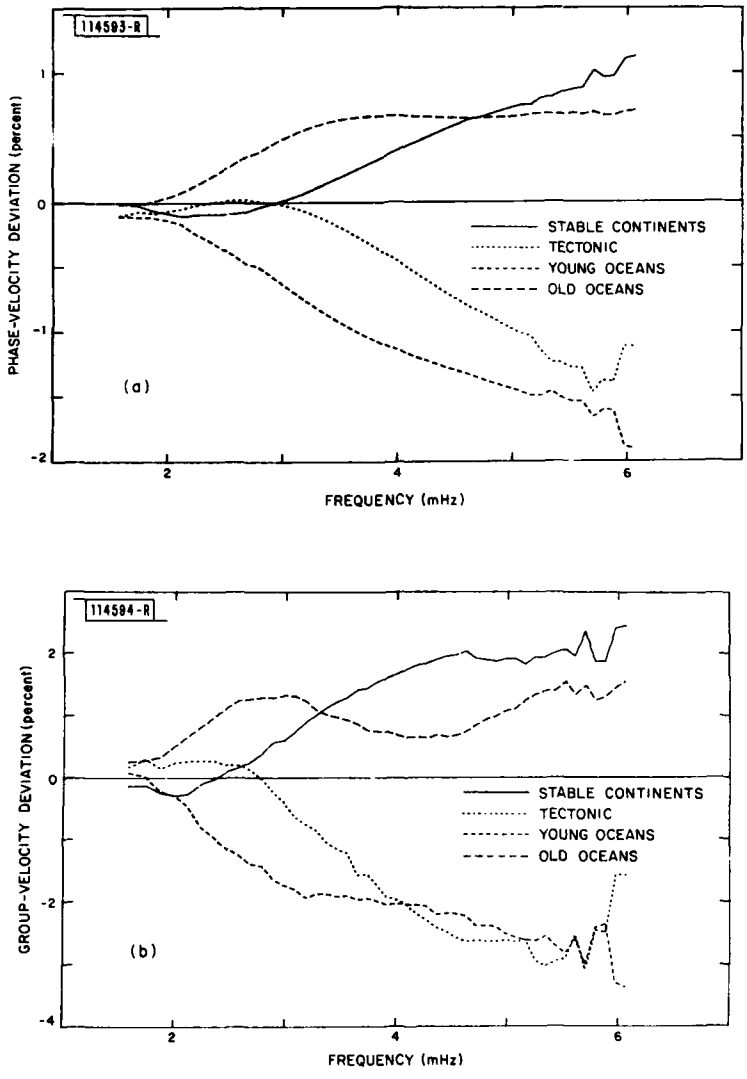

Fig. III-21. Pure-path phase velocities (a) and group velocities (b) obtained through decomposition of results of measurements for 37 great-circle paths.

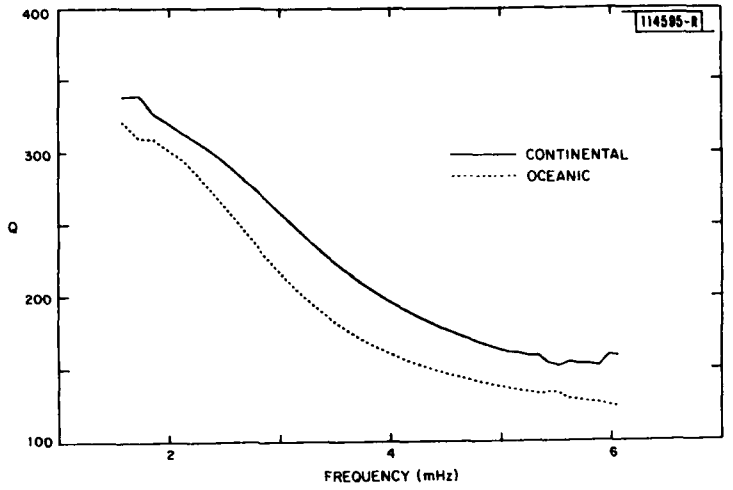

Fig. III-22. Attenuation (Q) for continental and oceanic regions; data are not sufficiently numerous and accurate to allow four-region analysis for Q. Differences between continental and oceanic Q values are statistically significant; see Table III-8.

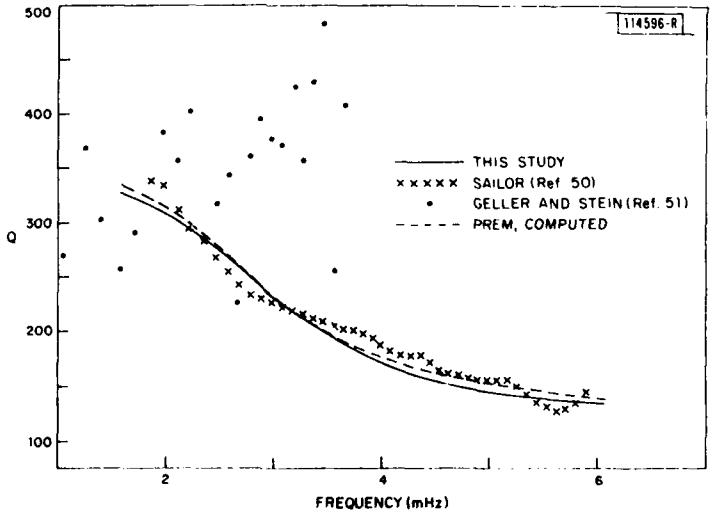

Fig. III-23. Comparison of Q data of Sailor[50] (traveling-wave approach), and Geller and Stein[51] (standing-wave approach) with those obtained in this study; values computed for PREM[16] are added for reference.

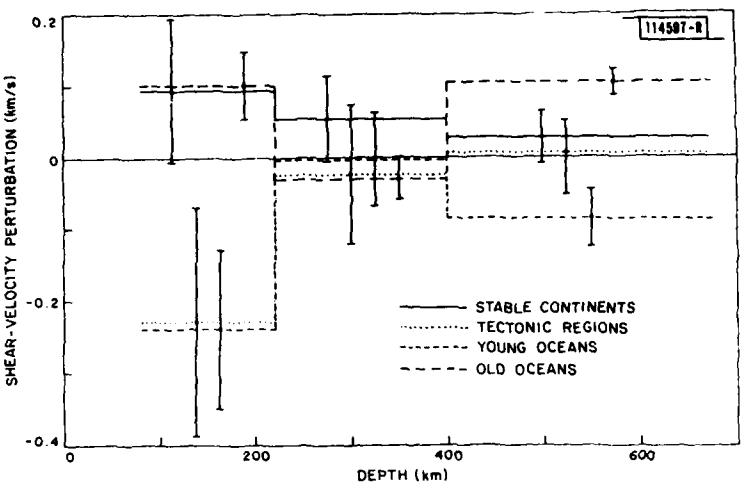

Fig. III-24. Pure-path shear-velocity models obtained through decomposition of structural parameters derived for each of 37 analyzed seismograms; bars indicate standard errors.

GLOSSARY

AA	Automatic Association
ABAR	Arrivals Based Analyst Review
ASL	Albuquerque Seismological Laboratory
ASRO	Abbreviated Seismic Research Observatory
ATN	Augmented Transition Network
DARPA	Defense Advanced Research Projects Agency
DBS	Database Subsystem
DEC	Digital Equipment Corporation
DMA	Direct Memory Access
DTW	Dynamic Time Warping
DWWSSN	Digital WWSSN Stations
FEL	Final Event List
GDSN	Global Digital Seismograph Network
IDA	International Deployment of Accelerometers
IESD	International Exchange of Seismic Data
IREM	Interim Reference Earth Model
LTA	Long Term Average
NEIS	National Earthquake Information Service
PDE	Preliminary Determination of Epicenters
PEL	Preliminary Event List
PREM	Preliminary Reference Earth Model
RAG	Related Arrival Group
RSTN	Regional Seismic Test Network
SAS	Seismic Analysis Station
SATS	Semiannual Technical Summary
SDAC	Seismic Data Analysis Center
SDC	Seismic Data Center
SNR	Signal-to-Noise Ratio
SRO	Seismic Research Observatory
STA	Short Term Average
USGS	U.S. Geological Survey
UUCP	UNIX-UNIX Copy
WIT	Waveform Inversion Technique
WWSSN	World-Wide Standard Station Network

UNCLASSIFIED

SECURITY CLASSIFICATION OF THIS PAGE *(When Data Entered)*

REPORT DOCUMENTATION PAGE	READ INSTRUCTIONS BEFORE COMPLETING FORM
1. REPORT NUMBER: ESD-TR-81-339	2. GOVT ACCESSION NO.: AD-A116 434
	3. RECIPIENT'S CATALOG NUMBER:
4. TITLE *(and Subtitle)*: Seismic Discrimination	5. TYPE OF REPORT & PERIOD COVERED: Semiannual Technical Summary, 1 April – 30 September 1981
	6. PERFORMING ORG. REPORT NUMBER:
7. AUTHOR*(s)*: Michael A. Chinnery	8. CONTRACT OR GRANT NUMBER*(s)*: F19628-80-C-0002
9. PERFORMING ORGANIZATION NAME AND ADDRESS: Lincoln Laboratory, M.I.T., P.O. Box 73, Lexington, MA 02173-0073	10. PROGRAM ELEMENT, PROJECT, TASK AREA & WORK UNIT NUMBERS: ARPA Order 512, Program Element No. 62714E, Project No. 1A10
11. CONTROLLING OFFICE NAME AND ADDRESS: Defense Advanced Research Projects Agency, 1400 Wilson Boulevard, Arlington, VA 22209	12. REPORT DATE: 30 September 1981
	13. NUMBER OF PAGES: 116
14. MONITORING AGENCY NAME & ADDRESS *(if different from Controlling Office)*: Electronic Systems Division, Hanscom AFB, Bedford, MA 01731	15. SECURITY CLASS. *(of this report)*: Unclassified
	15a. DECLASSIFICATION DOWNGRADING SCHEDULE:

16. DISTRIBUTION STATEMENT *(of this Report)*

Approved for public release; distribution unlimited.

17. DISTRIBUTION STATEMENT *(of the abstract entered in Block 20, if different from Report)*

18. SUPPLEMENTARY NOTES

None

19. KEY WORDS *(Continue on reverse side if necessary and identify by block number)*

seismic discrimination	surface waves	NORSAR
seismic array	body waves	ARPANET
seismology	LASA	

20. ABSTRACT *(Continue on reverse side if necessary and identify by block number)*

This Semiannual Technical Summary describes the Lincoln Laboratory Vela Uniform program for the period 1 April to 30 September 1981. During this period, the first working prototype of a Seismic Data Center has been completed. In this report, Sec. I describes this prototype system, Sec. II describes a series of activities in seismic processing related to the Center, and Sec. III describes a series of investigations in General Seismological Research.

DD FORM 1 JAN 73 1473 EDITION OF 1 NOV 65 IS OBSOLETE

UNCLASSIFIED

SECURITY CLASSIFICATION OF THIS PAGE *(When Data Entered)*

☆ U. S. GOVERNMENT PRINTING OFFICE: 1982--500-000--51